Electrochemical Reduction of Carbon Dioxide

Modeling the electrochemical conversion of CO_2 to Formic Acid under high pressure

by Vincent van Beusekom

TU Delft

Electrochemical Reduction of Carbon Dioxide

Modeling the electrochemical conversion of CO_2 to Formic Acid under high pressure

by

by Vincent van Beusekom

to obtain the degree of Master of Science
at Delft University of Technology,
to be defended publicly on Thursday 22th of February, 2018 at 13:30 PM.

Student number:	4031091	
Report number:	2884	
Project duration:	15th of March, 2017 – 22th of February 22, 2018	
Thesis committee:	Prof. dr. ir. W. de Jong,	Chairman, TU Delft (3mE)
	Dr. J. G. Buijnsters,	TU Delft (3mE)
	Dr. ir. J. W. Haverkort,	TU Delft (3mE)
	Dr. R. M. Hartkamp,	TU Delft (3mE)

An electronic version of this thesis is available at http://repository.tudelft.nl/.

TU Delft

Preface

Climate is changing. And it may be one of the biggest challenges that the world's people ever faced. The devastating risks of rising temperatures, changing weather patterns and extreme weather events are practically incalculable, and may include water crises, food shortages and limited economic growth. The solution for a sustainable future will require a combination of universal collaboration, ambitious governmental policies and legislation, and the development of new technologies. A key step will lie in eliminating the net rise of CO_2 in the atmosphere by closing the CO_2 cycle. As example, one solution might be the use of CO_2 as a feedstock for the production of fuels and raw materials for the chemical industry.

The research presented in this paper is part of a multi-company initiative in collaboration with the Delft University of Technology, in which the conversion of CO_2 to value-added products, in particular to formic acid, is actively researched. It has been a privilege to be part of this initiative during the last year or so. It has allowed me to learn from and work together with numerous skilled, ambitious and motivated people.

In this research, the electrochemical conversion of CO_2 towards formic acid is investigated. It includes a comparison between different possible reduction products and formic acid with respect to both commercial and technical feasibility. Furthermore, the electrochemical reduction to formic acid (or formate) is modeled and the effect of elevated pressure on both selectivity (faradiac efficiency) and production rate (current density) is researched. It has been found that a model which combines simplified mass transfer and electrochemical kinetic theory, is capable of reproducing the results from literature and satisfactorily predicting trends in efficiency and production rate for a range of operating conditions.

It would like to give a special thanks to my supervisors Wiebren de Jong and Peter van den Broeke for their advice and guidance during the many meetings and discussions over the last year. In addition, I would like to thank Andrew Morrison (Research associate) and Mahinder Ramdin (Research associate), for their willingness to help and offer advice whenever I reached out to them.

This work has been submitted for review to the members of the thesis committee: Prof. dr. ir. W. de Jong (thesis supervisor), Dr. J. G. Buijnsters, Dr. ir. J. W. Haverkort and Dr. R.M. Hartkamp.

This thesis was written as part of the master of Mechanical Engineering, Energy - & Process Technologies (EPT) offered by the faculty of 3mE at the Delft University of Technology.

by Vincent van Beusekom
Delft, February 2018

Abstract

Due to rising concerns about climate change, a lot of research is currently underway with respect to the development of new technologies which can contribute to the decline of atmospheric CO_2, and will allow further penetration of renewables into the energy mix. A promising technology which is currently actively researched is the electrochemical reduction of CO_2 (ERC). This technology utilizes otherwise polluting and unwanted CO_2 and converts it into value-added products under the influence of an electrical current. The process can therefore be designed as an energy storage mechanism since electrical energy is stored as chemical bonds. In this research, ERC towards formic acid has been investigated from two perspectives.

First, the feasibility of the commercial production of formic acid compared to other products of ERC was investigated. The electrochemical production of the most common reduction products have been compared based on production costs, energy storage capabilities, toxicity and manageability. Due to the relatively low energy consumption for 2-electron products, namely formic acid, carbon monoxide and oxalic acid, it is found that these products have the most promising business case. Additionally, ERC to formic acid is best studied compared to other products, and high selectivities are commonly reported. Formic acid and methanol are liquid at atmospheric conditions, which is beneficial as relatively large amounts of energy per unit volume can be stored without the need of additional compression or cooling. This will also allow for easy transportation. As hydrogen carrier, formic acid has the advantage that it can be decomposed in H_2 and CO_2 near room temperature.

In the second part of this research, the use of numerical modeling to study the reduction of CO_2 in an electrochemical cell towards formic acid/formate at elevated CO_2 pressures is presented. The model investigates to impact on the cathodic half-cell of a cell designed for the reduction of CO_2 in aqueous electrolyte solutions at a constant temperature of $25℃$, simultaneously assuming non-limiting conditions with respect to the anodic half-cell. The modeled part of the cell has been divided in three main regions, namely the bulk, cathode surface region and the electrode surface, which are discussed separately. The bulk is assumed to be the region of equilibrated concentrations which are constant in time, as they are not dynamically influenced by any mass transport phenomena. Reactants are supplied from the bulk to the electrode surface and products are removed vice versa via the cathode surface region, which is a thin region in the vicinity of the electrode. The transfer of species within this region and the chemical reactions between the species, form a system of diffusion-reaction equations. This system is solved numerically using appropriate boundary conditions. The actual reduction of CO_2 occurs on the electrode surface, and the kinetics of the electrochemical reactions towards $HCOO^-$, CO and H_2 are described using Tafel-type kinetics.

The electrochemical model has been verified and compared with experimental data, and despite various simplifications has proven to be predictive of the electrochemical reduction of CO_2. It is found that the potentially beneficial effects of an elevated CO_2 pressure on both the production rate and selectivity, as experimentally observed[1], can be reproduced with reasonable accuracy. The CO_2 concentration at the electrode surface is identified as the main limiting factor for achieving both a high selectivity towards formate and a higher production rate on formate producing metals. The model shows that with an increased CO_2 pressure the amount of CO_2 dissolved into the solution is increased significantly, resulting in a higher concentration of CO_2 at the electrode and less mass transfer limitations.

[1] Todoroki et al. (1995) [1]

Contents

Nomenclature

Abbreviations

$\%_{pp}$	Percentage point
CE	Current efficiency
CSR	Cathode Surface Region
CTC	Charge Transfer Control
ERC	Electrochemical Reduction of Carbon Dioxide
FE	Faradaic efficiency
HER	Hydrogen Evolution Reaction
$IUPAC$	International Union of Pure and Applied Chemistry
LHV	Lower Heating Value
MC	Mixed Control
MTC	Mass Transfer Control
$NIST$	National Institute of Standards and Technology
NPV	Net Present Value
O	Oxidant
$OCAP$	Organic CO_2 for Assimilation by Plants
$OFAT$	One-Factor-At-a-Time Approach
PCD	Partial Current Density
PDE	Partial Differential Equation
R	Reactant
RDS	Rate Determining Step

Physical Expressions

α_c	Anodic charge transfer coefficient	$[-]$
α_c	Cathodic charge transfer coefficient	$[-]$
ΔG_f	Change in Gibbs free energy	$[J]$
δ	Diffusion layer thickness	$[m]$
$\dot{E}$	Specific energy consumption	$[MWht^{-1}]$
$\dot{P}_{in}$	Total special energy input	$[Jcm^{-2}s^{-1}]$
$\dot{R}_i$	Rate of formation of species i	$[gcm^{-2}s^{-1}]$
η	Overpotential	$[V]$

η_{aux}	Efficiency of auxiliary processes	[%]
γ_i	Activity coefficient of species i	[−]
ρ_i	Density of species i	$[kgm^{-3}]$ or $[gl^{-1}]$
θ_i	Coverage of species i	[−]
$\vec{k_0}$	Rate constant of reduction at E=0V vs SHE	[dependant]
$\vec{k_s}(E_0)$	Rate constant of reduction at the equilibrium potential	[dependant]
C_i	Concentration of species i	$[M]$
C_{carbon}	Total concentration of carbon in the system	$[M]$
C_{ox}	Oxidant concentration at the electrode surface i	$[M]$
C_{tot}	Total electricity and carbon cost	$[€t^{-1}]$
CE/FE	Current efficiency/Faradaic efficiency	[%]
CE_{max}	Maximum current efficiency to $HCOO^-$	%
$CO_{2,consumption}$	Consumption rate of CO_2 at the cathode surface	$[kmolm^{-2}s^{-1}]$
D_i	Diffusion coefficient for species i in water at 25℃	$[m^2s^{-1}]$
E	Applied Potential	$[V]$
E_0^{cell}	Standard cell potential	$[V]$
E_0^{ox}	Standard oxidation potential	$[V]$
E_0^{red}	Standard reduction potential	$[V]$
E_0	Standard electrode potential	$[V]$
e_0	Elementary charge of an electron	$1.602e^{-19}$[C]
E_{opt}	Cathodic potential at CE_{max}	V
F	Faraday's constant	$96487[Cmol^{-1}]$
G_f	Change in Gibbs free energy	$[J]$
H_{CO_2}	Henry's constant for CO_2 in water at 25℃	$[molL^{-1}bar^{-1}]$
i_0	Exchange current density	$[mAcm^{-2}]$
i_j	Partial current density to product j	$[mAcm^{-2}]$
i_{tot}	(Total) current density	$[mAcm^{-2}]$
K^i	Equilibrium constant for reaction i	[dependant]
k_f^i	Forwards rate constant for reaction i	[dependant]
k_r^i	Backward rate constant for reaction i	[dependant]
k_B	Boltzmann Constant	$1.38e^{-23}[m^2kgs^{-2}K^{-1}]$
M_i	Molar mass of species i	$[gmol^{-1}]$
M_p	Molar mass of product	$[gmol^{-1}]$
n_i	Number of electrons exchanged in reaction i	[−]

$OH^-_{formation}$	Formation rate of OH^- at the cathode surface	$[kmolm^{-2}s^{-1}]$
p	Pressure	$[atm]$
$p^{sat}_{H_2O}$	Water saturation pressure at 25℃	$[bar]$
P_{CO_2}	CO_2 price	$[€t^{-1}]$
p_{CO_2}	Partial pressure of CO_2	$[bar]$
P_e	Electricity price	$[€MWh^{-1}]$
P_{sat}	Saturation pressure of CO_2 at 25℃	$[-]$
Q	Reaction quotient	$[-]$
R	Universal gas constant	$8.314[Jmol^{-1}K^{-1}]$
r	Electrical resistance of a electrochemical system	$[\Omega]$
s	Number of moles CO_2 used for each mole of product	$[-]$
S_{CO_2}	Concentration of CO_2 which can be dissolved in the electrolyte solution	$[M]$
T	Temperature	$[K]$
U_0^{cell}	Standard cell potential	$[V]$
u_i	Electrochemical mobility of an ion i	$[m^2s^{-1}V^{-1}]$
V_i	Net rate op formation of species i due to chemical reactions	$[Ms^{-1}]$
v_i	Velocity of the solution	$[ms^{-1}]$
y_i	Mole fraction of species i	$[-]$
z_i	Charge number of an ion i	$[-]$

List of Figures

List of Tables

1 Background

Introduction

Since the start of the industrial revolution, the concentration of carbon dioxide (CO_2) in the earth's atmosphere has been rising rapidly. The increase of this greenhouse gas in the atmosphere is largely induced by the burning of fossil fuels such as coal, oil and natural gas. As a result, global temperatures are rising, which poses a serious and potentially irreversible threat to people and ecosystems [9]. Reducing the global CO_2 emissions is becoming a top priority and many countries are setting increasingly ambitious emission reduction targets [10][11][12].

There are four main paths for the reduction of CO_2 emissions [13]: (1) increase the amount of non-carbon energy sources, (2) improving energy efficiency, sometimes referred to as the fifth fuel [14] next to coal, hydrocarbons (natural gas and petroleum), nuclear, and renewable energy, (3) carbon capture and storage and (4) carbon capture and CO_2 utilization. These solution all have the potential to contribute in solving the global warming challenge. The technology maturity, often expressed in technology readiness level (TRL), of the different proposed solutions vary from fully matured commercial scale technologies such as photo-voltaic cells or wind turbines to lab-scale initial research. One technology that has been researched for many years, but is not yet commercially developed and has a TRL of 3-5 [15], is the electrochemical reduction of CO_2 to value-added products.

Despite facing some large difficulties and obstacles, the electrochemical reduction of CO_2 (ERC) is a promising technology with some very appealing advantages. First of all, it utilizes CO_2 and converts it from an unwanted greenhouse gas into a value product which can be used in many different sectors. Secondly, the share of these renewable energy sources in the global energy market is steadily growing due to maturing technologies, large investments and ever increasing concerns about the climate. However, as long as large scale energy storage remains unavailable, the intermittent character of most renewables will limit the penetration of renewable energy sources into the overall energy mix. As the process of electrochemical reduction requires an applied potential, an electricity source is needed. If renewable energy sources such as wind and solar are used for the reduction of CO_2 during peak production hours, the intermittent character of these sources can be balanced whilst the renewable energy is secondarily stored in the products of the process.

COVAL Energy[1], a Dutch energy start-up, is actively researching the ambitious route of commercial scale CO_2 utilization by the electro-reduction of CO_2 to value-added products. Using this method and depending on the operating conditions and materials used, a variety of products can be produced. The products all have a variety of pro's and cons, which are carefully assessed in this research. The most promising products are evaluated for commercial scale implementation and the entire process is investigated with a systems approach. In this research the production of one of the most promising products, formic acid, is extensively looked at.

[1] http://www.covalenergy.com/

In previous studies [1][16], it was shown that reduction at elevated CO_2 pressure can have a positive effect on the production of valuable products, including formic acid. To further investigate this concept a numerical model is made, in which the key processes of CO_2 reduction are analyzed and modeled for an electrochemical cell with high selectivity for formic acid/formate. This model can be used to conduct initial research on the effect of different operational conditions on the process, without the need for expensive and time-consuming experiments. Furthermore it can be used to explore new potentially interesting cell configurations for new experimental research and help explain the effects observed in published experimental data.

This research has been commissioned by COVAL Energy in collaboration with Delft University of Technology, The Netherlands.

1.1. An Electrolytic Cell

In electrochemistry the interplay between electrical energy and chemical reactions is studied. One of the most typical examples of electrochemistry in our everyday life is a battery. A battery is an electrochemical cell in which electric current is produced via a spontaneous chemical reaction. Such a cell is called a galvanic cell. Another type of electrochemical cell is an electrolytic cell, which is a cell where a non-spontaneous chemical reaction takes place when electrical energy is supplied. In an electrolytic cell, electrical energy can therefore be converted into chemical energy stored in high energy compounds.

Here only an introductory summary of the working of an electrochemical cell will be given, for further reading the book ”Industrial Electrochemistry” by Pletcher and Walsh[17] is advised. Key in the working of electrochemical cells is the redox reaction. A redox reaction, short for reduction-oxidation reaction, is a process in which the oxidation states of the involved species are changed via electron transfer. Reduction is the part of the redox reaction where an atom, molecule or ion *gains* one or more electron(s), reducing the oxidation state and oxidation is the part of the reaction where an atom, molecule or ion *looses* one or more electron(s), increasing its oxidation state. During a redox reaction, both the oxidation and reduction proceed at the same time and cannot occur separately. Both processes are called half-reactions, as they each represent half of the total redox reaction. Each of the two half-reactions take place at a separate part of an electrochemical cell, called an half-cell. Each half-cell generally consist of an electrode and an electrolyte. The reduction and oxidation reactions takes place at the cathode and anode, respectively. The two half-cells both contain an electrolyte which allows for ion transport. Depending on the set-up of the cells, the two half-cells may or may not share the same electrolyte and may operate with or without a separator (e.g. membrane, salt-bridge).

Each half-reaction has a so called standard electrode potential (E^0). This is the potential difference at standard conditions (298.15K, 1 atm and concentrations of 1.0M) between the cathode half-reaction (the reaction where a electron is gained) and a reference anode reaction which is most commonly the oxidation of hydrogen on a platinized platinum electrode (Standard Hydrogen Electrode (SHE) or Normal Hydrogen Electrode (NHE)). The standard electrode potential is also known as the reduction potential as it is a measure of the tendency of the oxidant towards reduction. The more positive the standard potential, the more likely the substance is to be reduced. The standard reduction potentials of the reactions at the the cathode and anode can be combined to determine the overall cell potential of a redox:

$$E^0_{cell} = E^0_{red,cathode} - E^0_{red,anode} \tag{1.1}$$

For any reduction, there is a opposite oxidation, and the reaction at the anode is actually an oxidation reaction, thus explaining the minus sign. If the oxidation potential is used, the cell potential is calculated by addition, since the standard oxidation potential is defined as:

$$E^0_{ox} = -E^0_{red} \tag{1.2}$$

For an electrolytic cell, the thermodynamically determined overall cell potential, E^0_{cell}, indicates at which applied voltage the redox would ideally occur at standard conditions. However, due to inefficiencies in the reactor design, reaction mechanisms, and activation barriers, the actual voltage at which the reaction takes place is normally higher. In electrochemistry this difference between the standard potential and the measured or applied potential is called the overpotential. Normally, the additional energy needed to bridge the overpotential is dissipated as heat.

The maximum work that can be produced by an electrochemical cell, w_{max}, is the product of the cell potential, E_{cell} and the total charge transferred during the reaction, nF. Here n is the number of moles electrons transferred and F the charge of one mole electrons (Faraday's constant). The cell potential is related to the Gibbs free energy of the system, ΔG_f, because the Gibbs free energy is also a measure of the maximum work that can be performed during a chemical process. Therefore the cell potential and the Gibbs free energy are related via Equation 1.3. The Gibbs free energy is an indicator if a redox reaction will happen spontaneously or not and with which theoretical energy effort. A spontaneous reaction is characterized by a negative value ΔG_f, which corresponds to a positive value of E_{cell}, whereas a non-spontaneous reaction is indicated by a positive value for ΔG_f and a negative E_{cell}. In Chapter 4, the thermodynamics involving CO_2 reduction are further elaborated.

$$w_{max} = -nFE_{cell} = \Delta G_f \tag{1.3}$$

The standard electrode potential of half-reactions are listed in tabular form in many chemistry books and papers. For this research, standard electrode potentials as reported in "Electrochemical and Electrocatalytic Reactions of Carbon Dioxide" by Sullivan et al. [4] will be used.

1.2. The Electrochemical Reduction of CO_2

A electrolytic cell, in which electrical energy is converted into chemical energy, is used for ERC. Simplified, the process can be seen as the artificial electrochemical equivalent of photosynthesis, a process used by plants and other organisms in which CO_2 and water are converted into chemical energy under the influence of light (energy). As shown in Figure 1.1, both ERC and photosynthesis share the same building elements, namely CO_2, water and energy and both produce compounds containing chemically stored energy. The main difference is that where photosynthesis uses light energy (i.e. photons), the electrochemical reduction of CO_2 uses electrical energy (i.e. electrons).

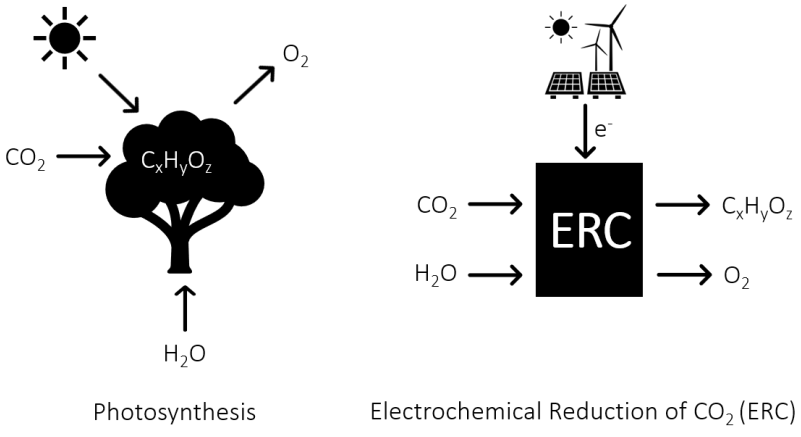

Figure 1.1: Schematic comparison between photosynthesis and ERC

Initial research on the concept of ERC started in the 1900's and intensified significantly in the 1980's, mainly as a reaction on the oil crises in 1973 and 1979. During these crises

the oil price rose rapidly, respectively up to 400% and 100% in a short period of time [18] and alternatives for the rapidly increasing oil-price were actively searched for. Due to environmental concerns regarding global warming, ERC research has gained momentum again in the last decade, as it potentially offers several advantages [19][20]:

- ERC utilizes the greenhouse gas CO_2 and converts it into potentially valuable products
- Electricity to drive the reduction process can be obtained from renewable and carbon neutral sources
- The electrical energy used for the electrochemical reduction can be stored as chemical energy for later use by oxidation of the products in fuel cells or heat engines
- The ERC process is controllable by varying the operating conditions as electrode potential, pressure and temperature
- Electrochemical systems can be designed to be compact, modular and scalable
- Water or even waste water can be used as reducing agent, donating electrons at the anode
- The process can be designed to minimize or even eliminate harmful waste products (e.g. by fully recycling the supporting electrolytes)

Despite these advantages, commercialization of ERC has proven to be difficult and researchers still struggle to bridge the difficult step from lab-scale reduction processes towards large scale and commercially viable reactors. Some of the remaining difficulties include:

- The kinetics of CO_2 reduction are slow, limiting the reaction rates and therefore the reduction process
- The solubility of CO_2 in water at standard conditions is low, limiting the availability of CO_2 at the cathode
- Reaching high selectivities towards the desired product(s)
- Low performance of electro-catalysts (low catalytic activity and poor stability)
- Still economically unattractive due to relatively cheap fossil fuels [20]

A variety of reduced products can be produced, depending on the operating conditions including pressure, temperature and applied voltage, as well as reactor design parameters such as electrode material, catalyst or electrolyte composition. The combination of these variables determines the amount of electrons transferred at the cathode and the mechanisms involved. These factors then determine the final distribution between reduction products. In Table 1.1, the half-reactions for the two-, four-, six- and eight-electron reduction products of CO_2 in an aqueous environment at standard conditions are given, together with their standard electrode potentials (vs. SHE) and standard Gibbs free energies [4][20].

Depending on the operating conditions and design of the cell, each of these reduction half-reactions can be balanced with an oxidation half-reaction in which water is the reducing agent:

$$H_2O \longrightarrow 2\,H^+(aq) + 2\,e^- + \frac{1}{2}\,O_2(g)$$

An example is the reduction of CO_2 towards formic acid under acidic conditions where CO_2 and water are converted to formic acid and oxygen. The total reaction then becomes:

$$\begin{aligned} CO_2(aq) + \cancel{2H^+} + \cancel{2e^-} &\longrightarrow HCOOH(aq) \\ H_2O &\longrightarrow \cancel{2H^+} + \cancel{2e^-} + \frac{1}{2}\,O_2(g) \\ \hline CO_2(aq) + H_2O &\longrightarrow HCOOH(aq) + \frac{1}{2}\,O_2(g) \end{aligned}$$

It is important to note that the standard potentials in Table 1.1 are based on standard conditions, including pH 0. The standard potential of a reaction is also pH dependent, as H^+ and OH^- are involved in the reactions occurring in aqueous solutions. This pH dependency of the reduction potential is also seen in the Pourbaix diagrams for the reduction of CO_2 shown in Chapter 4, which show the voltage potential (vs SHE) versus the acidity level (pH). With

Table 1.1: Standard Electrode Potentials (vs. SHE) at 298.15K, 1 atm and pH=0.0

Product:	**Reaction:**	**E^0**: [V]	ΔG^0: [kJmol^{-1}]
Oxalic Acid	$2\,CO_2(aq) + 2\,H^+ + 2\,e^- \longrightarrow H_2C_2O_4$	-0.475	+91.8
/Oxalate	$2\,CO_2(aq) + 2\,e^- \longrightarrow C_2O_4{}^-$ (anhydrous)	-0.590	+113.9
Formic Acid	$CO_2(aq) + 2\,H^+ + 2\,e^- \longrightarrow HCOOH(aq)$	-0.199	+38.4
/Formate	$CO_2(aq) + H_2O + 2\,e^- \longrightarrow HCOO^-(aq) + OH^-$	-1.078	+208.0
Carbon Monoxide	$CO_2(aq) + 2\,H^+ + 2\,e^- \longrightarrow CO(g) + H_2O$	-0.103	+19.9
”	$CO_2(aq) + H_2O + 2\,e^- \longrightarrow CO(g) + 2\,OH^-$	-0.934	+180.2
Formaldehyde	$CO_2(aq) + 4\,H^+ + 4\,e^- \longrightarrow HCHO(aq) + H_2O$	-0.071	+27.5
”	$CO_2(aq) + 3\,H_2O + 4\,e^- \longrightarrow HCHO(aq) + 4\,OH^-$	-0.898	+346.6
Methanol	$CO_2(aq) + 6\,H^+ + 6\,e^- \longrightarrow CH_3OH(aq) + H_2O$	+0.030	-17.3
”	$CO_2(aq) + 5\,H_2O + 6\,e^- \longrightarrow CH_3OH(aq) + 6\,OH^-$	-0.812	+470.1
Methane	$CO_2(aq) + 8\,H^+ + 8\,e^- \longrightarrow CH_4(g) + 2\,H_2O$	+0.169	-130.8
”	$CO_2(aq) + 6\,H_2O + 8\,e^- \longrightarrow CH_4(g) + 8\,OH^-$	-0.659	+508.7

respect to the electrochemical reduction, this means that depending on pH the reactions may vary. At pH 0 for example, the reactions with H^+ as proton donor are very thermodynamically favored. However, at increasing pH the standard potential may change and the proton donor may change from being H^+ to H_2O, producing formate instead of formic acid for example. Also depending on the pH of the solution, part of the formic acid formed may donate a proton to form formate or vice versa, to reach thermodynamic equilibria between the two. In Chapters 4 and 6, the thermodynamics as well as the reaction mechanisms of CO_2 reduction to various products is further elaborated.

1.3. Previous Work

In this section relevant literature on the ERC is summarized. It will elaborate on previous work, with the focus on ERC at elevated CO_2 pressures and commercial scale implementation. In this work, the feasibility of ERC for different products is looked at, the mechanisms of ERC are investigated, and a numerical model is build for the prediction of the selectivities and production rates at varying operating conditions. Therefore the literature study will be divided in three main section: feasibility studies, experimental work, and modeling work. Based on this study, a new possible field for research with respect to high pressure ERC is identified. This leads up to the objectives of this work, formulated in Section 1.4.

1.3.1. Feasibility and Product Comparison

The process of ERC can be designed to selectively make various products. These products all differ, as they have different characteristics and properties. Therefore from a feasibility aspect, the selective production of some products may be more attractive than others. Several studies on the characteristics of th different ERC products, and on the overall feasibility have been conducted. The most relevant finding, in scope of this work, are summarized.

A wide selection of products can be produced (theoretically), and they can be classified by the number of moles of electrons involved per mole of CO_2 reduced. Some of the most promising products include carbon monoxide (2 electrons), formic acid (2”), oxalic acid (2”), formaldehyde (4”), methanol (6”) and methane (8”) [20]. Looking at economic viability under current techno-economic conditions, carbon monoxide and formic acid were identified to be the only products with a positive end-of-life net present value (NPV) [21], comparing carbon monoxide, formic acid, methanol and higher-order alcohols (i.e n-propanol and ethanol).

Lu et al. [22] extensively reviewed the electrochemical reduction of carbon dioxide, in particular to formic acid. They state that amongst all the routes to ERC products (i.e. ERC to CO, formic acid, oxalate, alcohols and long chain hydrocarbons), the conversion of CO_2

to formic acid is favored for many reasons. They consider the commercialization of CO_2 to formic acid conversion to be feasible due to a broad market and wide application range, and therefore most likely to be profitable compared to other products.

Ma et al. [2], assessed formic acid, hydrocarbons, carbon monoxide and methanol, with respect to their current status and future challenges. They also developed a process cost analysis model for the selective production of CO, in order to get an idea of how the costs scale with current density. As shown in Figure 1.2, it was found that the total costs (capital and energy costs combined), levels off with production rate, due to the drop in capital costs. With increasing current density the capital costs drop significantly, and the energy costs becomes the dominant factor.

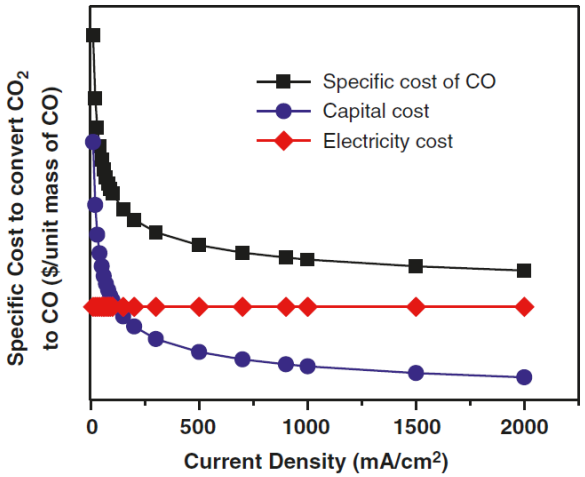

Figure 1.2: Schematic representation of a crude energy costs, capital investment, and the total CO cost for ERC to CO (From: Ma et al. [2])

1.3.2. Experimental

Many studies on the concept of the electrochemical reduction of CO_2 towards various products have been conducted in recent decades [20]. These studies often investigate the selective production towards one or more products, and the effect of various factors as operating conditions or cell design on the selectively and production rate. Often recognized as most promising products are carbon monoxide and formic acid/formate. Both species are products of a 2-electron reduction process, which reduces energy costs significantly compared to higher electron reactions. Selected experimental results of studies towards various ERC products are listed in Table 1.2. CO and $HCOO^-$ are the most commonly studied products, and can be formed with high selectivities up to 90%-95% [1][16][23][24]. High selectivities to the other products are less commonly reported in studies on ERC, and often involve more complex electrocatalysts. For all products, relatively low current densities ($\leq$ 60 $mAcm^{-2}$) are reported at atmospheric conditions, and therefore commercial scale production of these products remains difficult.

As mentioned, one of the main challenges of CO_2 reduction is the low solubility of CO_2 in water at standard conditions. The low solubility of CO_2 in water, 0.0325 moles CO_2 per liter at 1 bar and 298.15 K, significantly limits the electrochemical reaction rate and the overall production. The main reason for this limitation is the limited amount of CO_2 that is available at the cathode surface, the place where the electrochemical reaction occurs. Studies have shown that operation at elevated pressures can increase the reaction rate as well as the selectivity [1][16]. Hara et al. [16], investigated the possibility of high rate CO_2 reduction under high pressure conditions and found that formic acid was the main product with a FE of 92.3% at a pressure of 30 atm on Sn cathodes, reaching partial current densities of up to

163 mA/cm^2. Todoroki et al. [1] investigated the electrochemical reduction of CO_2 at Pb, Hg and In electrodes in an aqueous $KHCO_3$ solution with pressures up to 60 bar. They found that on Pb electrodes and at a current density of 200 mAcm^{-2}, the FE increased with an increasing CO_2 pressure of up to 20 bar, after which it remains fairly constant, as is seen in Figure 1.3. It was suggested that at a CO_2 pressure of about 20 atm, the rate limiting step changed from mass transfer to the cathode surface (i.e. CO_2 availability) to the electron transfer process at the surface, due to the high flux of CO_2 toward the cathode surface. At the same time the FE of the parasitic H_2 formation was suppressed with increasing pressure, because, in contrast to formic acid and CO production, the rate of H_2 formation was practically unaffected by increasing the CO_2 pressure. They also found that the maximum partial current density (PCD) for formic acid increased linearly with increasing CO_2 pressure, as is seen in Figure 1.4.

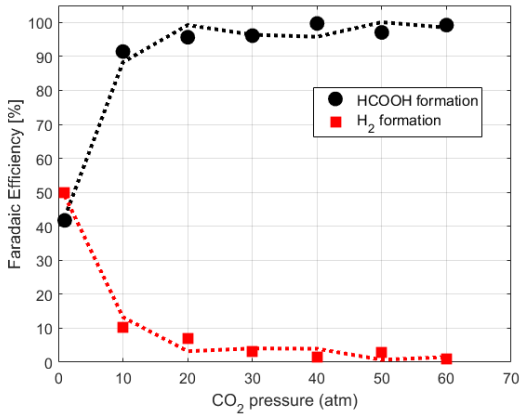

Figure 1.3: Effect of CO_2 pressure on FE of HCOOH formation on Pb-electrodes at a current density of 200 mAcm^{-2} (From Todoroki et al. [1])

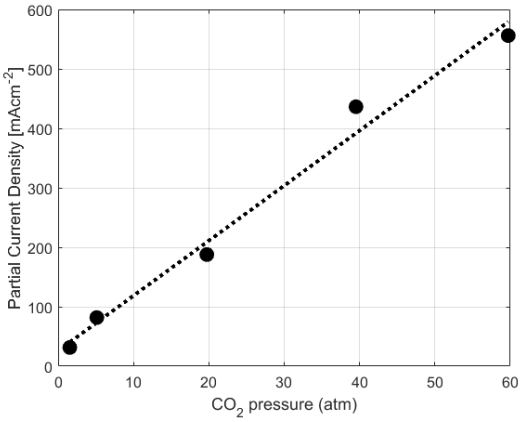

Figure 1.4: Effect of CO_2 pressure on the limiting PCD of HCOOH formation on In-electrodes (From Todoroki et al. [1])

Based on previous studies, including those mentioned earlier, it can be concluded that increasing the CO_2 pressure has a strong positive effect on the cathode potential and the partial current density for the formation of formate/formic acid [25]. This increase in reaction rate is said to be in a reaction order of about one with respect to CO_2 concentration in the catholyte.

Most research regarding the large-scale electrochemical CO_2 reduction focuses on the production of formate/formic acid, on tin (Sn) cathodes. Agarwal et al. [13] preferred the production of formate and formic acid over other products as the production has as a relatively low energy consumption, as described in Section 3.1.2. Furthermore, they chose to produce formic acid on tin as it is a highly selective electrocatalyst for ERC to formic acid/formate. Oloman and Li [26] did experimental work on the production of formic acid. Based on existing research as well as issues of convenience, cost and toxicity, Sn, was chosen as cathode material.

1.3.3. Modeling

Various researchers have attempted to model the phenomena and mechanisms involved in ERC. Modeling techniques can be very valuable in addition to experimental research, as it can offer insights into the mechanisms involved and on the influence of different process parameters on the overall performance. Furthermore, it can help to conduct initial research on the effect of process modifications, without the need for expensive and time-consuming experiments. In this section, key findings from relevant studies on the modeling of ERC are summarized.

Gupta et al. [27] presented a mathematical model that predicts the chemical cell conditions during ERC. The model focuses on the cathodic half-cell and assumes it to be divided into a bulk area of constant concentrations (i.e. in equilibrium), the electrode surface and a thin film between the bulk and the cathode surface, called the cathode surface region (CSR). In the CSR, diffusion and chemical reactions take place under the influence of cathode surface fluxes. They formulated partial differential equations (PDE) for each species in which they accounted for diffusion and chemical reactions, and they solved the system of PDE's numerically. They found that, under typical experimental conditions, the electrode surface concentration can be significantly different from the bulk concentration. The surface concentrations were found to be highly dependent on stirring rate (i.e boundary layer thickness), buffer capacity of the electrolyte concentration and current density.

Georgopoulou et al. [28], presented a model-based approach on the analysis of the different multidisciplinary processes involved in ERC. Their model structure comprised both the anodic and cathode domains in 2D for a cell where CO_2 is converted to formate/formic acid. The model is said to capture the molar transportation under the impact of an electric field, two-phase flow effects, and the key electrochemical reactions.

Delacourt et al. [29] analyzed experimental data for the reduction to CO and parasitic H_2 on gold and silver electrodes using a steady state mathematical model. The mathematical model is said to able to predict cell behavior including the current densities for varying time, potential and species concentrations. Despite being designed for this specific case study of reduction to CO on gold and silver electrodes, the mathematical model is said to be generic, and applicable for any electrochemical steady-state problem with a diffusion-layer of defined thickness. Under the assumption that the limiting step in reduction of CO_2 at the cathode is the formation of the radical $CO_2^{\cdot-}$ absorbed on the electrode, they derived both rate constants and charge transfer from experimental data.

1.4. Objectives

Taken previous studies into account, two main objectives for this work are identified. These objectives which will be introduced in this section.

First objective

As discussed above, many studies have looked at different aspects of ERC to added-value products, and the first part of this study aims to further elaborate on this. Objective is to conduct a comparative study between the different product and formic acid/formate, as this is the dominant product within the consortium. Several aspects need to be looked at, including: basic properties, production cost, energy/hydrogen storage, usability and toxicity. This will lead to a better understanding of the important elements of the process, reveal possible difficulties, and will identify opportunities. Additionally, goal is to propose a process cycle, which will visualize a possible route to commercialization of ERC. The process is investigated with a systems approach, grasping the most important features of the whole system. This all, leads to the first research question:

"What is the feasibility of the commercial production of formic acid compared to other different value-added products via the electrochemical reduction of CO_2 on a system level?"

The main subquestions which will need to be answered include:

- Which products can be produced via electrochemical reduction of CO_2, what are their individual advantages and disadvantages and how do they compare?
- What is the energy consumption and cost of production towards the most prospecting products via CO_2 reduction?
- What are the different process steps in the overall process chain of CO_2 reduction?

Second objective
The second part of this research zooms in, into the actual mechanisms of the electrochemical cell. Many experimental studies have looked at ERC, and several have shown a positive effect of CO_2 pressure on the production of formic acid/formate. However, questions remain on the exact mechanisms involved, and the interplay of pressure with other operational conditions with respect to formate/formic acid production. Also several efforts have been made on the modeling of (parts of) an electrochemical cell for the reduction of CO_2. These attempts have proven to be able to predict cell performance quite accurately, but rarely focus on the effect of CO_2 pressure on the reduction process and are mostly designed for cells that operate at ambient pressure and temperature.

Goal of this study is to fill in this discrepancy, and aims to develop a numerical model which describes the ERC to formic acid/formate, and the effect of elevated CO_2 pressures. The formation of formate is chosen to be further assessed, however many items discussed in this report are also applicable to the other reduction products. Goal is to identify the most essential theory for ERC with respect thermodynamics, mass transport, and kinetics, and investigate the effect of CO_2 pressure on these processes. The key findings will be combined and integrated in a numerical model, which is partly based on previous work. This model should give insight in the effects of high pressure ERC to formic acid/formate. It should be able to predict the production rates and product distribution under various conditions. The associated research question reads:

”Can the performance of an electrochemical cell with respect to selectivity and production rate towards formic acid/formate via CO_2 reduction, and the effect of an elevated CO_2 pressure, be effectively predicted using with a numerical model on a component level?”

The main subquestions regarding this question include:

- What are essential theories in thermodynamics, mass transfer phenomena, and kinetics, with respect to the electrochemical reduction of CO_2?
- What is the influence and effect of the operating conditions and cell design on the performance of an electrochemical cell designed for the reduction of CO_2?
- What are the rate determining steps in the electrochemical reduction of CO_2 with respect to mass transfer and kinetics?
- What is the effect of increased CO_2 pressure on thermodynamics, mass transfer phenomena, and kinetics, and how do these relate to the selectivity and production towards formic acid by CO_2 reduction in an aqueous solution?

1.5. Report Structure

In Chapter 2, the essentials of CO_2 are looked at, focusing on the solubility of CO_2 in aqueous solution and on the associated reactions upon dissolution. In Chapters 4, 5 and 6, key theory for the development of the model is studied and identified, with respect to thermodynamics, mass transport phenomena and kinetics, respectively. The development of the numerical model is explained in Chapter 7, followed by the discussion of the predicted results in 8. Finally in Chapter 9, conclusions regarding the research objectives and the model development are presented, and recommendations for future work are given.

Table 1.2: Selected data on ERC to selectively produce specific products

Information				Conditions					Results	
Product	**Author**	**Year**	**Ref.**	**Elctrd.**	**Pot. [V]**	**Elect.**	**Pres.**	**Temp.**	**FE [%]**	**CD[a]**
CO	Nakagawa et al.	1991	[30]	Pb (99.95%)	-1.8 (vs. Ag/AgCl)	0.1M $KHCO_3$	50 atm	30℃	57.9	-
	Lu et al.	2014	[23]	Ag (nanoporous)	-0.5 (vs. RHE)	0.5M $KHCO_3$	-	25℃	92.0	9.0
	Ikeda et al.	1987	[31]	Ag (99.98%)	-1.6 (vs. Ag/AgCl)	0.1M $KHCO_3$	-	25℃	64.7	-
$HCOOH/HCOO^-$	Ikeda et al.	1987	[31]	Hg	-1.6 (vs. Ag/AgCl)	0.1M $KHCO_3$	-	25℃	94.0	-
	Frankel et al.	2014	[32]	Sn	-1.8 (vs. SCE)	2.0M KCl	-	-	63.0	60.0
	Wu et al.	2012	[24]	Sn	-1.7 (vs. SCE)	0.1M Na_2SO_4	-	-	95.0	-
	Wu et al.	2012	[24]	Sn	-2.0 (vs. SCE)	0.5M $KHCO_3$	-	-	63.0	-
	Köleli and Balun	2004	[33]	Pb	-1.8 (vs. SCE)	0.2M K_2CO_3	50 bar	80℃	94.0	0.41
	Li and Oloman	2005	[34]	Sn/Cu	-	0.45M $KHCO_3$	-	25℃	86.0	22.0
	Hara et al.	1995	[35]	Fe	-1.61 (vs. Ag/AgCl)	0.1M $KClCO_4$	30 bar	25℃	59.6	120.0
	Hara et al.	1995	[16]	Sn	-1.39 (vs. Ag/AgCl)	0.1M $KHCO_3$	30 bar	25℃	92.3	163.0
	Hara et al.	1995	[16]	Pb	-1.57 (vs. Ag/AgCl)	0.1M $KHCO_3$	30 bar	25℃	95.5	164.0
	Todoroki et al.	1995	[1]	Pb	-	0.5M $KHCO_3$	50 atm	25℃	97.0	200.0
	Todoroki et al.	1995	[1]	Hg	-	0.5M $KHCO_3$	20 atm	25℃	100.9	200.0
	Todoroki et al.	1995	[1]	In	-	0.5M $KHCO_3$	20 atm	25℃	91.9	200.0
HCHO	Nakata et al.	2014	[36]	BDD[b]	-1.7 (vs. Ag/AgCl)	CO_2 sat. MeOH	-	25℃	74.0	-
	Nakata et al.	2014	[36]	BDD	-1.7 (vs. Ag/AgCl)	0.1M NaCl	-	25℃	62.0	-
CH_3OH	Frese	1991	[37]	Cu (preoxid. foil)	-0.4 (vs. SCE)	0.5M $KHCO_3$	-	25℃	100.0	33.0
	Le et al.	2011	[38]	Cu (preoxid. foil)	-1.1 (vs. SCE)	0.5M $KHCO_3$	-	-	38.0	-
	Frese and Leach	1985	[39]	Ru	-0.54 (vs. SCE)	0.2M Na_2SO_4	-	60℃	42.0	0.387
	Summers et al.	1986	[40]	Mo	-0.8 (vs. SCE)	0.2M Na_2SO_4	-	22℃	55.0	0.050
	Summers et al.	1986	[40]	Mo	-0.8 (vs. SCE)	0.2M Na_2SO_4	-	22℃	84.0	0.12
	Qu et al.	2005	[41]	RuO_2/TiO_2	-0.8 (vs. SCE)	0.5M $NaHCO_3$	-	25℃	60.5	-
$H_2C_2O_4/C_2O_4^{2-}$	Meser Ali et al.	1998	[42]	Ru	-1.65 (vs. Ag/AgCl)	CO_2 sat. CH_3CN	-	-	64.0	-
CH_4	Hori et al.	1995	[43]	Cu	-1.55 (vs. NHE)	0.1M $KClO_4$	-	18℃	49.5	5.0

[a] [$mAcm^{-2}$]
[b] Boron-doped diamond

2

Basics of Carbon Dioxide

Before discussing and evaluating the specific products of ERC, it is important to have a closer look at the main resource, namely carbon dioxide. The focus will be on the general properties such as solubility and phase behavior, as these are the most important aspects of CO_2 within the scope of this research. For further reading on CO_2 and its properties with respect to electrochemical and electro-catalytic reactions, the book "Electrochemical and Electrocatalytic Reactions of Carbon Dioxide" by Sullivan et al. [4] is recommended.

Carbon dioxide, exists as an odorless and colorless gas at atmospheric conditions and is found in relatively small quantities, about 400ppm, in Earth's atmosphere. CO_2 has a molar mass of 44.01 $gmol^{-1}$ and a density of 1.98 gL^{-1} at 25℃ and 1 bar. The CO_2-molecule consists of a carbon atom, which is covalently double bonded to two oxygen molecules, as is seen in Figure 2.1. Due to these bonds the molecule is chemically stable under normal conditions.

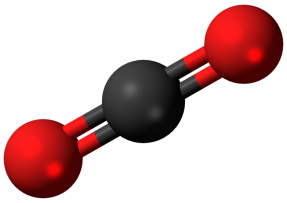

Figure 2.1: Schematic ball-and-stick model of CO_2

Solubility of CO_2

As described in Section 1.3, most research surrounding ERC is carried out in aqueous media. The current design of the electrochemical cell at the Process and Energy department of Delft University of Technology, is also based on the reduction of CO_2 in aqueous media, as CO_2 is dissolved in water (or an aqueous electrolyte), and fed into the electrochemical reactor. The solubility of CO_2 determines the amount of CO_2 that is available in the liquid phase, and therefore directly effects the rate of mass transfer to the cathode surface, and thus both the reaction rate and selectivity of the reaction.

The solubility of CO_2 in water at ambient conditions is quite low, around 0.03 mol CO_2 per liter water. Due to the low solubility under moderate conditions, the process is quickly limited by the mass transport of CO_2 towards the cathode surface. This is a major limitation for reaching high production rates, whilst simultaneously reaching high Faradaic efficiencies towards the desired product. Therefore, current densities are rarely reported to exceed 20 $mAcm^{-2}$ in previous studies surrounding the reduction of CO_2 eduction at moderate conditions. As the current density is a direct measure of the production rate (as explained in Chapter 6), the formation of useful products at moderate conditions is also very limited. For CO_2 reduction to be economically viable, the mass transport to the cathode surface needs to be optimized by any means. This research focuses on the concept of CO_2 reduction at an elevated CO_2 pressure, in order to increase the solubility, and thus decrease limitations of

the reduction process. The solubility of CO_2 in water (and aqueous electrolyte) is thoroughly investigated, focusing on the effect of elevated pressure.

Carbon dioxide can be dissolved in water, but the system can be complex. For this research the pressure dependence of the solubility of CO_2 in water will be analyzed around an isotherm of 25℃, as the reactor is initially designed to operate at ambient temperature. When CO_2 is dissolved in water, initially part of the CO_2 will be dissolved into the liquid phase according to:

$$CO_2\,(g) \rightleftharpoons CO_2\,(aq) \tag{2.1}$$

For low pressures and in a dilute solution (< 1% solute concentration), the solubility of CO_2 can be fairly accurately calculated using Henry's Law. Henry's Law states that along an isotherm the amount of gas which can be dissolved in solution is proportional to the partial pressure of the gas above the solution:

$$C_{CO_2}\,(aq) = H_{CO_2}\,p_{CO_2} \tag{2.2}$$

with:
C_{CO_2}: CO_2 concentration in aqueous phase [M]
H_{CO_2}: Henry's constant [$Mbar^{-1}$]
p_{CO_2}: Partial pressure of CO_2 above the liquid [bar]

Henry's constant for CO_2 at 25℃, H_{CO_2}, is 0.0345 $molL^{-1}bar^{-1}$ [44]. The supply of carbon dioxide is assumed to be a purely gaseous carbon dioxide feed, so the partial pressure of CO_2 will be almost equal to the total pressure above the liquid. Water vapor traces will be present in the mixture, of which the partial pressure is assumed to be the same as the pure water saturation pressure, $p_{H_2O}^{sat}$, which at 25℃ is 0.0316 bar [45] (as cited by NIST [46]). Thus:

$$p_{CO_2} = y_{CO_2}\,p_{total} \tag{2.3}$$

where the mole fraction of CO_2, y_{CO_2}, is calculated with:

$$y_{CO_2} = \frac{p_{total} - p_{H_2O}^{sat}}{p_{total}} \tag{2.4}$$

The linear solubility profile as described by Henry's Law for a temperature of 298.15K is plotted in Figure 2.2 as a black dotted line. It is calculated using Equations (2.2), (2.3) and (2.4).

The black crosses (**x**) in Figure 2.2 represent actual experimental data from CO_2 solubility measurements at 298.15K [47][48]. It can be seen that at relatively low pressures Henry's Law is accurate, but at higher pressures (>5 bar [49]), it starts to deviate from experimental data. For this research, the solubility at higher pressures must also be precisely known as the influence of CO_2 pressures higher than 5 bar is also to be investigated.

A model which describes the solubility accurately over a wider pressure range was therefore chosen. Based on on the equation of state of Duan et al. (1992) [50] and theory of Pitzer (1973) [51], Duan and Sun [52] set up a model for the calculation of CO_2 solubilities in H_2O in 2003 and an improvement on this model in 2006 [53]. For a wide range of temperatures and pressures (273K≤T≤533, 0 bar≤p≤2000 bar), the model's reliability is reported to be within, or close to, the experimental uncertainty (7% for CO_2 solubility [52]). The model of Duan and Sun may also be used to predict the solubility of carbon dioxide in water containing various ions. This will potentially be potentially useful, as in the actual cell CO_2 is dissolved in an electrolyte, which in addition to water also contains $KHCO_3$ or another salt. For this research, the model of Duan et Al. is used to predict solubilities for given pressures and the model is implemented in a MATLAB function. The solubility at 298.15K, predicted by this model, is seen as the red line in Figure 2.2. It is clearly seen that this model accurately follows the experimental data. Additional solubility curves for various temperatures have been plotted as well.

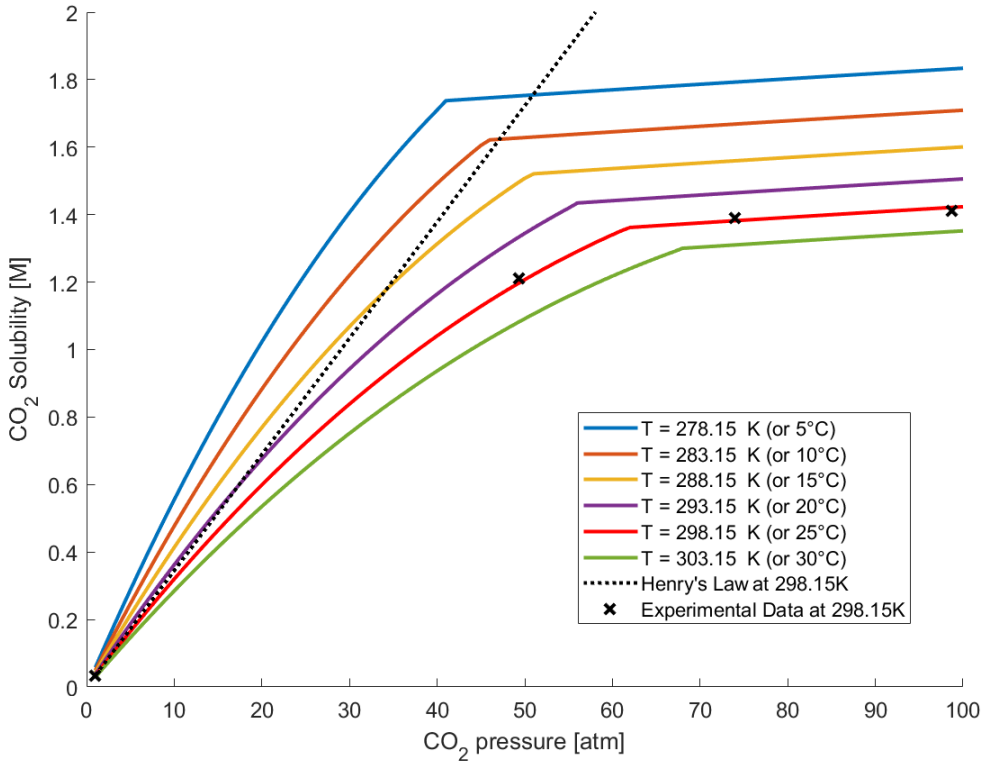

Figure 2.2: Solubility of Carbon Dioxide in Pure Water at 298.15K

Looking at Figure 2.2, some interesting trends are observed. It is seen that the solubility of CO_2 in water rapidly increases with rising pressures up to the saturation pressure (64.343 bar [54] at 25℃). At this point, the phase of CO_2 changes from being gaseous to being liquid, which results in a much smaller increase of solubility with increasing pressures. At 1 atm (298.15K) the CO_2 solubility is ~0.033M, compared to ~1.34M at 60 atm (298.15K), which is a 40x increase. With decreasing temperature the CO_2 solubility is also increased significantly, with the absolute solubility increase rising with pressure. At 20 atm, a decrease of 10℃ to 288.15K results in a ~28% solubility increase compared to the solubility at 298.15K. However, the influence of temperature on ERC is not looked on in this research. Further research on possible positive effects of temperature on ERC to value-added products is advised.

2.0.1. Dissolution of CO_2 in aqueous solutions

As mentioned, the system involved in dissolving CO_2 in water or an aqueous electrolyte can be complex. Using the solubility model of Duan and Sun [52] the amount of gaseous CO_2 that can be dissolved in water can be determined for a given pressure and temperature. However, when dissolved in water or an aqueous electrolyte solution a series of equilibrium reactions occur between CO_2 and more dissociated species, which may also be already present in the solution. Lower [49] extensively studied carbonate equilibria in waters and for further reading this work is advised. Furthermore, the equilibrium constants used in this section are taken from the book ”Electrochemical and Electrocatalytic Reactions of Carbon Dioxide” by Sullivan et al. [4].

The main reactions involved upon dissolution of CO_2 in aqueous solution are described below. The important reaction rates for reactions and the corresponding equilibrium constants are summarized in Table 2.1 [27] [4].

When gaseous CO_2 is brought into contact with H_2O, the first thing that happens is that

gaseous carbon dioxide is partly dissolved into water depending on the partial pressure of CO_2 above the liquid:

$$CO_2\,(g) \rightleftharpoons CO_2\,(aq) \tag{2.5}$$

The CO_2 (g) that is dissolved into the aqueous phase exists in a chemical equilibrium reversibly producing carbonic acid, H_2CO_3, according to (2.6):

$$CO_2\,(aq) + H_2O\,(l) \rightleftharpoons H_2\,CO_3(aq) \qquad (K_H) \tag{2.6}$$

The amount of CO_2 (aq) that is hydrated to H_2CO_3 (aq) is determined by the hydration equilibrium constant K_H, which is temperature dependent. At 25℃, K_H is approximately 2.6×10^{-3} in aqueous media. Carbonic acid has two protons which can be dissociated, making it a diprotic acid. After the dissociation of one proton a bicarbonate ion, HCO_3^-, is formed according to (2.7):

$$H_2CO_3(aq) \rightleftharpoons HCO_3^-(aq) + H^+(aq) \qquad (K_0) \tag{2.7}$$

This reaction has an equilibrium constant K_0 of approximately 1.7×10^{-4} at 25℃. However, from K_H it is evident that the concentration of H_2CO_3(aq) is much lower than the concentration of CO_2(aq), typically less than 1% [4] [49]. Furthermore, the protonation reaction of HCO_3^-(aq) is very rapid, effectively instantaneous and therefore reaction (2.7) can be assumed to be in chemical equilibrium. For these reasons, carbonic acid may be assumed to be an intermediate species in reaction (2.7). The ionization of CO_2 to produce HCO_3^-(aq) is better expressed [4] as reaction (2.8), in which CO_2^*(aq) represents both CO_2(aq) and H_2CO_3(aq).

$$CO_2^*(aq) + H_2O\,(l) \rightleftharpoons H^+ + HCO_3^-(aq) \qquad (K_{a1}) \tag{2.8}$$

Equilibrium constant K_{a1} can be calculated by combining both reactions (2.6) and (2.7): $K_{a1} = K_H K_0 = 4.4\times10^{-7}$.

Bicarbonate can be dissociated further into carbonate, CO_3^{2-}, as shown in (2.9). The equilibrium constant of this reaction, K_{a2}, is approximately 4.7×10^{-11} at 25℃.

$$HCO_3^-(aq) \rightleftharpoons CO_3^{2-}(aq) + H^+(aq) \qquad (K_{a2}) \tag{2.9}$$

Aqueous solutions, like the electrolyte under study, contain both H^+ and OH^- ions as part of the water molecules split via an autoprotolysis reaction, as seen in (2.10):

$$H_2O\,(l) \rightleftharpoons OH^-(aq) + H^+(aq) \qquad (K_W) \tag{2.10}$$

The solubility product of this reaction, K_W, at 25℃, is approximated to be 10^{-14} M^2, meaning that the product of the two species concentrations is always 10^{-14} M^2. The pH of an aqueous solution is determined by the amount of H^+ in solution. When assuming ideal solutions (i.e. γ_{H^+}=1 for H^+), the pH than varies between 1 and 14 and is calculated as:

$$pH = -\log(\gamma_{H^+}[H^+]) = -\log[H^+] = 14 - \log[OH^-]$$

In more alkaline solution, with a relatively high OH^- concentration, CO_2(aq) may also react directly with OH^- ions, as shown in reaction (2.11), with resulting equilibrium constant K_{b1}:

$$CO_2(aq) + OH^-(aq) \rightleftharpoons HCO_3^-(aq) \qquad (K_{b1}) \tag{2.11}$$

Also in alkaline solutions, the bicarbonate ion may than be directly neutralized by an OH^- ion, with an equilibrium constant K_{b2} of approximately 4.7×10^3 [M^{-1}]:

$$HCO_3^-(aq) + OH^-(aq) \rightleftharpoons CO_3^{2-}(aq) + H_2O\,(l) \qquad (K_{b2}) \tag{2.12}$$

Summarized, whilst dissolving CO_2 in an aqueous solution several constants are important to determine the composition of the electrolyte under different pressures. The reactions described above all have corresponding forward- and reverse reaction rates, which together

result in the reported equilibrium constant. It can be easily proved [55] that for reaction i, the equilibrium constant K_i is defined as:

$$K_i = \frac{k^i_{forward}}{k^i_{reverse}}$$

with $k^i_{forward}$ and $k^i_{reverse}$ being respectively the forward and reverse rate constant.

Table 2.1: Relevant reaction rates and equilibrium constants for the dissolution of CO_2 in water at 25℃

i	Reaction:	k^i_f	k^i_r	K^i	pK^i_a
a1	$CO_2 + H_2O \underset{k_r^{a1}}{\overset{k_f^{a1}}{\rightleftharpoons}} H^+ + HCO_3^-$	-	-	$\approx 4 \times 10^{-7}$M	6.35
a2	$HCO_3^- \underset{k_r^{a2}}{\overset{k_f^{a2}}{\rightleftharpoons}} CO_3^{2-} + H^+$	-	-	$\approx 4.7 \times 10^{-11}$M	10.33
b1	$CO_2 + OH^- \underset{k_r^{b1}}{\overset{k_f^{b1}}{\rightleftharpoons}} HCO_3^-$	$7.7 \times 10^3 M^{-1}s^{-1}$	$2.3 \times 10^{-4}s^{-1}$	$\approx 4 \times 10^7 M^{-1}$	-
b2	$HCO_3^- + OH^- \underset{k_r^{b2}}{\overset{k_f^{b2}}{\rightleftharpoons}} CO_3^{2-} + H_2O$	$1 \times 10^8 M^{-1}s^{-1}$	$2.15 \times 10^3 s^{-1}$	$\approx 4.7 \times 10^3 M^{-1}$	-
W	$H_2O \underset{k_r^W}{\overset{k_f^W}{\rightleftharpoons}} OH^- + H^+$	-	-	$\approx 10^{-14}M^2$	14

It is to be mentioned that the reported reaction rates and resulting equilibrium constants are highly temperature dependent. Whilst increasing or decreasing the temperature, the equilibrium shifts toward the products or reactants, depending on whether the reaction is respectively exothermic or endothermic. Pressure however, does not have an effect on reaction rates in liquid and solid media, because it will not increase the number of collisions between particles [56] (simplistically explained).

Phase behavior of CO_2

As described earlier, the solubility of carbon dioxide in water can be improved significantly by increasing the pressure. The fact remains that as long as CO_2 remains in its gaseous phase, the amount of CO_2 that can be dissolved in water is limited, even at high CO_2 pressures.

When looking at pressures above the saturation pressure, where CO_2 changes to its liquid phase, a interesting route for future research appears. ERC using liquid CO_2 will possibly allow for much higher production rates, mainly because mass transfer limitations of CO_2 towards to the electrode surface are diminished. When compared to the maximum CO_2 density in aqueous CO_2 reduction, the CO_2 density for liquid CO_2 reduction is much higher. Along the isotherm of 25℃, CO_2 becomes liquid when held at a pressure above the saturation pressure of CO_2 of approximately 64.3 bar [54], as can also be seen in Figure 2.3. It can also be seen that another possibility for liquid CO_2 operation would be to operate at a lower temperature as this will lower the saturation pressure, allowing liquid CO_2 reduction at a lower temperature.

Of course certain other issues arise when liquid CO_2 will be reduced, for example the supply of protons for the electrochemical reaction as less H_2O or H^+ is present or finding a suitable reductant which donates electrons at the anode electrode instead of H_2O. For the scope of this research however, the focus will be on the area where CO_2 is in a gaseous phase and ERC occurs in aqueous solvents. Further research on ERC in liquid phase however is highly recommended, as it might offers some big opportunities with respect to the current operating constrains and to the successful implementation of large scale reduction of CO_2 towards value-added products.

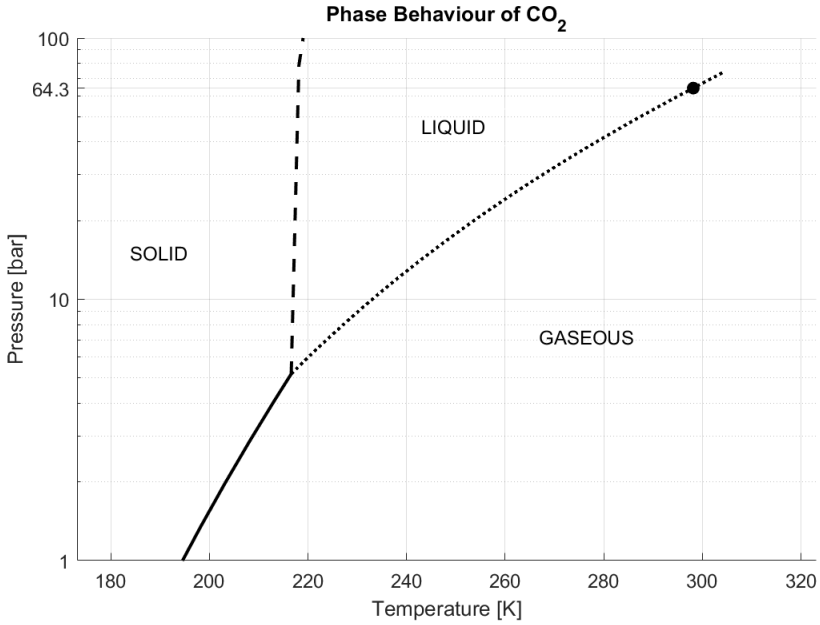

Figure 2.3: Phase behavior of CO_2 for varying temperature and pressure with sublimation line (—), saturation line (····), melting line (- -) and P_{sat} at 298.15K (●). (Data borrowed from NIST [3])

3

Feasibility and Comparison of Products

Introduction

The electrochemical reduction of CO_2 is an interesting method to utilize CO_2 for the production of useful chemicals. ERC can be customized to produce specific products with high selectivities by choosing appropriate cell properties as electrocatalysts, electrolytes and by optimizing operating conditions such as applied potential. In this chapter the most promising ERC products will be evaluated and compared. As this work is part of a larger research project led by Delft University of Technology in which formic acid and formate are researched, the comparison is primarily made between the different products and formic acid/formate. Rather than dismissing specific products, the aim of this chapter is to identify the possibilities of ERC. Also the process of ERC towards formic acid will be generally looked at from a system-level perspective, determining the different parts relevant in the process chain. The chapter aims to answer the first main research question: What is the feasibility of the commercial production of formic acid compared to other different value-added products via ERC on a system level?

3.1. Comparison of the Different Products

Depending on the process conditions, electrode material (i.e. electrocatalyst) and electrolyte, the process can be designed to be selective for different products. These products have different characteristics, and the production of these products via the proposed routes may be commercially interesting depending on different factors. ERC to some products is better studied and understood than to others, and the best recorded product selectivity and production rate for each product may differ significantly. In this section various products will be introduced and discussed, with the aim to finally select the most promising, based on both technological and commercial purposes (criteria being profitability primarily). The products are assessed for their properties with respect to several important factors, such as basic properties, production cost, current market value, usability, toxicity and energy density. The most commonly researched products of the 2-, 4-, 6- and 8 electron reactions, namely oxalic acid, formic acid, carbon monoxide, formaldehyde, methanol and methane are looked at.

3.1.1. Introduction to Different Products of ERC

Oxalic Acid

Oxalic acid (and its derivative oxalate) is less commonly studied as a product of ERC. Its formation in a CO_2 saturated and non-aqueous solution of CH_3CN on ruthenium complexes has been reported to have a selectivity of 64% [42]. Pure oxalic acid exists as odorless white crystals. It has a high acid strength, and is one of the strongest organic acids. The applications of oxalic acid mainly focus on cleaning and bleaching, pharmaceuticals, dying and other more niche markets as developing photographic films. The estimated current market price for oxalic acid is around 500 €/t [57], with a global production capacity of 0.45 million t/year [58]. With respect to ERC, the route to produce oxalic acid involves the addition of 2 electrons and requires 2 moles of CO_2 for each mole of product.

Formic Acid
Formic acid (and its derivative formate) is one of the major products of ERC on electrodes including Sn, In, Pb and Hg, with reported selectivities up to 90-95% [1][16][31][33]. Formic acid is used in various sectors and products including farming, leather, rubber, pharmaceuticals, and in the chemical industry. At atmospheric conditions it exists in liquid form, and is primarily sold in solutions with concentrations between 85-99% [59]. The current market price is approximately 600 €/t [60] and in 2017, the global production capacity was estimated to be 0.8 million t/year [61]. Via ERC the formation of formic acid involves 2 electrons and 1 mole of CO_2 per mole of product.

Carbon Monoxide
Next to formic acid, carbon monoxide is a major product of ERC with reported selectivities of 90-100% on several electrodes including Ag, Au and Zn. At atmospheric conditions carbon monoxide, is a gas which consists of one carbon atom triple bonded to an oxygen atom. CO can be formed via the partial oxidation of carbon, fossil fuels and other organic compounds. Carbon monoxide is industrially produced on quite large scale, as it is a important compound for bulk chemicals manufacturing. In combination with hydrogen it forms syngas, which can be converted into hydrocarbons via the Fischer–Tropsch process. The market price is estimated to be 850 €/t [62]. The formation of CO via ERC also involves a two-electron process and requires 1 mole of CO_2 for each mole of carbon monoxide.

Formaldehyde
The electrochemical production of formaldehyde is scarcely reported in literature, but a selectivity of 74% on a boron-doped diamond electrode, using seawater as electrolyte solution, is reported by Nakata et al. [36]. Formaldehyde is a flammable gaseous compound at standard conditions. In industry, formaldehyde is currently mainly synthesized by the catalytic oxidation of methanol at high temperatures. Formaldehyde is very toxic for both humans and animals, and ingestion of very small quantities have been reported fatal [63]. In solution, formaldehyde has many functionalities and is used in many industries such as construction, automotive, plastics and the textile industry. The market price is estimated to be 300 €/t [64], with a large global capacity of 52 million t/year in 2017 [65]. By ERC, formaldehyde can be produced in a four-electron process and requires 1 mole of CO_2 per mole of product. Formaldehyde is closely related to formic acid as it will oxidize to formic acid in aqueous solutions.

Methanol
The selective ERC to methanol is not commonly reported. However, on several electrodes including pre-oxidized copper electrodes, methanol has been reported to be formed selectively [37][38]. Methanol, CH_3OH, is liquid at atmospheric conditions. From an industrial perspective, methanol is one of the most produced and used chemicals worldwide. It is currently primarily used as a feedstock chemical for the production of other chemicals such as formaldehyde, olefins [66] or gasoline [67]. It is also used as a fuel in specific specialized vehicles such as fuel cell based cars. It can either be used in a combustion engine, pure or mixed with other fuels, or as a hydrogen carrier for fuel cells. To split methanol into hydrogen and carbon dioxide it has to be treated in a methanol reformer operating at approximately 20 bar and temperatures between 250℃ and 360℃ [68]. The current global capacity to produce methanol is approximately 110 million t/year [69], with an estimated market price of 300 €/t [70]. By ERC, methanol can be produced in a six-electron process with 1 mole of CO_2 per mole methanol.

Methane
Methane has been reported to be selectively formed on copper electrodes with FE's up to ~50% [71]. However, its formation is not commonly reported in research. Despite its gaseous state at standard conditions, it is a commonly used fuel as there is a relative abundance of methane on earth as main compound in natural gas. Methane is most commonly used as a fuel for vehicles, water- and home heating and has additional functionality as a common

ingredient in fabric, plastic, anti-freeze and fertilizer production. The methane or natural gas price is generally given in \$/mmBTU (million metric British Units), but converted to €/t the price of methane roughly approximately 150 €/t [72]. Methane can be produced in an eight-electron process via ERC, requiring 1 mole of CO_2 per mole methane.

3.1.2. Cost of Electrochemical Reduction

For every production process, an important requirement for success is an effective business case. This means that the benefits must be larger than the costs. Depending on the product and process the benefits and costs can include various aspects, such as financial profitability, social benefit, growth potential and safety hazards. In this section the minimum cost of production for each product is compared, based on energy requirement and CO_2 consumption, and balanced against the current market price. Additional costs such as the fixed costs for the reactor design and costs for separation and purification are ignored for the moment.

The specific energy consumption, $\dot{E}$, can be expressed in $\mathrm{MW\,h\,t^{-1}}$. For an electrochemical process, the specific energy consumption can be calculated using Equation (3.1):

$$\dot{E} = \frac{n \cdot (U_{cell} \cdot F)}{\eta_{aux} \cdot FE} \times \frac{1}{M_p} \times \frac{10^6[\frac{\mathrm{g}}{\mathrm{t}}]}{3.6 \times 10^9[\frac{\mathrm{J}}{\mathrm{MWh}}]} \tag{3.1}$$

with:

n: The number of electrons involved in the reaction [-]

$\dot{E}$: Specific energy consumption [MWh/t]

U_{cell}: Applied cell potential (= U_{red} + U_{ox} [V])

F: Faraday's constant (=96485.3 [C/mol])

FE: Faradaic Efficiency [%]

M_p: Molar Mass of product [g/mol]

η_{aux}: Efficiency of additional processes (pump, valves, etc..) [%]

The efficiency due to additional losses are assumed to be the same for all products, and chosen to be 90%. Equation (3.1) shows that the difference in cost of production for each product is dominated by the cell potential U_{cell}, the Faradaic efficiency, the molar mass of the product M_p and the number of number of electrons involved in the reaction n. Here the molar mass and number of electrons are fixed for each reaction, the cell potential and faradiac efficiency are highly dependent on a specific cell design and will potentially improve with future research and development. Based on the literature survey, of which the results are shown in Table 1.2, typical established values for U_{cell} and CE are chosen for each product which correspond to best-case experimental data. These values, together with the approximate market price [$€t^{-1}$] for oxalic acid, formic acid, carbon monoxide, formaldehyde methanol and methane are plotted in Figure 3.1. The cell potential can be calculated by combining the reduction potential (cathode) and the oxidation potential (anode). Although in reality anodic losses will be present, it is assumed that the oxidation potential for the water oxidation, U_{ox}, at the anode is equal to the thermodynamically calculated standard reduction potential at pH 7 (around which most measurements are performed). This value is -0.81V (vs. SHE) [4].

The electricity price [$€MWh^{-1}$], P_e, is assumed to be €85 per MWh, based on the 2017 S1 average electricity price for non-households in The Netherlands [73]. Furthermore the CO_2 price per tonne, P_{CO_2}, is assumed to be €50, which is the OCAP reference price for CO_2 in The Netherlands [74]. OCAP is a Dutch initiative which manages a CO_2 transport network delivering CO_2 to the Dutch greenhouse sector. Using the information provided above, the total electricity and carbon cost of production can be easily calculated:

$$C_{tot} = \dot{E} \cdot P_e + s\frac{M_{CO_2}}{M_p} \cdot P_{CO_2} \tag{3.2}$$

Table 3.1: Product Comparison

Product	CE[%]	U_{red}[V]	U_{ox}[V]	M_p	Market Price [€/t]	n [−]
Oxalic Acid	65%	-1.6	-0.81	90	500 [57]	2
Formic Acid	95%	-1.7	-0.81	46	600 [60]	2
Carbon Monoxide	65%	-1.6	-0.81	28	850 [62]	2
Formaldehyde	70%	-1.7	-0.81	30	300 [64]	4
Methanol	50%	-0.8	-0.81	32	350 [70]	6
Methane	50%	-1.6	-0.81	16	150 [72]	8

where s is the number of moles CO_2 necessary for each mole of product (NB: s=1 for all products except oxalic acid with s=2). The cost per tonne (C_{tot}) and the approximate market price for each product is plotted in Figure 3.1.

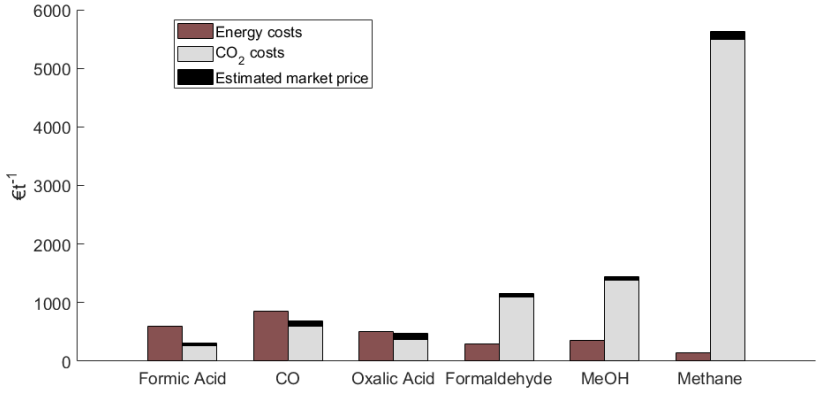

Figure 3.1: Cost and market price for various ERC products

Although the calculation of the total cost involved several simplifications, and the assumed market prices may vary significantly with source and package size, Figure 3.1 still offers some clear insights with respect to product comparison. Most evident is the rapid increase of specific energy costs with an increasing number of electrons per reaction. The costs of production for the 2-electron products formic acid, carbon monoxide and oxalic acid are all lower than the current market price, and might therefore be commercially viable. As calculated, the potential for formic acid is largest with approximately €290 per tonne, followed by carbon monoxide (€170 per tonne) and oxalic acid (€25 per tonne). The production costs for formaldehyde (4 electrons), methanol (6 electrons) and methane (8 electrons) however, greatly exceed the market price and are therefore financially unattractive.

3.1.3. Energy Storage

Renewable energy sources are often characterized by a highly intermittent energy production, regularly causing a dis-balance between supply and demand. Storage of electrical energy during periods of overproduction might offer a solution for this problem. However, long term storage of electrical energy in batteries might be problematic as batteries typically lose 1-5% of their energy content per hour [75] by self discharge. The usage of ERC for the storage of electrical energy from renewable sources (e.g. solar, wind) into chemicals is commonly studied [75][76][77]. In periods of high demand and low supply these chemicals can be converted back into electrical energy, effectively balancing the energy load. All together, such a system will possibly allow for a larger penetration of renewable energy into the energy balance.

One way to compare the energy storage capabilities of the products is by comparing the heat of combustion, which is the total energy that is released as heat during the reaction with oxygen to produce carbon dioxide and water. The thermodynamic heat of combustion

can be expressed per mole, per mass or per volume and via the molar mass and density they can be calculated interchangeably. In Table 3.2, the approximate heat of combustion of the different products as well as that of hydrogen are reported for standard conditions of 1 atm and 298.15K.

Table 3.2: Heat of combustion of ERC products at standard conditions and volumetric hydrogen density in typical liquid/solid state

Product	**MJkg^{-1}**	**kJmol^{-1}**	**MJL^{-1}**	**g H_2 per dm^3**
Oxalic Acid (s)	2.8	253 [78]	5.3	42 (atmospheric)
Formic Acid (l)	5.5 [79]	254	6.7	53 (atmospheric)
Carbon Monoxide (g)	10.1 [79]	283	0.01	0
Formaldehyde (g)	19.0 [79]	571	0.02	54 (-20℃)
Methanol (l)	22.7 [79]	726	18.0	99 (atmospheric)
Methane (g)	55.5 [79]	891	0.04	106 (-162℃)
Hydrogen (g)	141.6 [79]	286	0.01	71 (700 bar)

From the values reported in Table 3.2 it is clear that from the ERC products, methane has the largest energy content per unit of mass with 55.5 MJkg^{-1}. Furthermore, methane already has a very dominant share in the current energy mix, especially compared to the other ERC products. However, as methane is a gas at standard conditions, the energy density per volume is impractically low. Likewise, carbon monoxide and formaldehyde, with a volumetric heat of combustion of respectively 0.01 MJ per liter and 0.02 MJ per liter. Effective storage of these products would therefore require costly compression or cooling measures. Methanol and formic acid, are liquids at standard conditions and can therefore easily store significant amounts of energy without the need for compression and/or cooling. Purified oxalic acid exists in solid form and this may also complicate handling as compared to a liquid [80].

Methanol has a volumetric heat of combustion of 18.0 MJ per liter, compared to 6.7 MJ per liter found for formic acid. Storage of both products comes with several disadvantages and difficulties and needs to be done with great care. However, both products, especially methanol with global market of 100 million ty^{-1}, are already used and stored in large quantify today [61][69]. As methanol stores almost three times more energy per volume than formic acid (18MJL^{-1} and 6.7MJL^{-1}, respectively), from an energy content point of view methanol may be the most promising product.

As seen in Table 3.2, hydrogen has the highest gravimetric energy density with 141.2 MJkg^{-1} and additionally hydrogen can be turned into energy in fuel cells or in a combustion engine with water as only byproduct. Furthermore, as described by Centi et al. [81], various industrial relevant products such as syngas, methanol, methane, formic acid, ammonia and short chain olefins, can be produced from H_2. Therefore, it is suggested that H_2 produced with renewable energy will play a key role in connecting renewable energy and basic chemical production. Furthermore, it will allow for a larger penetration of renewables into the energy mix. A large obstacle for the hydrogen economy however, are the difficulties in cost-effective storage and transport of H_2 [82]. Main problem is the fact that hydrogen is gaseous and effective storage will typically require compression up to 700 bar. Furthermore, liquid hydrogen will have a volumetric hydrogen density of ~71 gl^{-1}, which is actually lower or comparable to that of methanol (~99 gl^{-1}) or formic acid (~53 gl^{-1}), which as explained are liquid at atmospheric conditions and relatively easily stored. Large scale adoption of renewable hydrogen is therefore expected to fail, as long as such issues are not solved. Hydrogen storage in chemicals as formic acid and methanol might therefore offer an interesting route, enabling relatively easy storage and distribution.

Methanol carries a relatively large amount of hydrogen per volume, but conversion from methanol back to H_2 typically requires steam reforming at temperatures higher than 200℃ and a special reforming unit [68]. Research has shown that formic acid, with approximately

half of the volumetric hydrogen density of methanol, can however be decomposed to H_2 and CO_2 on several catalysts near room temperature [83]. One possible advantage of this over methanol, is that hydrogen can be produced from formic acid on site more easily. Although technologically feasible, economics will be determining the success of commercial success [82]. Costs and other important considerations such as catalyst activity, sustainability and lifetime of a catalytic formic acid converter system are not assessed in this research. For future work a detailed assessment is advised.

3.1.4. Industry applications

Besides energy- and hydrogen storage, the products may also be used in industry either directly or as platform molecules for the production of other chemicals. When looking at the current industry size there is a clear distinction between the products. Methane (i.e. natural gas), formaldehyde and methanol currently all have large, mature markets and are produced in quantities higher than 50 million tonnes per year. Formic acid and oxalic acid currently have much smaller markets with respectively $0.8 \mathrm{Mty}^{-1}$ and $0.45 \mathrm{Mt} y^{-1}$. The large market size for methane, formaldehyde and methanol might suggest that there are many applications for these products or that there is a large demand from dominant sectors. A smaller current market however, might allow for more future growth, but as demand is lower this may also lead to a surplus of production. The actual effects of current market size with respect to the commercial production of value-added products via ERC are much more complicated however, and would require additional research.

As explained in Section 1.3, research has shown that CO and HCOOH can be produced with high selectivity via ERC. Despite having smaller global markets than methane, methanol or formaldehyde, both molecules can be used as platform molecules for industry. Carbon monoxide is used to make syngas which can be utilized to synthesis other chemicals as synthetic natural gas, ammonia or methanol and formic acid can be seen as a feedstock compound from which important other chemicals can be made.

3.1.5. Toxicity and manageability

The toxicity and manageability of the various products, may also effect the choice of product. All ERC products should be handled with care and great caution, as they are all hazardous to a certain degree with respect to aspects as flammability, toxicity and environmental pollution. In concentrated form, all products are known to be toxic. In Table 3.3, the NFPA-704 ratings with respect to the flammability, health and instability/reactivity of the different products are listed. NFPA-704 is a standard maintained by the National Fire Protection Association of the U.S [84]. It rates the products on a scale from 0 (not hazardous) to 4 (most hazardous).

Table 3.3: NFPA ratings of the different ERC products [8]

Product	Flammability	Health	Instability
Oxalic Acid (s)	1	3	0
Formic Acid (l)	2	3	0
Carbon Monoxide (g)	4	3	0
Formaldehyde (g)	2	3	0
Methanol (l)	3	1	0
Methane (g)	4	2	0

Up to a certain degree, all products pose a threat will respect both flammability and health concerns. Carbon monoxide, methane and methanol are found to be most hazardous with respect to flammability. From a health perspective, oxalic acid, formic acid, carbon monoxide, and formaldehyde pose the biggest risk. From a manageability perspective, the fact that formic acid and methanol are liquid at atmospheric conditions is a big plus. Storage of these products does not require extreme pressures or temperatures which reduces cost and risk.

3.1.6. Conclusion

After comparing the ERC products with respect to the criteria discussed above, several conclusions can be drawn. It has been shown that the energy consumption for the 2-electron addition products oxalic acid, formic acid and carbon monoxide is much lower compared to the 4-, 6- and 8-electron addition products. At current market prices, only the 2-electron addition products seem to allow for a profitable business case. Formic acid is found to be most profitable looking at energy costs. The energy and hydrogen storage capabilities of the products were also compared. Formic acid and methanol are liquid at atmospheric conditions, which is a large advantage as they can store relatively large amounts of energy per unit of volume without the need of additional compression or cooling. It will also allow for more easy transportation. As hydrogen carrier, formic acid has the advantage that it can be decomposed to H_2 and CO_2 near room temperature. In additional to methanol and despite having smaller markets, the most commonly reported products of ERC, namely formic acid and carbon monoxide, may also serve as platform molecules for industry.

Compared to the other ERC products, formic acid a promising, with some large advantages. Formic acid can be produced cost effectively due to the low energy requirements. ERC to formic acid is also actively studies, and high selectivities are commonly reported. It can be effectively used to store energy and act as hydrogen carrier, while being in the liquid state at atmospheric conditions.

3.2. Process Overview for Formic Acid

In this chapter the electrochemical production of formic acid via the reduction of CO_2 has been identified as having several advantages over other possible products of ERC, especially with respect to production costs, energy storage, manageability and as platform molecule for industry. A possible process configuration with respect to these findings can give an inside in how the entire system may function, and has been visualized in Figure 3.2. Summarized, the general workings of the proposed process are as follows.

The electrical energy needed for ERC is preferably produced by renewable energy sources such as photovoltaics, wind turbines and hydro-power. The electricity is supplied to the grid manager (i.e. distribution network operator), who monitors the demand and supply of electricity. In periods of overproduction of renewable electricity, and after rectification of the current, part of the electricity is used for ERC. In addition, part of the electricity may be used in the process of carbon capture, either at large point sources such as power plants, cement production plants, steel works and refineries, or for direct CO_2 capture from the air. If necessary, the gaseous CO_2 is subsequently pressurized and fed into an continuous electrochemical cell, containing an aqueous electrolyte. The CO_2 is dissolved into H_2O, activated, and selectively reduced into formic acid/formate. The product needs to be separated and purified to industrial purities between 85-99% [59]. After product separation and purification of the formic acid (which is not studied in this research), formic acid may be transported and stored long term at atmospheric conditions.

The diverse usability of formic acid offers several possibilities for further use. First of all, formic acid can be used to produce electricity again via a direct-formic acid fuel cell or via a fuel cell after reforming into hydrogen under the influence of a catalyst. The electricity can be used, after inversion, by the grid manager to balance the supply and demand during a period of low renewable production using renewable based electricity. In addition to grid management, formic acid can be valuable as a platform molecule for industry, from which a diverse range of chemical and material derivatives are possible. Furthermore, formic acid can be used in today's main industries: farming, the treatment of leather and rubber production.

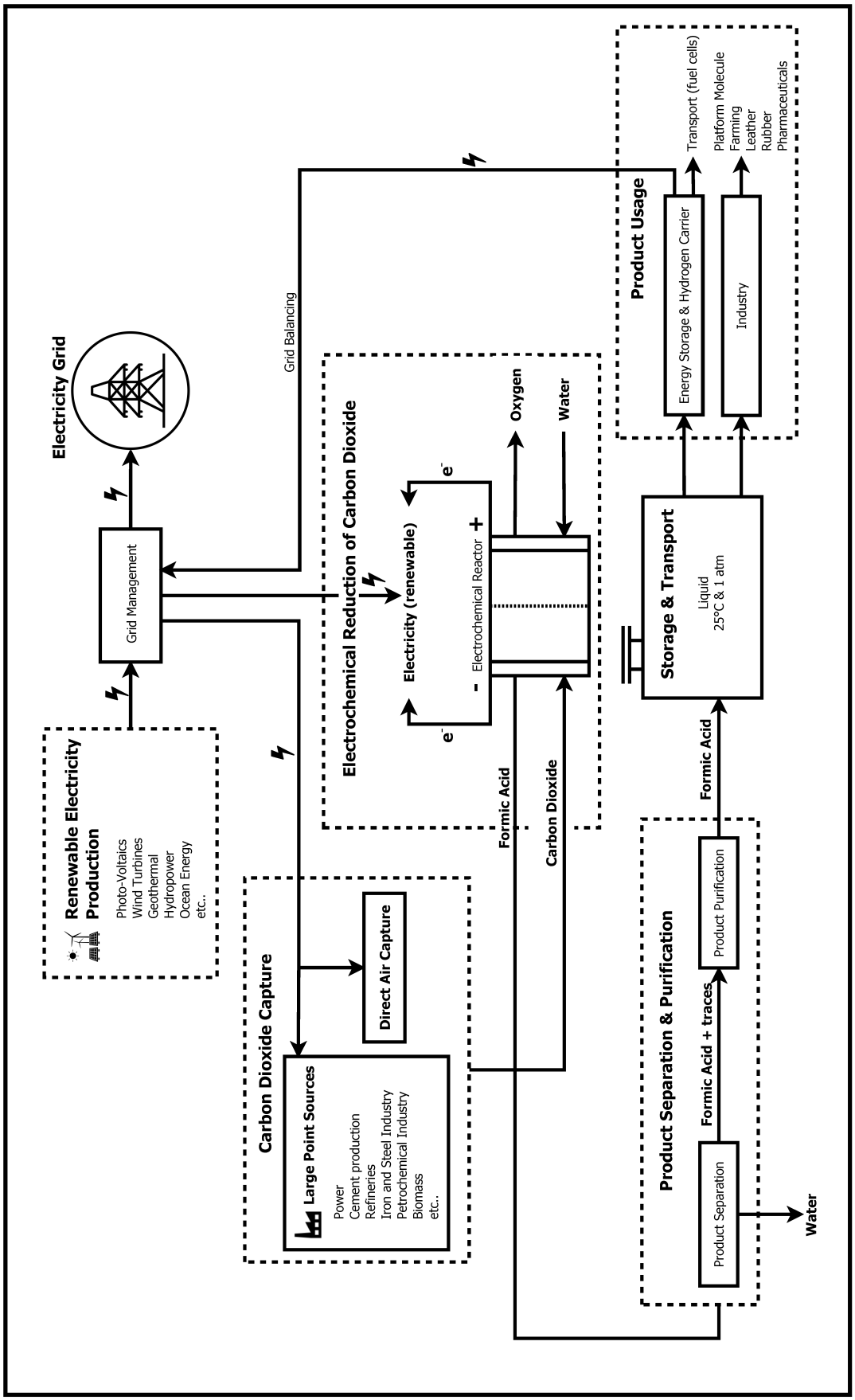

Figure 3.2: Flowchart of a proposed ERC process for selective production of formic acid

4

Thermodynamics

Introduction

As already mentioned in Chapter 1, electrochemical cells can be categorized into two groups based on the spontaneity of the involved redox reaction. If a cell is driven by a spontaneous redox, such as a battery, it is called a galvanic cell and when a cell relies on a non-spontaneous redox, such as with electrolysis or electroplating, it is classified as an electrolytic cell. Whether or not a specific redox reaction will be spontaneous or not and to what degree is determined by thermodynamic principles and may vary with factors as temperature, pressure, pH level and concentrations. Thermodynamic calculations, within the scope of this research, offer a theoretical insight in the cell behavior at equilibrium conditions. Despite the fact that experiments often show different results than theoretically expected, thermodynamics offers a good reference and starting point. This chapter gives a brief summary of the thermodynamic principles used for this research.

4.1. Electrode Potential

An essential principle in the understanding of redox reactions and therefore electrochemical cells is the electrode potential. In a cell there are generally two main electrodes, namely the cathode and the anode, and depending on the reaction of interest, one is referred to as the working electrode and the other as the counter electrode. At the working electrode the reaction of interest occurs. Within the study on the electrochemical reduction of CO_2 this is the cathode, as the cathode surface is the place where the reduction occurs. Throughout this research focus will be on the cathodic half cell, assuming that the anodic reactions will be non-limiting and merely supportive of the cathode half-reactions. Experimentally, this can be done by making the surface area of the counter electrode much larger than that of the working electrode.

Between the cathode and the anode, depending on the half-reactions, a electric potential difference will arise. This potential difference is referred to as the cell potential and is a measure of the spontaneity of a redox reaction. A positive cell potential indicates a spontaneous reaction, whereas a negative cell potential is a sign of a non-spontaneous reaction. The cell potential is the difference between the cathode's reduction potential and the anode's oxidation potential, which can be calculated thermodynamically and are widely tabulated for standard conditions. Standard potentials are listed for separate half-reactions and are given versus a reference electrode, which will be the Standard Hydrogen Electrode (SHE), for this research. As explained, the total cell potential of a redox reaction can be calculated by combining the reduction potentials for the two half-reactions.

Looking at the reactions relevant within the scope of CO_2 reduction it is seen that most redox reactions have a negative cell potential and will therefore not occur spontaneously. Normally, electrochemical reactions will not happen at the theoretical value calculated via thermodynamics and, for electrolytic cells, the cathode's potential will need to be more negative and thus will require more energy than thermodynamics predicts. Overpotential is preferably minimized as it directly relates to the losses of the system, and the energy associated with the overpotential is normally dissipated as heat, eventually. Methods to reduce the

overpotential may include the use of a good electrocatalyst, improved mass transport, and cell design. There are three main types of overpotential: activation overpotential, concentration overpotential and resistive overpotential.

Activation overpotential, η_{act}, is the part of the potential difference between the equilibrium potential and the actual potential which is caused by the activation energy to drive the redox reaction. With respect to ERC, it is suggested that this type of overpotential is present primarily due to the formation of the radical anion $CO_2^{\cdot-}$ as intermediate in the mechanism of CO_2 reduction. The activation overpotential may be lowered by the use of electrocatalyst, which can lower the activation energy as is schematically shown in Figure 4.1.

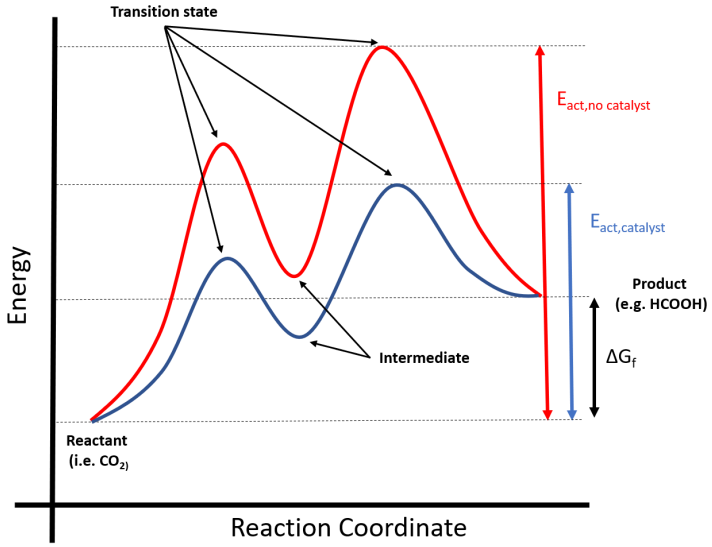

Figure 4.1: Schematic potential energy diagram for the reduction of CO_2 via transient intermediate $CO_2^{\cdot-}$

Concentration overpotential, η_{conc}, is caused by mass transfer limitations and for ERC it becomes predominant when the CO_2 concentration at the surface becomes smaller than the CO_2 concentration in the bulk (i.e. mixed and mass transfer control). It is therefore expected that losses due to concentration overpotential become larger for increasing current densities.

Resistive overpotential or Ohmic drop, iR (=V), is caused by the electrical resistance of a cell which causes a potential drop between the working electrode and the reference electrode. It is typically influenced by the electrolyte conductivity, the magnitude of the current and the distance between the electrodes. Cell design may therefore help in lowering the ohmic drop.

The total overpotential, η, is the sum of all overpotentials:

$$E - E_0 = \eta = \eta_{act} + \eta_{conc} + iR \tag{4.1}$$

with E the applied potential [V], E_0 the thermodynamically theoretical voltage [V] and R the resistance of the system [Ω].

4.1.1. Gibbs free energy and potential

The Gibbs free energy is the thermodynamic energy which described the maximum reversible work that a system can perform at a given temperature and pressure. The change in Gibbs free energy, ΔG_f, equals the work done when a reaction or system moves from its initial state to its final state. The change in Gibbs free energy at standard conditions for a given electrochemical reaction, can be calculated via Equation (4.2) if the standard Gibbs free energies of formation for the components involved are known. For each compound this is the

change of Gibbs free energy which accompanies its formation.

$$\Delta G^o = \sum \Delta G^o_{f,products} - \sum \Delta G^o_{f,reactants} \tag{4.2}$$

with ΔG^o being Gibbs free energy change per mole of reaction at standard conditions [$kJmole^{-1}$].

As already briefly explained in Section 1.1, the change in Gibbs free energy can be related to the standard potential as they both relate to the maximum work done by an electrochemical system. For an electrochemical reaction, depending on the reaction and source, either one of them may be measured and reported in literature. For further reading on this matter and in particular on the relation between the Gibbs Free energy and the electrochemical reduction potential, "Electrochemical science and technology: fundamentals and applications" (chapters 1-6) by Oldham et al. [85] is recommended.

An equation that connects ΔG_f and the reduction potential is the Nernst equation. This equation relates the reduction potential to the concentration of the involved species as shown in Equation (4.5), and allows you to calculate the reduction potential for a specific reaction at non-standard conditions. For a given reaction:

$$aA + bB \rightleftharpoons cC + dD \tag{4.3}$$

with reaction quotient:

$$Q = \frac{[A]^a[B]^b}{[C]^c[D]^d} \tag{4.4}$$

the Nernst equation reads:

$$E = E_0 - \frac{RT}{nF} \ln Q \tag{4.5}$$

Here E is the actual reduction potential, E_0 the reduction potential at standard conditions including concentrations of 1M and R,T,n and F have their usual meaning. At 298.15K and after a conversion of the natural log to base-10 log, this equation can be rewritten to:

$$E = E_0 - \frac{0.059}{n} \log_{10}(Q) \tag{4.6}$$

When in equilibrium, the reaction quotient Q is equal to the equilibrium constant K. Therefore, for a equilibrium the Nernst equation may also be written as [86]:

$$E = E_0 - \frac{RT}{nF} \ln K \tag{4.7}$$

4.1.2. Standard reduction potentials and pH

The standard reduction potentials for many common reactions, are reported in literature. With respect to the electrochemical reduction of CO_2, the potentials (vs. SHE) for the 2-, 4-, 6- and 8 electron reduction products at standard conditions have been listed in Table 1.1. These potentials are calculated at standard conditions, including an hydrogen ion concentration of 1M (i.e. 0 pH). Most research concerning the reduction of CO_2 is done at more neutral pH levels between 6 and 10. At lower pH values, hydrogen evolution becomes very dominant, and at higher pH values CO_2 barely exists, as equilibria are shifted towards HCO_3^- and CO_3^{3-}. H_2O is taken to be the proton donor in this pH range [7][87][88] and formate instead of formic acid is produced in the cell. Formate and CO are assumed to be the main reaction products of CO_2 reduction on most electrocatalytic metals [1]. H_2O can also be reduced, producing H_2, in an Hydrogen Evolution Reaction (HER). In order to maximize the efficiency of the process, generally the selectivity of the desired product should be maximized. Within this research, CO and H_2 are referred to as byproducts. The dominant overall reactions, assuming that H_2O is the proton donor, then become:

$$CO_2(aq) + H_2O + 2\,e^- \rightleftharpoons HCOO^-(aq) + OH^-$$
$$CO_2(aq) + H_2O + 2\,e^- \rightleftharpoons CO(g) + 2\,OH^-$$
$$H_2O + 2\,e^- \rightleftharpoons H_2(g) + 2\,OH^-$$

In Table 4.1, the corresponding standard potentials are given for pH 0 and more conveniently for pH 7 (vs. SHE) [87][20]. Part of the information is already given in Table 1.1, and listed here for convenience.

Table 4.1: Standard Electrode Potentials (vs. SHE) at pH=0.0 and pH=7.0

Reaction:	**E^0 at pH 0**: [V]	**E^0 at pH 7**: [V]
$CO_2(aq) + H_2O + 2\,e^- \rightleftharpoons HCOO^-(aq) + OH^-$	-1.08	-0.43
$CO_2(aq) + H_2O + 2\,e^- \rightleftharpoons CO(g) + 2\,OH^-$	-0.93	-0.53
$H_2O + 2\,e^- \rightleftharpoons H_2 + 2\,OH^-$	-0.83	-0.41

From Equation (4.6) it can be concluded that with varying pH, the reaction quotient of the half-reactions change and therefore also the actual reduction potential. This change of reduction potential with pH can be plotted on a pH-E plot, also known as a Pourbaix diagram.

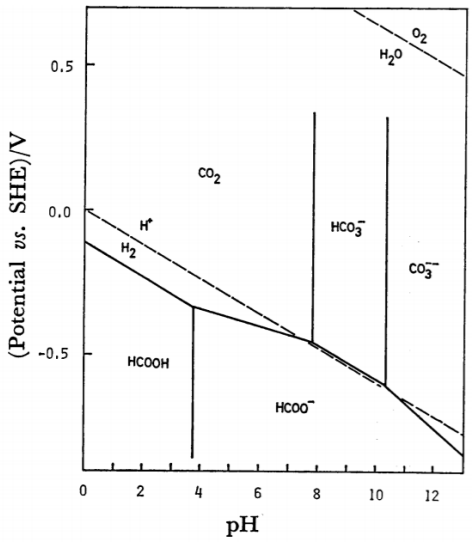

Figure 4.2: Pourbaix diagram with for ERC to formic acid/formate in an aqueous system (from Sullivan et al. [4])

In Figure 4.2, the Pourbaix diagram for ERC to formic acid/formate in an aqueous system is plotted. It shows the reduction potentials toward $HCOOH/HCOO^-$ and H_2 for varying pH. Depending on the number of electrons (n) and H^+ (m) (or OH^-) involved, the slope varies according to Equation 4.6. For n=2 and and m=1 the slope is $-\frac{1}{2}\cdot 0.059$ mV pH^-, for n=2 and and m=2 the slope is $-1\cdot 0.059$ mV pH^{-1} and for for n=2 and and m=3 the slope is $-\frac{3}{2}\cdot 0.059$ $mVpH^{-1}$.

Table 4.2: Dissociation constants and pKa values related to the electrochemical reduction of CO_2

Acid/base reaction:	**K_a**:	**pK_a**:
$CO_2{}^* + H_2O \rightleftharpoons H^+ + HCO_3{}^-$	4.5×10^{-7}	6.35
$HCO_3{}^- + H_2O \rightleftharpoons H^+ + CO_3{}^{2-}$	4.7×10^{-11}	10.33
$HCOOH \rightleftharpoons H^+ + HCOO^-$	1.8×10^{-4}	3.75

The diagram also shows the dominant species for each region based on equilibrium constants, pK_a's, which are listed in Table 4.2. Equilibrium reactions concerning CO_2 in aqueous systems are discussed in Chapter 2, and for further reading on the Pourbaix diagram regarding CO_2 reduction, "Electrochemical and Electrocatalytic Reactions of Carbon Dioxide" by Sullivan et al. [4] is recommended. Furthermore, in contrary to the assumption made for this research that CO_2 is the only active species (as explained later in Section 7.1, Model

Assumptions), the diagram shows theoretical reduction potentials of other carbon species available in the electrolyte, namely HCO_3^- and CO_3^{2-}, for the region where they become dominant.

To simplify the development of the model at this stage, the assumption is made that the standard reduction potentials towards $HCOO^-$, CO and H_2 are constant at a pH of 7. During ERC however, due to the involvement of H^+ and OH^- in reactions at the electrode surface, the pH at the electrode surface (where the reduction reaction occur) may be different from the bulk pH, and not constant for varying applied potential, current and or electrolyte concentration. The assumption will lead to a maximum theoretical deviation of approximately 120mV between the actual potential and assumed potential for formate within the studied range from pH 6 to pH 11. Compared to the E^0 for $HCOO^-$ at pH 7 of -0.43V, this is a 28% deviation of the standard reduction potential. This may lead to significant changes in the output and further research on the addition of the reduction potential dependency on the electrode surface pH to the model is recommended.

5

Mass Transport Phenomena

Introduction

The complete reduction process in the electrochemical (half)cell, consisting of electrode and electrolyte solution, will be divided into of a series of three elementary steps [20] and discussed accordingly. Each has the ability to limit the rate of the reduction process, and it is therefore important to carefully assess these, in order to identify the rate determining step (RDS). The three steps are:

1. Supply of Reactants: Mass transport (or supply) of reactants species from the bulk to the electrode surface
2. Electrochemical: The electrochemical reactions at the electrode via electron transfer across the electrode surface
3. Removal of Products: Mass transport (or removal) of product species away from the electrode surface into the bulk

Both the supply of reactants from the bulk onto the electrode and the removal of products from the electrode surface into the bulk, as mentioned above, are related to mass transport phenomena. Within an electrochemical cell, three main transport phenomena can be identified for ions and species in solution, namely diffusion, migration and convection. These topics are extensively covered in the book "Modern analytical chemistry" by Harvey [89] and the essentials will be reviewed here.

5.1. Diffusion

Diffusion is a mass transport phenomenon which describes the movement of particles (e.g. atoms, molecules and ions) from a region of high concentration to a region of low concentration. Due to the statistics of these movements, diffusion will cause a net mass transfer in favor of a more uniform concentration, and thus movement of particles down a concentration gradient.

Fick's second law of diffusion predicts how diffusion causes the concentration to change with time. The law is expressed as a PDE, which in 1 dimension describes linear diffusion normal to the cathode. With simultaneously occurring reactions between the involved chemical species (as explained in Section 2.0.1) which directly effect the concentration of the species, Fick's second law can be extended and written as:

$$\frac{\partial C_i}{\partial t} = D_i \frac{\partial^2 C_i}{\partial x^2} + V_i(x,t) \tag{5.1}$$

with:

- C_i: concentration of species i [M]
- D_i: diffusion coefficient for species i at 25℃[$\frac{m^2}{s}$]
- V_i: net rate of formation of species i (due to chemical reactions) [$\frac{M}{s}$]
- i: species (CO_2, HCO_3^-, CO_3^{2-} and OH^-, respectively)

In an electrochemical cell, concentration gradients occur in the region next to the electrode due to species which are consumed and formed at the electrode surface. Due to these gradients a small layer is formed between the bulk and the electrode in which diffusion occurs. This layer is called the diffusion layer and is defined by the IUPAC as the "region in the vicinity of an electrode where the concentrations are different from their value in the bulk solution". Via this layer reactants are supplied from the bulk onto the electrode and removed vice versa. It is assumed that in the diffusion layer other mass transport phenomena are negligible, and diffusion may only occur in combination with additional chemical reactions.

When dissolving CO_2 in water or an aqueous electrolyte, a variety of species are involved. For this research aqueous potassium bicarbonate ($KHCO_3$) is chosen as electrolyte solution, as it has proven to be successful in supporting the reaction towards formate under both atmospheric conditions and at elevated CO_2 pressures [1][16][31]. The species involved in a system of CO_2 dissolution in an aqueous $KHCO_3$ electrolyte solution are: CO_2(aq), HCO_3^-, CO_3^{2-} and OH^- (or H^+ for an acidic system). The relevant forward- and reverse reaction rates and equilibrium constants for the dissolution of CO_2 in water at 25℃ are summarized in Table 2.1.

The diffusion coefficients D_i, as seen in Equation (5.1) are a measure of how fast a pair of species diffuse into each other. Values for the diffusion coefficients, D_{CO_2}, $D_{HCO_3^-}$, $D_{CO_3^{2-}}$, D_{OH^-} and the product formate D_{HCOO^-} at 25℃ at infinite dilution in water or electrolyte solutions are reported in various sources such as the 'Handbook of Chemistry and Physics' by Haynes [90] (used by Gupta et al. [27]) and 'Electrochemical Systems' by Newman and Thomas-Alyea [91] (used by Delacourt et al. [29]). Gupta et al. [27] preformed a correction on the diffusion coefficients for the changing viscosity of the electrolyte solution with changing concentration. The effect of viscosity on the diffusion coefficients was investigated and it was found to small too significantly change and improve the model reliability at this stage of development. As the values vary slightly among the different sources, and the actual values for the specific cell design are hard to determine, rounded values are taken initially (see Table 5.1). In Chapter 8, the sensitivity of the model with respect to the diffusion coefficients will be analyzed.

Table 5.1: Diffusion coefficients at 298.15K at infinite dilution in water [m^2s^{-1}]

D_{CO_2}	$D_{HCO_3^-}$	$D_{CO_3^{2-}}$	D_{OH^-}	D_{HCOO^-}
2.0×10^{-9}	9.2×10^{-10}	1.2×10^{-9}	5.3×10^{-9}	1.5×10^{-9}

5.2. Thickness of the Diffusion Layer

In the scope of this research, the thickness will be estimated using experimental data provided by Todoroki et al. [1] on the limiting current density towards formate for a given CO_2 pressure. The thickness of the diffusion layer (δ), is an important parameter as it determines over which length species have to diffuse. The rate of supply of CO_2 from the bulk towards the electrode surface is therefore largely dependent on this thickness. It is however very hard to measure the actual thickness of the layer, partly because it very much depends on cell conditions, and it can be chosen arbitrarily as the concentrations approach the bulk concentration asymptotically. Therefore, the determination of the precise thickness is outside the scope of this work.

The estimation of the diffusion layer thickness, can be done as follows. For the extreme case where the CO_2 surface concentration becomes zero, the availability of CO_2 at the surface is fully limited by the flux of CO_2. In this situation the limiting current density for ERC, i_{lim,CO_2}, can be expressed roughly as [29]:

$$i_{lim,CO_2} = \frac{FD_{CO_2}(C_{bulk}^{CO_2} - \cancelto{0}{C_{surface}^{CO_2}})}{\delta} = \frac{FD_{CO_2}C_{bulk}^{CO_2}}{\delta} \tag{5.2}$$

If it is assumed that the current densities to CO and other products of ERC beside formate are negligible, $i_{lim,HCOO^-}$ is equal to i_{lim,CO_2} and it is possible to estimate δ using the experimentally measured limiting current density to $HCOO^-$ and the bulk concentration of CO_2 for a given pressure. Based on this estimation the diffusion layer thickness is 0.05mm for the scope of this research.

5.3. Convection

Convection, with respect to an electrochemical cell, is the bulk movement of solution species caused by an applied mechanical force, for example by stirring or flow through the cell. Convection can be divided into two main types, natural convection and forced convection. When forced convection is present it normally dominates the other mass transfer phenomena, but electrochemical experiments are possible in the absence of forced convection. This can be done, for example, by using unstirred conditions in the cell. When forced convection is absent, natural convection can arise due to density differences in the solution originating from the reactions at the electrodes as explained more extensively by Novev and Compton [92]. They explain that, despite these phenomena, mass transport by natural convection is normally assumed negligible. For laminar flows, the effect of convection in time for 1D can be mathematically expressed as:

$$\frac{\partial C_i}{\partial t} = -v_x \frac{\partial C_i}{\partial x} \tag{5.3}$$

with:
C_i: concentration of species i [M]
v_x: velocity of the solution [m^s-1]

In this work, convection as a mass transfer phenomenon is assumed non-present. This assumption can be justified experimentally as explained above, and will allow for a more simplified initial model in which the transfer of species via diffusion will be analyzed more elaborately.

5.4. Migration of Charged Particles

In response to the local electric field (i.e. a potential gradient), charged particles tend to move in a specific direction as they are, either attracted or repelled to the charged interface (i.e. electrode). Migration is the mechanism by which charge passes through the electrolyte. Mathematically the migratory flux can be expressed in 1D as:

$$\frac{\partial C_i}{\partial t} = -z_i u_i \frac{\partial^2 \theta_i}{\partial x^2} \tag{5.4}$$

with:
C_i: concentration of species i [M]
u_i: electrochemical mobility of an ion i [$m^2 s^{-1} V^{-1}$]
z_i: charge number of the ion i [-]
θ_i: electrostatic potential of ion i [V]

Using the Nernst-Einstein relation the electrochemical mobility can be related to the diffusivity of a species [93]:

$$u_i = \frac{e_0 D_i}{k_B T} = D_i \frac{F}{RT} \tag{5.5}$$

with e_0 being the elementary charge on an electron [C] and k_B is the Boltzmann constant.

Migration is however assumed negligible for the scope of this research, as it is not necessarily an important form of mass transport for the electro-active species [17]. Migration is an electrostatic force, thus the charge is carried without discriminating between ions. If the reaction is carried out in an excess of inert, supporting electrolyte (compared to the electro-active species), the electrolyte will carry most of the charge and the effect of migration on the electro-active species is small [94] [95] [96]. The ratio of supporting electrolyte to bulk

concentration of electro-active species needs to exceeds ~30 to make a electrochemical experiment quantitatively diffusional [97]. If the contribution of the supporting electrolyte to the ionic strength is 97%, the contribution to migration may be lower than 1%, as suggested by Bamford et al. [98]. With increasing CO_2 pressure the ratio of active species against the supporting electrolyte concentration will increase, however. Therefore it should be remembered that this assumption might become less valid with increasing pressure. This effect will be smaller for higher electrolyte concentrations, as the ratio will be larger.

5.5. Nernst-Planck Equation

In the sections above, the three dominant mass transfer phenomena in electrochemical systems are considered. When combined they represent a conservation of mass equation which is used to describe the motion of charged species in a fluid, known as the Nernst-Planck equation. The time-dependent Nernst-Planck equation is shown in equation (5.6).

$$\frac{\partial c}{\partial t} = \nabla \bullet \Big(\underbrace{D\nabla c}_{\text{diffusion}} - \underbrace{uc}_{\text{convection}} + \underbrace{D\frac{Dz\epsilon}{k_b T}c(\nabla\phi)}_{\text{migration}} \Big) \tag{5.6}$$

As explained, convective and migrative terms are neglected and therefore the Nernst-Planck equation reduces to Fick's law of diffusion with reaction-diffusion terms as shown in Equation (5.1).

6

Kinetics of Electrochemistry

Introduction

The field of electrochemical kinetics is the study concerning the rates of electrochemical processes. These processes occur at the electrode surface, or in other words the interface between the electrode and the electrolyte. The electrochemical kinetics are influenced by both the reactor design (e.g. electrolyte type, electrocatalyst, size) and operating condition (e.g. temperature, pressure, electrolyte concentration). In this chapter the aspects of electrochemical kinetics which are important for the mathematical model described in Chapter 7, are discussed.

6.1. Electrocatalyst

The selectively towards different products is dependent on different factors such as temperature, pressure and applied voltage. The material of the cathode, the electrocatalyst, is upon the most important in determining product selectivity in CO_2 reduction in aqueous systems.

The electrode surface, is the site at which the actual electrochemical reactions occur, which often consists of various consecutive reaction steps. The electrocatalyst may catalyze the reduction process towards a specific product with high Faradaic efficiencies. For example the strength of adsorption of involved species highly affect the product selectivity, as it determines which reactions may or may not occur. The selection of the appropriate electrode material should therefore be considered carefully in order to optimize the effective production of the desired product.

Azuma et al. [5] investigated the effect of several different metals on ERC in an aqueous solution, supported by $KHCO_3$ as the electrolyte and hey visualized their finding in the periodic table in which they labeled the main CO_2 reduction products per metal type. The electrocatalysts are broadly categorized in 4 groups: CO producing metals, $HCOO^-$/HCOOH producing metals, metals producing higher carbon species and metals on which mainly water is reduced into H_2. In Figure 6.1, a similar representation of the different electrocatalysts is shown.

Ignoring the metals that do not selectively reduce CO_2 (grey), there are broadly speaking two main groups of practical electrode metals based on their product selectivity [5][87]: (1)Pb, Sn, In, Hg, Cd and Tl primarily yield $HCOO^-$/HCOOH as major product and (2)Au, Ag, Cu, Zn, Pd and Ga form mainly CO. Cu, Ru and Ir may also produce higher carbon species such as CH_4 and C_2H_4 or even alcohols, but research suggests that on these metals CO is formed initially, after which it may be further reduced into more complex molecules [99].

In this work, the focus will be on the formic acid/formate formation metals. For large-scale production of formic acid, tin (Sn) has been suggested as practical electrocatalyst based on existing research results as well as cost and toxicity. Experimental data however, especially under high CO_2 pressure, is scarce and therefore for the mathematical model, indium (In) and lead (Pb) will be used as electrocatalyst, as Todoroki et al. [1] conducted extensive research on ERC at elevated CO_2 pressured using these metals as electrocatalyst.

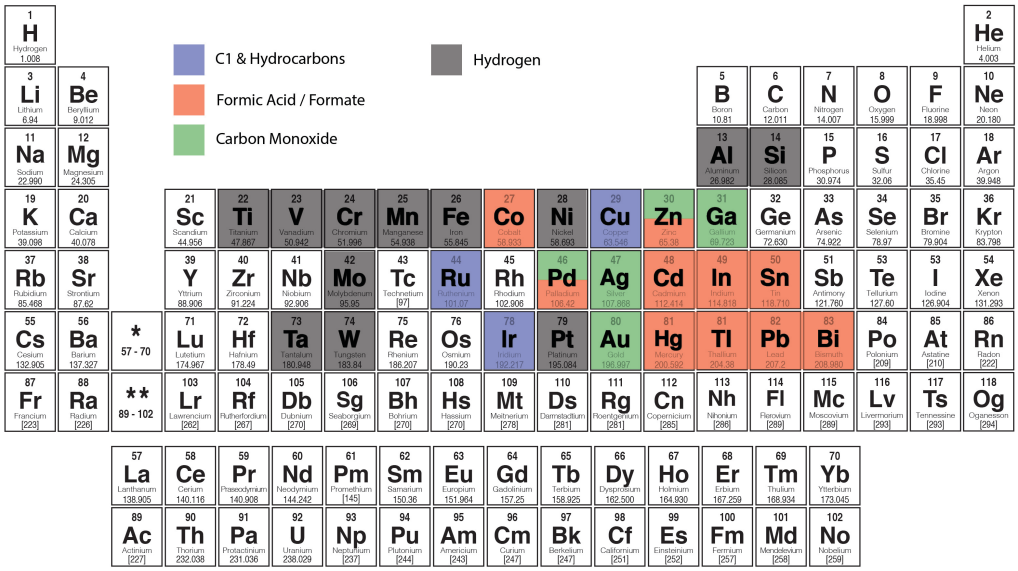

Figure 6.1: Metals shaded based on their predominant selectivity for a particular product of CO_2 reduction products either in pure form or as oxide in aqueous solutions (based on: Azuma et al. [5] & Rakowski Dubois [6])

6.2. Reaction Mechanism

In this section the reaction mechanism for the ERC will be briefly discribed. The mechanisms is vastly researched, but still heavily debating among researchers. The reaction mechanisms towards $HCOO^-$ and CO may be both initiated by the formation of the radical anion $CO_2^{\bullet-}$. The standard potential of $CO_2^{\bullet-}$ formation is much higher than the standard reduction potential of both $HCOO^-$ and CO, which may partly explain the high overpotential necessary for successful reduction. Depending on the electrode metal, the radical anion may be strongly adsorbed on the electrode producing CO (and possibly further reaction products) or primarily weakly adsorbed on the electrode (or even not adsorbed at all) producing $HCOO^-$ [99] [7]. In this sudy, the focus is on formate producing metals. Based on previous work by Todoroki et al. [1] and Hara et al. [16], it is assumed that the production of any other products beside $HCOO^-$, CO and H_2 is negligible and that therefore $HCOO^-$, CO and H_2 are the only reduction products. This assumption is valid for all formate producing metals, as well as most metals with an affinity for CO formation (excluding copper).

As researchers have proposed different plausible mechanistic pathways for ERC, one of the most commonly proposed pathways is chosen and assumed to be valid for the scope of this work.

The pathway towards both formate and CO may be initialized by the binding of the CO_2 to the electrode surface in a first electrochemical step. Feaster et al. suggested that on $HCOO^-$ forming metals CO_2 may bind via the oxygens atoms resulting in the adsorption intermediate $^*OCHO$ and that on CO forming metals CO_2 binds via the carbon atom forming the adsorption intermediate $^*COOH$. They found that this distinction may be explained by differences in binding energy for both intermediate species and that this therefore may explain the difference in the preference of metals to selectively form $HCOO_2$, CO or H_2. Summarized the reaction pathways to $HCOO^-$ and CO are to be as follows:

$$\begin{aligned} CO_2(aq) + e^- &\rightleftharpoons CO_2^{\bullet -}(aq/ad) \\ CO_2^{\bullet -}(aq) + H_2O\,(\text{or}\,H^+) &\rightleftharpoons {}^{\bullet}OCHO(aq/ad) + OH^-(aq) \\ {}^{\bullet}OCHO(aq/ad) + e^- &\rightleftharpoons HCOO^-(aq) \\ \hline CO_2(aq) + H_2O + 2\,e^- &\rightleftharpoons HCOO^-(aq) \end{aligned}$$

$$\begin{aligned} CO_2(aq) + e^- &\rightleftharpoons CO_2^{\bullet -}(ad) \\ CO_2^{\bullet -}(ad) + H_2O\,(\text{or}\,H^+) &\rightleftharpoons {}^{\bullet}COOH\,(ad) + OH^-(aq) \\ {}^{\bullet}COOH\,(ad) + e^- &\rightleftharpoons CO\,(g) + OH^-(aq) \\ \hline CO_2(aq) + H_2O + 2\,e^- &\rightleftharpoons CO\,(g) + OH^-(aq) \end{aligned}$$

Schematically, these proposed routes to either $HCOO^-$ and CO may be visualized as shown in respectively Figure 6.2 and 6.3

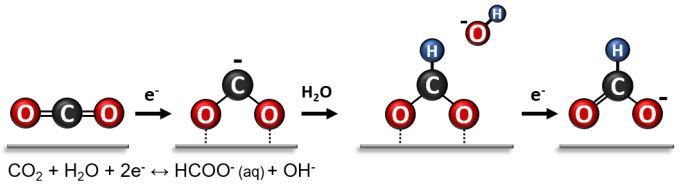

Figure 6.2: Schematic visualization of the assumed mechanistic pathway towards $HCOO^-$ for neutral or alkaline conditions as proposed by Feaster et al. [7] (2017)

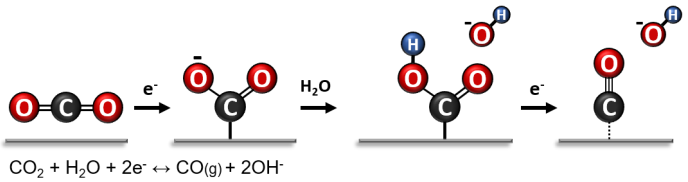

Figure 6.3: Schematic visualization of the assumed mechanistic pathway towards CO for neutral or alkaline conditions as proposed by Feaster et al. [7] (2017)

As the reduction potentials of CO_2 to formate and carbon monoxide are very similar to that of water reduction, water may also be reduced. This process is may follow different consecutive steps [100] as is shown below and visualized in Figure 6.4.

$$\begin{aligned} H_2O + e^- &\rightleftharpoons H^{\cdot}\,(ad) + OH^-\,(aq) \\ H^{\cdot}\,(ad) + H_2O + e^- &\rightleftharpoons H_2\,(g) + OH^-\,(aq) \\ 2\,H^{\cdot}\,(ad) &\rightleftharpoons H_2\,(g) \\ \hline 2\,H_2O + 2\,e^- &\rightleftharpoons H_2(g) + 2\,OH^-(aq) \end{aligned}$$

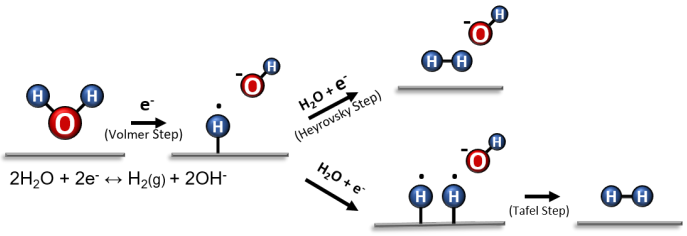

Figure 6.4: Schematic visualization of the assumed mechanistic pathway towards H_2 for neutral or alkaline conditions

6.2.1. Surface Coverage

As explained above, the electrochemical mechanisms towards $HCOO^-$, CO and H_2 all require an initial adsorption step in which the species is bounded to the electrode surface. The extent of adsorption of each species i, can be expressed as the surface coverage, θ_i, with 0 (no coverage) $\leq \theta_i \leq 1$ (full coverage). With a limited electrode surface area it may be important to assess competition of coverage between CO_2 and H^+, especially as the reduction at elevated CO_2 pressures (i.e. CO_2 concentration) is researched. If CO_2 and H_2O compete for the same adsorption sites, a model to describe the competitive adsorption is the competitive Langmuir model [101]. For competing species a and b this model states:

$$\theta_a = \frac{K_a C_a}{1 + K_a C_a + K_b C_b} \tag{6.1}$$

$$\theta_b = \frac{K_b C_b}{1 + K_a C_a + K_b C_b} \tag{6.2}$$

with:

θ_i: Coverage of species i [-]

K_i: The equilibrium constant for species i

C_i: Concentration of species i [M]

It may be hypothesized that as pressures will become larger, all adsorption sites will become occupied (θ_1 = 1), limiting further adsorption of CO_2 with increasing pressure. This might explain the flattening of measured Faradaic efficiency at high pressure (>20 atm) as seen in Figure 1.3. However, this direct relation between coverage and Faradaic efficiency towards $HCOO^-$ may be dismissed and the effect is not important in the scope of this work. Main reason is that the concentration difference between CO_2 and H_2O is very large even at 60 atm (1.34M:55M), which makes it unlikely that the occupation of reaction sites is already maximum even at the modeled extreme of 60 atm. Also the limiting partial current density towards $HCOO^-$ increases near linearly with increasing pressure (i.e CO_2 concentration) from 1 atm to 60 atm [1]. This suggests that mass transfer instead of adsorption of CO_2 is likely to be the limiting step.

6.3. Reaction Rate

On a given electrode, the electrochemical reaction(s) involve a back-and forth reaction between the reduction of a oxidant (O) and the oxidation of a reductant (R):

$$O + ne^- \rightleftharpoons R \tag{6.3}$$

The rate of the forward reduction process is proportional with the cathodic current, i_c and the rate of the reverse oxidation process scales with the anodic current, i_a[1], with the sum of both being the overall current on the electrode. The current is caused by a deviation from the equilibrium potential, the overpotential. Without any mass transfer limitations of CO_2 to the electrode surface, this relation can be described by the Butler-Volmer equation.

6.3.1. Butler-Volmer Equation

The Butler-Volmer equation is one of the fundamental equations in electrochemical kinetics, as it describes the relation between the (partial) electrical current (i.e. production rate) on an electrode and the applied electrode potential. It considers both a cathodic and an anodic reaction occurring at the same electrode. In compact form the equation can be expressed as [17]:

$$i = i_o \exp\left[\frac{\alpha_a n F}{RT}\eta\right] - i_o \exp\left[\frac{-\alpha_c n F}{RT}\eta\right] \tag{6.4}$$

[1] anodic current on the cathode

with:

i: Current density on the electrode [$mAcm^{-2}$]

i_o: Exchange current density [$mAcm^{-2}$]

α_a: Anodic charge transfer coefficient [-]

α_c: Cathodic charge transfer coefficient [-]

η: Overpotential i.e. $E-E_0$ [V]

T: Temperature [K]

F: Faraday's constant (=96485.3) [$Cmol^{-1}$]

n: Number of electrons involved in electrochemical reaction [-]

R: Universal gas constant (=8.3144598) [$Jmol^{-1}K^{-1}$]

The reduction of CO_2 involves large overpotentials, supposedly due to the involvement of the anion radical $CO_2^{\cdot-}$, of which the formation requires a highly negative potential. For $\eta \ll 0$ (i.e. $E \ll E_o$), the anodic term of the Butler-Volmer equation goes to zero quickly and simplifies to the Tafel equation:

$$i_{\eta \ll 0} = \cancelto{0}{i_o \exp\left[\frac{\alpha_a nF}{RT}\eta\right]} - i_o \exp\left[\frac{-\alpha_c nF}{RT}\eta\right] = -i_o \exp\left[\frac{-\alpha_c nF}{RT}\eta\right] \tag{6.5}$$

From the Tafel equation it becomes clear that the current density increases exponentially with an increasing overpotential. Therefore, it is useful to express the current density on a base 10 logarithmic scale:

$$\log_{10}(-i) = \log_{10}(i_o) + \log_{10}\left(\frac{\ln\left(e^{\left[\frac{-\alpha_c nF}{RT}\eta\right]}\right)}{\ln(10)}\right) = \log_{10}(i_o) - \underbrace{\frac{\alpha_c nF}{2.3RT}}_{\text{Tafel slope}}\eta \tag{6.6}$$

The Tafel equation assumes that the reverse reaction, the oxidation of reductant R, is negligible compared to the forward reduction reaction (i.e. $i_a = 0$, so $i = i_c$).

With n, F and R being constants for a given reaction product and for operation at a isotherm of 298.15K, the relation between the partial current density i and the overpotential η according to the Tafel equation is fully determined by the exchange current density i_o and the cathodic charge transfer coefficient α_c.

6.3.2. Exchange current density, I_o

At the equilibrium potential, there will be no observed net current. There will, however, be a dynamic equilibrium at the electrode surface, with an equal rate of reduction and oxidation. As the back- and forth rate are equal, there will be no change of composition of the electrolyte solution or the electrode. The reduction partial current density and the oxidation partial current density are of opposite sign (by convention reduction leads to a negative current) and at the equilibrium potential they can be expressed as:

$$-I_c(E_0) = I_a(E_o) = I_0 \tag{6.7}$$

i_o is known as the exchange current density which can be expressed mathematically as:

$$i_o = -nF\overrightarrow{k_s}(E_0)C_{ox} \tag{6.8}$$

with $\overrightarrow{k_s}(E_0)$ being the rate constant of the reduction at the equilibrium potential and C_{ox} the oxidant concentration on the electrode surface. It is assumed, as is generally found experimentally, that the rate constant k_s is potential dependent as [17]:

$$k_s = k_0 \exp\left[\frac{-\alpha_c nF}{RT}E\right] \tag{6.9}$$

with k_0 being the rate constant at a potential of 0V. Despite these mathematical expressions, which suggests that i_0 can be readily calculated, the exchange current density is normally determined experimentally. The main reason for this is that the exchange current density is highly effected by many variables which may vary significantly per cell and are difficult to measure independently. Some important variables of i_0 include [102]:

- Composition of electrode material - As explained in Section 6.1
- Geometrical surface area - Dependant of the surface roughness of the electrocatalyst. The larger the surface area, the higher the exchange current density.
- Concentration of active species in the electrolyte solution
- Impurities on the electrode surface - If more impurities dissolve on the surface of the electrode, the exchange current density tends to decrease.

For ERC at elevated pressures experimental data is scarce, especially for research with accurately reported E-I data on the type of cell comparable with the one in this research. Therefore, i_0 is taken as is, based on experimental data by Todoroki et al.[1]. Assuming that $k_s(E_0)$ is only temperature dependent for a specific cell design and not dependent on any effects caused by a varying pressure, $k_s(E_0)$ will be determined by fitting on this data at 5 atm on In electrodes (as Todoroki et al. [1] presented the E-I data in their paper best at 5 atm and 40 atm on Indium). i_o has a dependency on the oxidant concentration at the electrode surface, as is seen in Equation 6.8, and therefore i_0 will vary accordingly with varying pressure (i.e. CO_2 surface concentration).

6.3.3. Cathodic charge transfer coefficient, α_c

The physical interpretation of the charge transfer coefficient is the fraction of interfacial potential at an electrode-electrolyte interface that goes to either the reduction reaction (α_c) or the oxidation reaction (α_a). Similar to the exchange current density, the charge transfer coefficient is not readily calculable and is normally determined for a given electrode via experimental analysis. Based on the IUPAC recommendations [103] and on the fact that very limited data on ERC for varying pressures is available, the charge transfer coefficient a_c is assumed pressure independent and similar to the exchange current density fitted on data from Todoroki et al. [1] at 5 atm in indium electrodes, as listed in Table 6.1.

6.3.4. i_o and α_c from experimental data

As the exchange current density and the charge transfer coefficient are highly dependent on the electrode design as explained earlier, they are normally determined via experimental analysis of a specific cell. Todoroki et al. [1] researched the effect of an elevated CO_2 pressure on ERC on electrodes with a high selectivity towards formic acid/formate. This work will be used to determine i_o and α_c, for the scope of this research.

In Figure 6.5 the Tafel plot for the reduction of CO_2 towards $HCOO^-$ at 5 atm on an indium electrode is shown and in Table 6.1 the E-I measurements for $HCOO^-$, CO and H_2 at 5 atm on In electrodes are given. The data from these measurements are used as reference for the modeled cell and for the charge transfer controlled regime, $k_s(E_0)$ (i.e. i_o for a given CO_2 surface concentration) and α_c are fitted on this data. At 298.15K, for $HCOO^-$, CO and H_2 the approximate Tafel slopes of respectively 125 mV dec^{-1}, 235 mV dec^{-1} and 210 mV dec^{-1} are found. For all reactions being 2 electrons processes (n=2), the respective pressure independent charge transfer coefficients $\alpha_{c,HCOO^-}$, $\alpha_{c,CO}$ and α_{c,H_2} are calculated to be: 0.236, 0.126 and 0.140.

Within the charge transfer controlled regime the CO_2 surface concentration is assumed not to be effected by any mass transfer limitations. This implies that the surface concentration is equal to the bulk concentration of CO_2 (aq). At 5 atm, the bulk concentration of CO_2 is calculated to be 0.165 M via the system described is Chapter 2 and as explained more elaborate in Section 7.1.2 on the modeling of the bulk region. Using the slopes found from

Table 6.1: E-I measurements for $HCOO^-$, CO and H_2 at 5 atm (T=298.15K & 0.5M $KHCO_3$) on In electrodes (Data from Todoroki et al. [1])

E [V]	$\mathbf{I}_{HCOO^-}$ [$mAcm^{-2}$]	$\mathbf{I}_{CO}$ [$mAcm^{-2}$]	$\mathbf{I}_{H_2}$ [$mAcm^{-2}$]
-1.15	0.169	0.099	0.175
-1.30	2.975	0.467	0.906
-1.45	42.336	1.889	6.980

the data from Table 6.1, the exchange current densities for $HCOO^-$, CO and H_2 can be calculated via extrapolation. With n, F and the CO_2 concentration at 5 atm known, $k_s(E_0)$ can be calculated via Equation (6.8). As the rate constant k_s is assumed pressure independent [104], the fitted values for $k_s(E_0)$ will remain valid for all pressures levels, and are a property of the electrocatalyst. The results are shown in Table 6.2

Table 6.2: Summary of the fitted Tafel coefficients used for the model

Product:	**Slope: [mV dec^{-1}]**	$\alpha_{c,i}$	$\mathbf{E}_{0,i}$ **at pH 7** [V]	$\mathbf{k}_{s,i}$ at E_0	$\mathbf{i}_{0,i}$ at 5 atm
$HCOO^-$	125	0.236	-0.43	9.38e-12	2.98e-7
CO	235	0.126	-0.53	6.93e-09	2.21e-4
H_2	210	0.140	-0.41	5.00e-12	5.36e-5

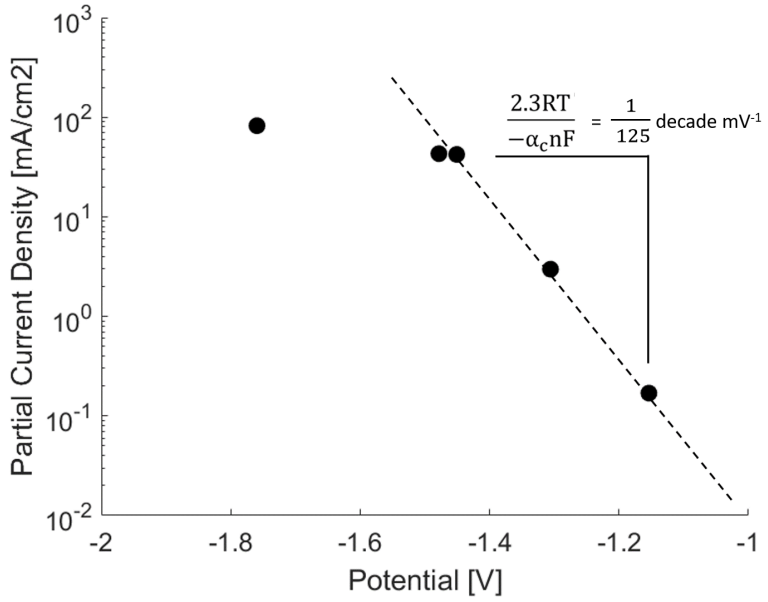

Figure 6.5: Tafel plot of $HCOOH/HCOO^-$ at 5 atm on In electrodes (T=298.15K & 0.5M $KHCO_3$) (Data from: Todoroki et al. [1])

7
Modeling

Introduction

This chapter discusses the modeling of the electrochemical cell and the effect of operation at elevated CO_2 pressures. It further elaborates on the methods used to implement the principles identified earlier with respect to thermodynamics, kinetics and mass transport. In the field of electrochemistry, modeling can be very helpful for researchers as well as businesses for a variety of reasons. A good model can give insight in the mechanisms involved and help understand cell behavior, which in effect can lead to cell design improvements. Furthermore, it can offer a cheap and quick alternative to expensive experiments to investigate cell behavior at varying operating conditions. It can also help in identifying potential new fields of research and explore new areas for future experiments.

ERC is a complex process which, despite being actively researched, still offers many questions, especially with respect to the mechanistic understanding. The model has been build based on various assumptions, which simplify the modeling problem. It is important to recognize that a model is only as accurate as is allowed by its assumptions. It is therefore important to understand the assumptions and the limitations they imply for the usability of the model and the reliability of the results. However, if done correctly, even a modest and highly simplified model can have large predictive power.

The mathematical model presented in this research focuses on the cathodic part of the electrochemical cell, as this is the working electrode. The coupled reactions occur at the counter electrode in the anodic compartment and are assumed to be non-limiting. In this model the cathodic compartment is divided into three main regions:

- Bulk: The bulk solution is the part of the electrolyte solution where the species concentrations are not dynamically influenced by any mass transport phenomena or (electro-) chemical reactions. Therefore the bulk species concentrations are assumed equilibrated and constant in time. The electrolyte solution is formed when CO_2 is dissolved into a aqueous solution containing dissolved $KHCO_3$ salt. The bulk concentrations are assumed to be exclusively dependent on temperature, (CO_2-)pressure and the amount of electrolyte salt added per liter H_2O.
- Cathode Surface Region (CSR): The species concentrations in the vicinity of the cathode are different from the bulk concentrations. The concentration gradients between the bulk and the electrode surface are triggered by the electrochemical reactions occurring at the cathode surface which produce and consume specific species. The supply and removal of species between the bulk and electrode surface is facilitated by diffusion, for which this thin layer is also referred to as the cathode surface region or diffusion layer of thickness δ.
- Electrode Surface: The surface of the cathode is the location where the electrochemical reaction and thus the reduction of CO_2 occurs. Upon polarization the cathode becomes more negatively charged and electrons are added to the electrode surface, which initiates the reduction mechanism. Because the applied overpotentials for the products $HCOO^-$,

CO and H_2 are high, the reduction reactions are assumed to follow Tafel-type kinetics as described more elaborate in Chapter 6.

In Figure 7.1, a schematic representation of the modeled part of the reaction is given. It shows the bulk, the CSR and electrode surface with the respective reactions and involved species.

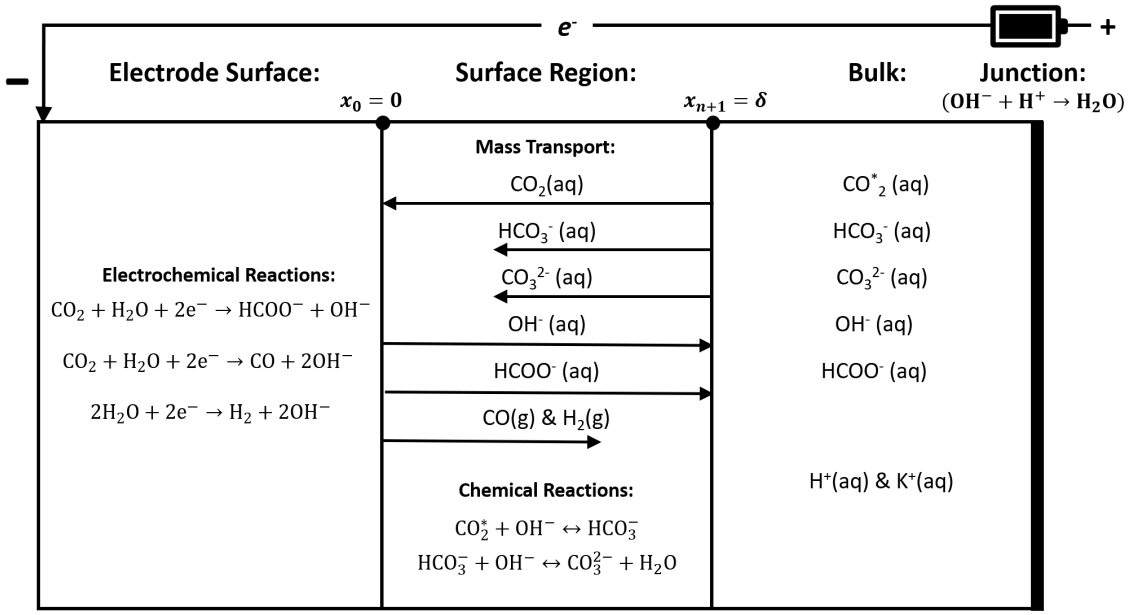

Figure 7.1: Schematic overview of the modeled part of the reactor

7.1. Assumptions

7.1.1. General:

1. The oxidation of H_2O, occurring in the anodic compartment of the electrochemical cell, is assumed to be non-limiting. Here the supporting half-reaction for ERC, the oxidation of H_2O, takes place and supplies the electrons for the reduction process and possibly, depending on the cell design and conditions, also H^+-ions.

2. The modeled process is assumed to operate at a constant temperature of 298.15K. In reality the temperature in the cell may vary due to both endothermic and exothermic reactions as well as overpotential losses with are dissipated as heat.

3. The modeled ERC occurs in slightly acidic/neutral and alkaline conditions, where the pH is high enough for reactions b1 and b2 from Table 2.1 to be dominant. Furthermore, H_2O is the proton donor and OH^- is produced at the surface in the reactions to $HCOO^-$, CO and H_2. The pH limit, for which this assumption is valid is assumed to be 6. The model therefore does not allow for operation in acidic media.

7.1.2. Bulk:

1. The volume of the bulk is assumed to be very large with respect to the electrode area. Any variation to the bulk species concentrations due to the removal and addition of species caused by the electrochemical reactions at the electrode are therefore assumed negligible.

2. For neutral or alkaline conditions, OH^- ions are formed at the electrode in the electrochemical reactions to $HCOO^-$, CO and H_2. Due to the concentration gradient between

the bulk and the electrode surface, these ions diffuse to the bulk. In this model, these ions are assumed to chemically recombine to H_2O with H^+ ions formed at the anode. In reality this may occur at the separator (junction) between the cathodic and anodic compartment as shown in Figure 7.1.

3. For this study, CO_2(g) is assumed to be in equilibrium with the liquid at all times. Therefore despite that CO_2 is being consumed at the electrode, the CO_2 concentration in the bulk is assumed to be constant for a given temperature and pressure.

4. The bulk concentration of $HCOO^-$ is kept constant at zero, as variation to the bulk species concentrations due to the addition of species is assumed negligible (see first bulk assumption). In reality, with time $HCOO^-$ needs to be removed, as the concentration will eventually build up to significant levels. This is not covered in this work.

7.1.3. Cathode Surface Region (CSR) / Diffusion Layer:

1. The mass transfer phenomena in the CSR are limited to one spacial direction perpendicular to the electrode surface. The spacial discretization is therefore done in one dimension (1D).

2. Mass transfer phenomena are limited to diffusional fluxes within a thin film layer between the bulk and the electrode surface. Convection and the migration of charged particles under the influence of an electrical potential gradient are not accounted for, as further explained in Chapter 5.

3. All reactions are carried out in an excess of supporting electrolyte (compared to the electro-active species), the electrolyte will therefore carry most of the charge and the effect of migration on the electro-active species is negligible.

4. The products CO and H_2, which are produced at the electrode surface are produced in gaseous form and both have a very low solubility in water at 298.15K of respectively $9.3e^{-4}$M and $8.0e^{-}4$M[105]. It is therefore assumed that they both bubble off as soon as they are formed.

5. After $HCOO^-$ is formed, it transports from the surface to the bulk, without reacting with other species.

7.1.4. Surface Kinetics:

1. $HCOO^-$/HCOOH, CO (via CO_2 reduction) and H_2 (via H_2O reduction) are the only products of ERC at the cathode and the selectivity towards other species is assumed to be negligible. This assumption is based on research done by Hara et al. [16] on ERC under high pressure on various electrodes. They found that on the $HCOO^-$/HCOOH producing metals Sn, In and Pb, other species as CH_4, C_2H_6 and C_2H_4 are either not produced or produced with very low selectively (Faradaic efficiency < 0.3%).

2. CO_2(aq) and H_2O, are the only active species to be reduced. This implies that the possible direct reduction of the other carbon species available in the electrolyte, H_2CO_3, HCO_3^- and CO_3^{2-} is neglected. Some researchers have suggested that HCO_3^- is also reduced effectively, but most researchers agree that it does not act as an electro-active species. It is suggested that HCO_3^- is likely decomposed to CO_2 first and which is then reduced at the cathode [87].

3. The electrons which flow from the cathode interface to adsorbed species are produced at the anode where the electrons flow from the species towards the anode surface. As the anodic half reaction is assumed to be non-limiting, the kinetics at the cathode are rate-determining, with the water oxidation at the anode as supporting half-reaction.

7.2. Bulk

7.2.1. Theory

CO_2 is dissolved into the aqueous electrolyte containing $KHCO_3$ under a given temperature (298.15K) and pressure. It is assumed that the CO_2(aq) concentration is constant within the bulk, as the CO_2(g) is always in equilibrium with the electrolyte solution. Furthermore, the bulk is defined as the part of the electrolyte where mass transport phenomena are assumed to be negligible. In addition, the bulk volume is also assumed to be very large with respect to the electrode area. Combining these assumption results in the fact that all the bulk species concentrations are equilibrated and d not vary in time.

As explained in Section 2.0.1, the system of dissolved CO_2 in water or an aqueous solution can be rather complex as many different species are involved. The relevant chemical reactions necessary to calculate the equilibrated species concentrations are shown in reactions (7.1)-(7.5):

$$CO_2\,(aq) + H_2O\,(l) \rightleftharpoons H_2CO_3(aq) \qquad K_H \qquad (7.1)$$

$$H_2CO_3(aq) \rightleftharpoons HCO_3^-(aq) + H^+(aq) \qquad K_{a0} \qquad (7.2)$$

$$CO_2^*(aq) + H_2O\,(l) \rightleftharpoons H^+ + HCO_3^-(aq) \qquad K_{a1} \qquad (7.3)$$

$$HCO_3^-(aq) \rightleftharpoons CO_3^{2-}(aq) + H^+(aq) \qquad K_{a2} \qquad (7.4)$$

$$H_2O\,(l) \rightleftharpoons OH^-(aq) + H^+(aq) \qquad K_W \qquad (7.5)$$

As H_2CO_3 is only present in very small quantities (roughly: $[CO_2] = 650[H_2CO_3]$ [49]), it is considered to be an intermediate in the dissolution of CO_2 towards HCO_3^-. CO_2^* in reaction (7.3) therefore actually represents $[CO_2] + [H_2CO_3]$. The equilibrium constant K_{a1} is therefore calculated from K_H and K_{a0}: $K_{a1} = K_H K_{a0}$. With this simplification the bulk concentrations are calculated using reactions (7.3),(7.4),(7.5).

In addition to the chemical reactions given above, the equilibrium in the bulk is also determined by the carbon balance (7.6) and a zero charge requirement (7.7) within the bulk:

$$[CO_2] + [HCO_3^-] + [CO_3^{2-}] = C_{carbon} \qquad (7.6)$$

$$[K^+] + [H^+] - [HCO_3^-] - 2\,[CO_3^{2-}] - [OH^-] = 0 \qquad (7.7)$$

The total amount of carbon, C_{carbon}, in the system is fixed by the number of moles $KHCO_3$ dissolved in the aqueous solution, forming the electrolyte and the amount of CO_2 dissolved in the aqueous solution. Each mole of $KHCO_3$ dissolved into the system accounts for 1 mole of carbon atoms (C) and 1 mole of potassium ions (K^+). The rest of the carbon in the system comes from gaseous CO_2 that is being dissolved in the electrolyte solution. Per liter, this amount is referred to as the solubility of CO_2, which depends on both the temperature and the partial pressure of CO_2 above the liquid. In Section 2, the solubility of CO_2 in aqueous solutions for varying conditions is further investigated.

For a given electrochemical reactor, which is assumed to be operating at a constant temperature of 25℃, the amount of carbon carbon in the system is therefore fully determined by the amount of electrolyte salt added per liter and the pressure of the gaseous carbon dioxide above the liquid (assuming pure CO_2(g), which is continuously in equilibrium with the liquid). C_{carbon} is therefore calculated as:

$$C_{carbon} = C_{electrolyte} + S_{CO_2}(p) \qquad (7.8)$$

7.2.2. Calculation

Using the reactions and balances identified above, the equilibrated bulk concentrations can be calculated as follows:

From (7.3):

$$[HCO_3^-] = K_{a1}\frac{[CO_2]}{[H^+]} \tag{7.9}$$

From (7.4):

$$[CO_3^{2-}] = K_{a2}\frac{[HCO_3^-]}{[H^+]} \tag{7.10}$$

From (7.9) and (7.10):

$$[CO_3^{2-}] = K_{a1}K_{a2}\frac{[CO_2]}{[H^+]^2} \tag{7.11}$$

Substituting (7.9) and (7.11) in the carbon balance gives an expression in which $[CO_2]$ and $[H^+]$ are the only unknowns:

$$[CO_2] + K_{a1}\frac{[CO_2]}{[H^+]} + K_{a1}K_{a2}\frac{[CO_2]}{[H^+]^2} = C_{carbon} \tag{7.12}$$

Reordering expression (7.12) for gives:

$$[CO_2] = \frac{C_{carbon}[H^+]^2}{[H^+]^2 + K_{a1}[H^+] + K_{a1}K_{a2}} \tag{7.13}$$

From (7.5), $[OH^-]$ can be expressed in terms of $[H^+]$:

$$[OH^-] = \frac{K_w}{[H^+]} \tag{7.14}$$

Substituting (7.9), (7.11) and (7.14) in the charge balance gives:

$$[K^+] + [H^+] - K_{a1}\frac{[CO_2]}{[H^+]} - 2\,K_{a1}K_{a2}\frac{[CO_2]}{[H^+]^2} - \frac{K_w}{[H^+]} = 0 \tag{7.15}$$

In Equation (7.15), the concentration of potassium ions, $[K^+]$, is fixed and equal the to amount of moles of $KHCO_3$ added to the system as electrolyte salt (i.e. $C_{electrolyte}$). Therefore with equations (7.13) and (7.15), we have two equation and only two unknowns, namely $[CO_2]$ and $[H^+]$.

By substituting $[K^+]$ for $C_{electrolyte}$ and by combining (7.13) with (7.15), we get a rather complex polynomial expression, in which $[H^+]$ is the only unknown:

$$\begin{aligned}[C_{electrolyte}] + [H^+] - \frac{K_{a1}C_{carbon}[H^+]^2}{[H^+]^3 + K_{a1}[H^+]^2 + K_{a1}K_{a2}[H^+]} \ldots \\ \ldots - \frac{2\,K_{a1}K_{a2}C_{carbon}[H^+]^2}{[H^+]^4 + K_{a1}[H^+]^3 + K_{a1}K_{a2}[H^+]^2} - \frac{K_w}{[H^+]} = 0\end{aligned} \tag{7.16}$$

Solving (7.16) for $[H^+]$ (with $0 \le pH \le 14$ i.e. $10^{-14} \le [H^+] \le 1$) using MATLAB, gives an unique solution for the H^+ equilibrium concentration in the bulk. With $[H^+]$ known, $[CO_2]$, $[HCO_3^-]$, $[CO_3^{2-}]$, $[OH^-]$ can be calculated subsequently via respectively equations (7.13), (7.9), (7.11) and (7.14).

In Tables 8.1, 8.2 and 8.3 in Chapter 8, the calculated bulk concentration of the species CO_2, HCO_3^-, CO_3^{2-}, OH^- and H^+ (represented as pH) are given at a CO_2 pressure of 1 atm, 20 atm and 40 atm, respectively.

7.3. Cathode Surface Region (CSR)

7.3.1. Theory

Within the scope of this research, the cathode surface region (CSR) is evaluated as a boundary layer in which the concentrations of the various involved species differ from their equilibrated bulk concentrations due to electrochemical reactions occurring around - and at the cathode surface. Due to these concentration gradients, diffusion causes the ions and molecules to move within the CSR. Simultaneously, there are local chemical reactions between the species caused by the broken equilibria. Therefore the local species concentrations within the CSR can be approximated by a system of reaction-diffusion equations of the form:

$$\frac{\partial C_i}{\partial t} = D_i \frac{\partial^2 C_i}{\partial x^2} + V(C_1, C_2, \cdots, C_n) \tag{7.17}$$

where c_i is the respective species concentration and D_i the corresponding diffusion coefficient.

Generally speaking, hydrogen evolution becomes more dominant in comparison with CO_2 reduction in increasingly acidic media. HER increases proportional to H^+ (proton) activity or concentration, whereas research [87] suggests that CO_2 reduction is pH independent as H_2O acts as proton donor. In addition, for highly alkaline media (~ pH 10 and higher), CO_2 is non existent due to shifting equilibria towards HCO_3^- and eventually CO_3^{2-}. Most studies have therefore focused on ERC in neutral or slightly alkaline media, with 6.0 < pH < 10. The assumption made for the scope of this research is that, due to the relatively high concentration of carbonate, bicarbonate, and hydroxides in the electrolyte, the pH is high enough for reactions b1 and b2 from Table 2.1 to be dominant:

$$CO_2(aq) + OH^-(aq) \underset{k_{b1}^r}{\overset{k_{b1}^f}{\rightleftharpoons}} HCO_3^-(aq) \tag{7.18}$$

$$HCO_3^-(aq) + OH^-(aq) \underset{k_{b2}^r}{\overset{k_{b2}^f}{\rightleftharpoons}} CO_3^{2-}(aq) + H_2O(l) \tag{7.19}$$

These chemical reactions are used to express the net rate of formation of each species, V_i. By combining Ficks' second law of diffusion and the net rate of formation via inter-species reactions for each species, the relevant diffusion-reaction equations for the CSR can be derived. The equations are:

$$\frac{\partial [CO_2(aq)]}{\partial t} = D_{CO_2} \frac{\partial^2 [CO_2(aq)]}{\partial x^2} - [CO_2(aq)][OH^-]k_{b1}^f + [HCO_3^-]k_{b1}^r \tag{7.20}$$

$$\frac{\partial [HCO_3^-]}{\partial t} = D_{HCO_3^-} \frac{\partial^2 [HCO_3^-]}{\partial x^2} + [CO_2(aq)][OH^-]k_{b1}^f - [HCO_3^-]k_{b1}^r \ldots - [HCO_3^-][OH^-]k_{b2}^f + [CO_3^{2-}]k_{b2}^r \tag{7.21}$$

$$\frac{\partial [CO_3^{2-}]}{\partial t} = D_{CO_3^{2-}} \frac{\partial^2 [CO_3^{2-}]}{\partial x^2} + [HCO_3^-][OH^-]k_{b2}^f - [CO_3^{2-}]k_{b2}^r \tag{7.22}$$

$$\frac{\partial [OH^-]}{\partial t} = D_{OH^-} \frac{\partial^2 [OH^-]}{\partial x^2} - [CO_2(aq)][OH^-]k_{b1}^f + [HCO_3^-]k_{b1}^r \ldots - [HCO_3^-][OH^-]k_{b2}^f + [CO_3^{2-}]k_{b2}^r \tag{7.23}$$

The H^+ concentration, and therefore the pH, for each position in space and time can be directly calculated from the OH^- concentration via (7.5). Furthermore, at the electrode $HCOO^-$, CO and H_2 are formed. CO and H_2 are assumed to bubble off directly when they are formed. Formate is assumed to diffuse from the electrode surface through the diffusion

layer into the bulk, without interacting with other species. The partial differential equation for formate therefore becomes:

$$\frac{\partial[\mathrm{HCOO^-}]}{\partial \mathrm{t}} = \mathrm{D_{HCOO^-}} \frac{\partial^2[\mathrm{HCOO^-}]}{\partial\, \mathrm{x}^2} \tag{7.24}$$

The system of partial differential equations (7.20-7.24) is an initial-and boundary value problem, for which the solution can be approximated using numerical analysis.

The diffusion layer is discretized in a 1D spacial domain (x) perpendicular to the electrode surface from $x_0 = 0$ at the electrode surface to $x_{n+1} = \delta$ at the bulk interface, with n+1 equidistant intervals of length $\Delta x = \frac{\delta}{(n+1)}$. δ represents the diffusion layer thickness, which is initially chosen to be 0.05mm based on experimental data on the limiting current density towards formate by Todoroki et al.[1], as explained in Chapter 5. For each time step Δt from t=0 to $t=t_{end}$, the solution to the system of partial differential equations is approximated in the nodes, which are given by $x_i = i\Delta x$ for i = 0,1,...,n,n+1.

Initial Conditions

At time t=0, just before the reactor is switched on, the initial concentrations of all species are considered to be in equilibrium everywhere in the spacial domain ($0 \leq x \leq \delta$) and therefore equal to the bulk concentrations. In mathematical form the initial conditions (at time t=0) for the concentration of CO_2(aq), HCO_3^-, CO_3^{2-} and OH^- are:

$$\begin{cases} [\mathrm{CO_2}]_{\mathrm{x}}^{\mathrm{t=0}} = [\mathrm{CO_2}]_{\mathrm{bulk}} & \text{for: } 0 \leq x \leq \delta \\ [\mathrm{HCO_3^-}]_{\mathrm{x}}^{\mathrm{t=0}} = [\mathrm{HCO_3^-}]_{\mathrm{bulk}} & \text{for: } 0 \leq x \leq \delta \\ [\mathrm{CO_3^{2-}}]_{\mathrm{x}}^{\mathrm{t=0}} = [\mathrm{CO_3^{2-}}]_{\mathrm{bulk}} & \text{for: } 0 \leq x \leq \delta \\ [\mathrm{OH^-}]_{\mathrm{x}}^{\mathrm{t=0}} = [\mathrm{OH^-}]_{\mathrm{bulk}} & \text{for: } 0 \leq x \leq \delta \end{cases}$$

At time t=0 the electrolyte does not carry any formate, which is mathematically expressed as follows:

$$\{ [\mathrm{HCOO^-}]_{\mathrm{x}}^{\mathrm{t=0}} = 0 \text{ [mol/l]} \quad \text{for: } 0 \leq x \leq \delta$$

Boundary Conditions

A solution to the system of partial differential equations is only unique if it satisfies certain defined constraints, so called boundary conditions, at the CSR-electrode interface (x=0) and the CSR-bulk interface ($x=\delta$) for t>0.

At $x=\delta$, the boundary conditions for the species concentrations are equal to the concentrations in the bulk solution. Therefore the concentrations at $x=\delta$ are constant and equilibrated for a given pressure, temperature and electrolyte concentration and the following set of Dirichlet boundary conditions should be satisfied:

$$\begin{cases} [\mathrm{CO_2}]_{\mathrm{x=\delta}}^{\mathrm{t}} = [\mathrm{CO_2}]_{\mathrm{bulk}} & \text{for: } t > 0 \\ [\mathrm{HCO_3^-}]_{\mathrm{x=\delta}}^{\mathrm{t}} = [\mathrm{HCO_3^-}]_{\mathrm{bulk}} & \text{for: } t > 0 \\ [\mathrm{CO_3^{2-}}]_{\mathrm{x=\delta}}^{\mathrm{t}} = [\mathrm{CO_3^{2-}}]_{\mathrm{bulk}} & \text{for: } t > 0 \\ [\mathrm{OH^-}]_{\mathrm{x=\delta}}^{\mathrm{t}} = [\mathrm{OH^-}]_{\mathrm{bulk}} & \text{for: } t > 0 \\ [\mathrm{HCOO^-}]_{\mathrm{x=\delta}}^{\mathrm{t}} = 0 & \text{for: } t > 0 \end{cases}$$

At x=0, the boundary conditions for the different species are related to the fluxes caused by the electrochemical reactions at the electrode surface. As described in Chapter 6, their are three electrochemical reactions occurring at the cathode. CO_2 is reduced to either $HCOO^-$ according to reaction (7.25) or to CO according to reaction (7.26). In addition via hydrogen evolution, water can be reduced to H_2 according to reaction (7.27).

$$CO_2 + H_2O + 2\,e^- \rightleftharpoons HCOO^- + OH^- \tag{7.25}$$
$$CO_2 + H_2O + 2\,e^- \rightleftharpoons CO + 2\,OH^- \tag{7.26}$$
$$2\,H_2O + 2\,e^- \rightleftharpoons H_2 + 2\,OH^- \tag{7.27}$$

Based on the reactions above, the consumption or formation of each species at the electrode surface can be expressed as a reaction flux and calculated using the partial current densities (PCD) towards $HCOO^-$, CO and H_2. At x=0, a Neumann boundary condition can be expressed mathematically for each species:

$$\begin{cases} D_{CO2}\dfrac{d[CO_2]}{dx}|_{x=0} = CO_{2\text{consumption}} = -10^{-2}\left(\dfrac{i_{HCOO^-}}{n_{HCOO^-}F} + \dfrac{i_{CO}}{n_{CO}F}\right)\ [\text{kmol/m}^2\text{s}] \\ D_{HCO3^-}\dfrac{d[HCO_3^-]}{dx}|_{x=0} = 0\ [\text{kmol/m}^2\text{s}] \\ D_{CO3^{2-}}\dfrac{d[CO_3^{2-}]}{dx}|_{x=0} = 0\ [\text{kmol/m}^2\text{s}] \\ D_{OH^-}\dfrac{d[OH^-]}{dx}|_{x=0} = OH^-_{\text{formation}} = 10^{-2}\left(\dfrac{i_{HCOO^-}}{n_{HCOO^-}F} + 2\,\dfrac{i_{CO}}{n_{CO}F} + 2\,\dfrac{i_{H_2}}{n_{H_2}F}\right)\ [\text{kmol/m}^2\text{s}] \\ D_{HCOO^-}\dfrac{d[HCOO^-]}{dx}|_{x=0} = HCOO^-_{\text{formation}} = 10^{-2}\left(\dfrac{i_{HCOO^-}}{n_{HCOO^-}F}\right)\ [\text{kmol/m}^2\text{s}] \end{cases}$$

with:

i_j: Partial Current Density for reaction j $[\text{mA/cm}]^2$

n_j: # of electrons exchanged in reaction j [-]

As the boundary conditions are related to the fluxes of species at the electrode surface, the boundary condition for a specific species is directly linked to the amount of current per area (i.e. number of electrons) that facilitates the reaction(s) in which the species is involved, also known as the partial current density. The current density distribution between reactions (7.25), (7.26) and (7.27) for a fixed total current density or applied potential, is determined by both kinetics and mass transport phenomena and will be further elaborated in Section 7.4.

7.3.2. Calculation

The system of partial differential equations (7.20-7.24), with the described initial- and boundary conditions is solved using MATLAB's build-in numerical solution 'PDEPE' solver. PDEPE is a numerical solver, which can be used to solve initial-boundary value problems for PDEs or systems of PDE's in an 1D domain [106][107]. Here the essentials with respect to the methods used by the numerical solver are discussed. Skeel and Berzins [108] cover the actual numerical theory behind the solver in great detail.

PDEPE is designed to solve systems of PDEs in the spatial dimension x and in time. It implements a numerical approach, called the method of lines. In the method of lines approach the PDEs are spatially discretized after which a set of ordinary differential equations, ODEs, remain. Subsequently, the ODEs are then integrated using a suitable numerical procedure for solving ordinary differential equations to obtain the approximate solutions. In Figure 7.2, a schematic visualization of the method of lines in presented, which shows the approximated nodes in both the spatial x-direction and time.

As suggested by Skeel and Berzins [108], PDEPE discretizes the set of PDEs along the spatial dimension using finite differences techniques, more precisely the Petrov/Galerkin-Galerkin method. This results in a system of ODEs, with one ODE for each grid node along your spatial dimension. The set of ODEs are solved using the MATLAB ODE solver ODE15s.

ODE15s implements numerical differentiation formulas in terms of 5th order (by default) backward differences [109]. Simplified this means that the derivative of a function is approximated using information from earlier computed times. This is an implicit method, which are known to be computationally more demanding, but also very stable, which allows for large time steps.

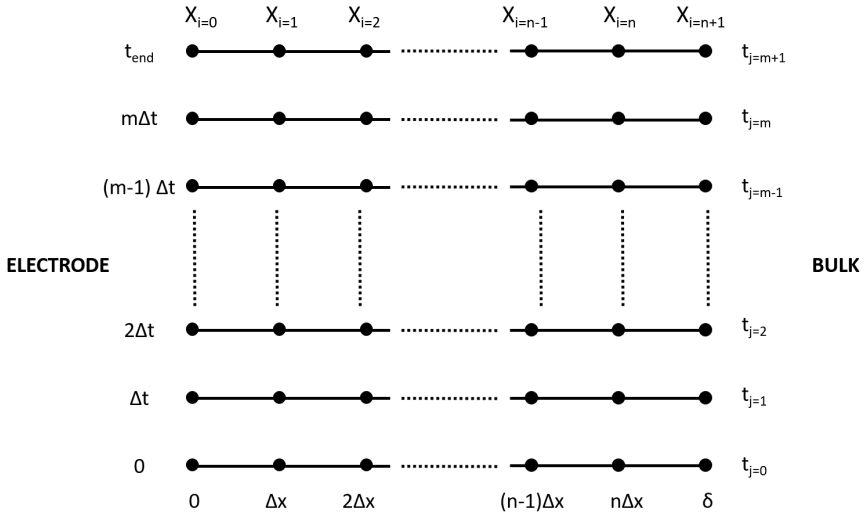

Figure 7.2: Numerical approach - Method of lines

7.4. Electrode Surface (Kinetics)

The ERC towards $HCOO^-$, CO and H_2 occurs at the electrode surface. As explained in Chapter 6, the rate of reactions occurring at the electrode surface are characterized by the catalytic properties of the material it is made of. As the reactions occur at high overpotential, typically much larger than 52 mV [17], the reaction kinetics are modeled using the Tafel equation. The modeled reactions to $HCOO^-$, CO and H_2 are shown in respectively reaction (7.25), (7.26) and (7.27). Using the fitted values for α_c and $k_s(E_0)$ given in Table 6.2, the following equation is used to describe the partial current densities towards $HCOO^-$, CO and H_2 for a given potential:

$$i_j = i_{0,j} \exp\left[\frac{-\alpha_{c,j} n_j F}{RT}\eta_j\right] = i_j = C_{ox} n_j k_{s,j}(E_{0,j}) F \exp\left[\frac{-\alpha_{c,j} n_j F}{RT}(E - E_{0,j})\right] \tag{7.28}$$

with j being 1,2 or 3 for $HCOO^-$, CO or H_2, respectively.

The partial current densities towards the three products are calculated for an applied potential (E) varying between 0 V and -2.0V. As the standard reduction potentials towards $HCOO^-$, CO and H_2 are all slightly different, the overpotentials also vary for each reaction. From Equation (7.28) it is clear that for linearly increasing overpotentials the partial current densities increase exponentially, depending mainly on the Tafel coefficients i_0 and α_c.

The exchange current density, i_0, is dependent on the oxidant concentration, C_{ox}, at the electrode surface, being $[CO_2]_{surface}$ for CO_2 reduction to $HCOO^-$ and CO and $[H_2O]_{surface}$ for water reduction to H_2. As the reduction occurs in an aqueous environment, the water concentration is assumed to be constant and calculated via:

$$[H_2O]_{surface} = \frac{\rho_{H_2O}}{M_{H_2O}} \approx= \frac{1000}{18} \approx 55M \tag{7.29}$$

with ρ_{H_2O} being the density of water in gl^{-1} and M_{H_2O} the molar mass of water $gmol^{-1}$. As the water concentration at the electrode surface is assumed to be constant (i.e. independent of

CO_2 pressure or potential), there will be no mass transfer limitation and the electrochemical conversion to H_2 will be fully charge transfer controlled over the entire potential range looked at. This assumption is in line with measurements done by Todoroki et al. [1]. They studies the effect of elevated CO_2 pressures on the selective formation of $HCOO^-$ via the reduction of CO_2 and they saw no indications of mass transfer limitations with respect to H_2 formation. Furthermore, another effect of this assumption will be that the rate of H_2 formation will be unaffected by an increasing CO_2 pressure. This also corresponds to the findings of Todoroki et al. [1], who found that "H_2 formation is almost unaffected by CO_2 pressure".

As the potential E increases, the partial current densities to formate and carbon monoxide will also increase, which will in effect increase the consumption of CO_2 at the cathode surface. Depending on the mass transfer rate of CO_2 from the bulk to the surface, the CO_2 concentration at the surface may be either almost equal to the bulk concentration, smaller than the bulk concentration or zero. Under the influence of these variations in CO_2 concentration at the surface, the relation between potential (E) and the partial current densities (i) start to change. This relation is commonly expressed in an i-E curve, which can be divided into three areas [17]: charge transfer control, mixed control and mass transfer control. A schematic representation of a typical I-E curve and the hypothesized effect of an elevated CO_2 pressure is seen in Figure 7.3.

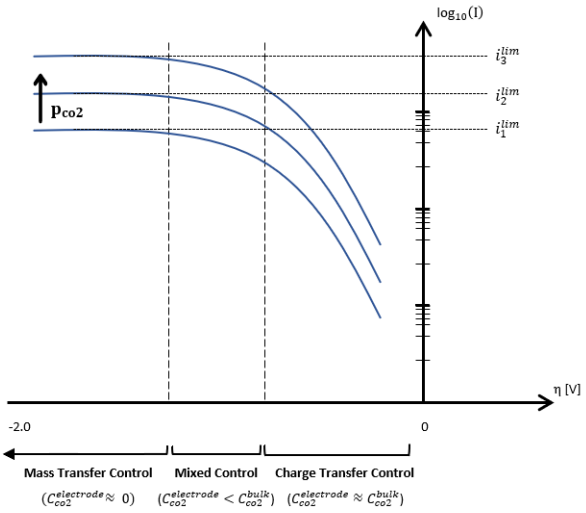

Figure 7.3: Schematic representation of a complete I-E curve for CO_2 reduction and the assumed effect of an elevated CO_2 pressure.

Initially a small reduction current towards $HCOO^-$, CO and H_2 will be observed when a small negative potential is applied. The CO_2 consumption will be relatively small and $[CO_2]_{surface}$ will be close to $[CO_2]_{bulk}$. In this region, the reduction rate is charge transfer controlled and the I-E curve follows the Tafel equation. For more negative potentials the current density increases quickly, rapidly increasing the CO_2 consumption which will eventually lead to a situation where the transport of CO_2 towards the surface will start to be limiting and $[CO_2]_{surface}$ will be lower than $[CO_2]_{bulk}$. This region is called the region of mixed control and is characterized by a non linear Tafel plot. For even more negative potential, the current densities may become so large that the surface concentration of CO_2 decreases to zero. At this point the currents densities are no longer potential dependent and are fully determined by mass transfer. This region is therefore referred to as the region of mass transfer control. When operating in this region, the current densities are limited and therefore stay constant even for more negative potential. The value of the limiting current densities is determined by mass transfer and will therefore strongly relate to the mass transfer conditions in the cell.

The mathematical model describes the regions of charge transfer control, mixed control and mass transfer control. For applied potentials (E) between 0.0 V and -2.0 V, starting with 0.0 V, the partial current densities are calculated using the Tafel equation for each product. With the calculated current densities to $HCOO^-$, CO^- and H_2, the CO_2 consumption, OH^- formation and $HCOO^-$ formation can be calculated as described in Section 7.3. The CO_2 consumption, OH^- formation and $HCOO^-$ formation then serve as the boundary conditions at x=0 (electrode surface) for the mass transfer model described earlier. With the mass transfer calculations, an updated steady-state CO_2 surface concentration is calculated which will be used for the next calculation loop with slightly more negative potential. If the model calculated CO_2 surface concentration is smaller than 95% of the CO_2 bulk concentration, the regime is said to switch from being charge transfer controlled to mixed control and at 5 atm on an indium electrode this is found to be at a potential of -1.31 V ($E_{CTC>MC}$). If the calculated CO_2 surface concentration reaches or if the partial current densities are calculated to become smaller with more negative potentials, the model is assumed to be in the mass transfer region and the CO_2 surface concentration is set to zero and the last calculated partial current density is set to be the limiting current density. For reduction at 5 atm on an indium electrode, this is found to be at a potential of -1.57 V ($E_{MC>MTC}$), with a limiting partial current density to formate of approximately 63 $mAcm^{-2}$. Both values found for $E_{CTC>MC}$ and $E_{CTC>MC}$, respectively -1.31V and -1.57V , correspond to values found by Todoroki et al. [1]. The modeled CO_2 surface concentrations at 5 atm on indium electrodes, together with the lines of switching region, are shown in Figure 7.4.

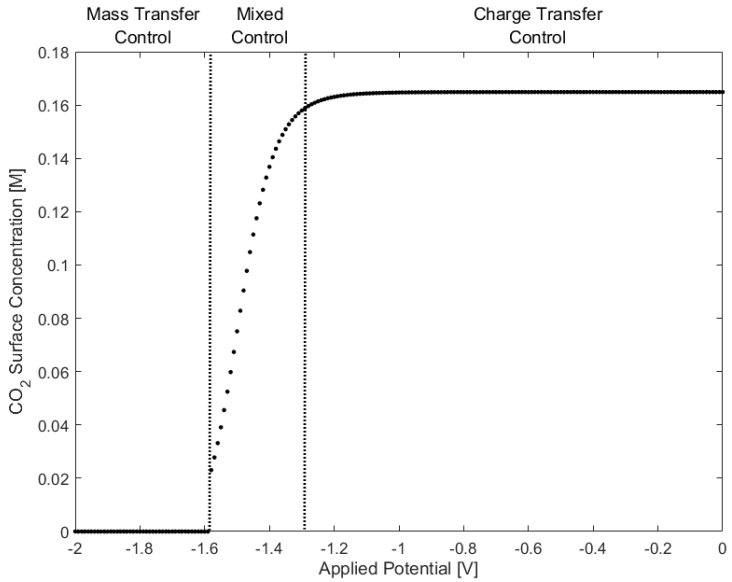

Figure 7.4: Modeled effect of potential on the CO_2 surface concentration at 5 atm on In electrodes (T=298.15K & 0.5M $KHCO_3$).

7.5. Model Overview

The theory described in this chapter is combined in a mathematic model using MATLAB R2017a. In Figure 7.5, a summarized mathematic overview of the model is given. It shows the most input parameters, most relevant equations and theory, and the output of the model for respectively the bulk, cathode surface region and the electrode surface.

In the bulk region, the bulk concentrations of the species CO_2(aq), HCO_3^-, CO_3^{2-}, OH^- and H^+ are calculated. Input parameters for the bulk region are the CO_2 pressure and the electrolyte, $KHCO_3$, concentration. The calculation involves solving the equilibrium reactions with reaction constants at 298.15K, together with the carbon - and charge balance.

In the cathode surface region, the mass transport of involved species between the bulk and the electrode surface is calculated using numerical analysis techniques. Main inputs are the diffusion layer thickness, δ, the spacial step size, Δx and the time step, Δt. The system of reaction–diffusion equations is an initial-and boundary value problem. At the initial condition ($t=0$) and at the boundary with the bulk ($x=\delta$, $t\leq 0$), the species concentrations are equal to the bulk concentrations (**arrow 1**). The boundary conditions at the electrode surface ($x=0$) are determined by the electrochemical reaction rates at the electrode surface (**arrow 3**). For CO_2 and OH^-, the boundary conditions depend on the partial current densities towards $HCOO^-$, CO and H_2 for a given potential and are equal to respectively the consumption of CO_2 and formation of OH^- at the surface. For HCO_3^- and CO_3^{2-} a no-flux boundary conditions is assumed.

The surface kinetics are describes using the Tafel Equation, with parameters α and i_0 (more precisely: k_s at E_0) for each reaction fitted from experimental data. According to the Tafel equation, the kinetics are dependent on the oxidant concentration at the surface. The CO_2 surface concentration is therefore updated for every step of increasing overpotential (**arrow 2**). Outputs are the partial current densities (i.e. production rates) and Faradaic efficiencies (i.e. selectivity) to $HCOO^-$, CO and H_2 for potentials between 0.0V and -2.0V.

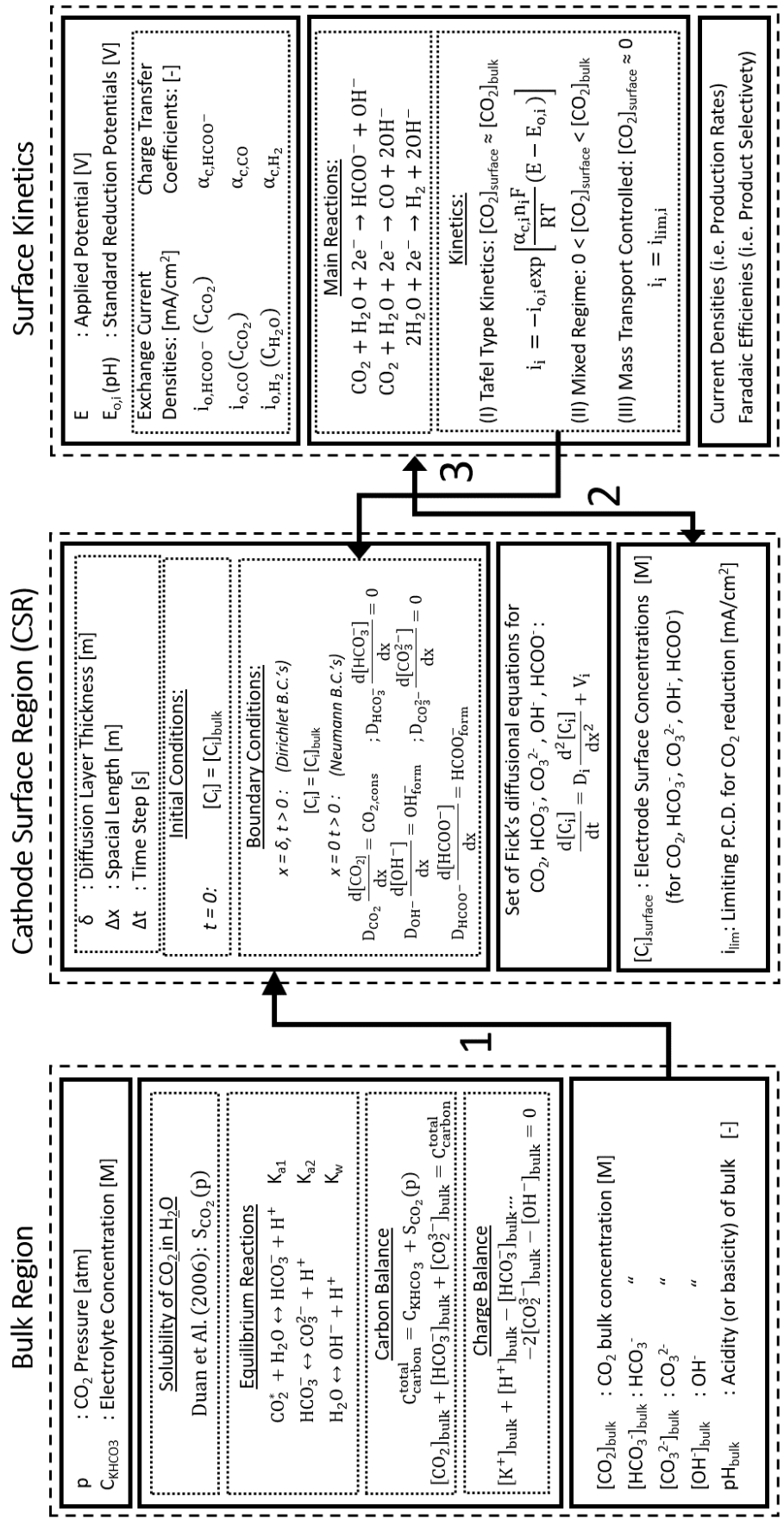

Figure 7.5: Schematic summary of the mathematical modeling

8

Results & Discussion

In this chapter, important and relevant results from the model will be presented and discussed. In order to validate the results, part of them are modeled using conditions similar to that presented in literature. First, key results with respect to the pressure effects on selectivity and production rate are presented. Furthermore, general results specifically regarding the bulk and CSR discussed. Finally, the sensitivity of the model to variations of important parameters is looked at.

8.1. Overall Results of the Model

In Figure 8.1a, the modeled effect of CO_2 pressure on the Faradaic efficiencies towards $HCOO^-$, CO and H_2 is shown for a current density of 200 $mAcm^{-2}$ on an Indium electrode. Both experimental results [1] and predictions from the model are shown. The FE to $HCOO^-$ is found to increase rapidly from <5% at a CO_2 pressure of 1 atm to ~90% at 20 atm, after which the FE remains almost constant. The selectivity towards H_2 decreases from being higher than 95% at 1 atm to <5% at 20 atm. This observed trend is in good accordance with the experimental results. The observed plateau with a FE of approximately 90%-95% for pressures of 20 atm and higher, seen in both the experimental and the model results, suggest that the kinetics change from mass transfer control via diffusion to charge transfer control at approximately 20 atm for a current density of 200$mAcm^{-2}$. With an increasing current density, CO_2 will be consumed even more rapidly at the surface. It is therefore expected that for higher current densities the FE will reach its maximum at a higher CO_2 pressure. In Figure 8.1b the modeled effect of CO_2 pressure on the Faradaic efficiencies for a current density of 400 $mAcm^{-2}$ is shown and it is found that the region changes from mass transfer control to charge transfer control at 35 atm.

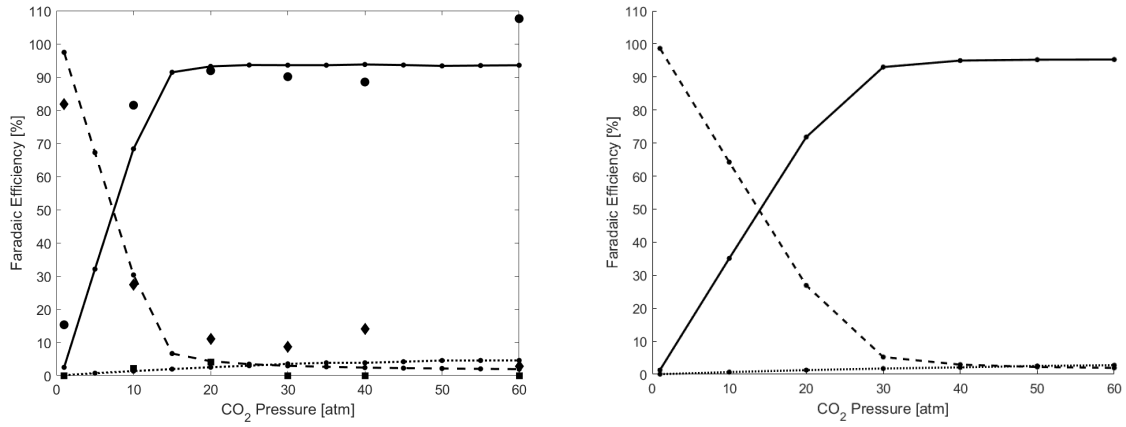

(a) Current density of 200 $mAcm^{-2}$ (b) Current density of 400 $mAcm^{-2}$

Figure 8.1: Modeled effect of CO_2 pressure on the Faradaic efficiencies of $HCOO^-$ (—), CO (····) and H_2 (- -) (T=298.15K & 0.5M $KHCO_3$). Data points from Todoroki et al. [1] for $HCOO^-$ (●), CO (■) and H_2 (♦) at 200 $mAcm^{-2}$ on In electrodes

Although the overall trends of the modeled and experimental results are in good accordance with each other, differences up to 15%-20% percentage points between the modeled- and experimental results are observed. One obvious difference is the selectivity toward H_2 at elevated CO_2 pressure. In the experimental data the H_2 formation is suppressed to an efficiency of approximately 10-15%, whereas the model predicts a much larger suppression of H_2 selectivity all the way down to <5%. Differences can possibly be attributed to the model assumptions as explained in Chapter 7, and it may also be that experimental errors are part of the blame for the deviation.

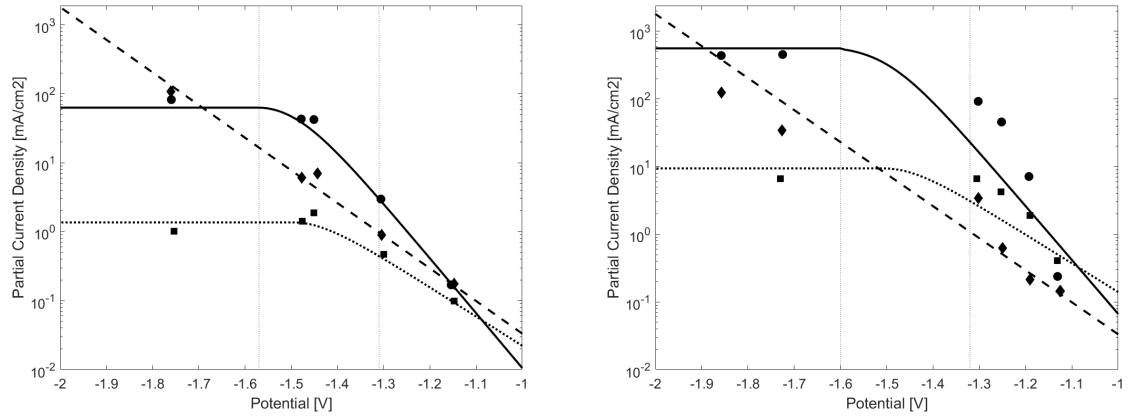

(a) 5 atm (b) 40 atm

Figure 8.2: Modeled Tafel plots of $HCOO^-$ (—), CO (····) and H_2 (- -) (T=298.15K & 0.5M $KHCO_3$). Data points from Todoroki et al. [1] for $HCOO^-$ (●), CO (■) and H_2 (⧫) at 40 atm on In electrodes

In Figure 8.2a the modeled Tafel plot for ERC at 5 atm and with 0.5M $KHCO_3$ on an Indium electrode is shown, together with experimental data [1]. As explained in Chapter 6, the kinetics parameters i_0 and α_c are fitted on this dataset, which can be seen by looking at the charge transfer region (i.e. were the Tafel slope is linear) for which the experimental data and the modeled results are identical. At a more negative potential, the overpotential becomes larger, and thus the current density increases. The model predicts that at a potential of -1.31V. At which point, the CO_2 concentration at the surface becomes significantly lower than the CO_2 concentration at the bulk, due to the increasing CO_2 consumption at the surface. The electrochemical reduction of CO_2 is then said to be in a mixed regime. Due to increasing current densities towards $HCOO^-$ and CO, at approximately -1.57V the CO_2 consumption becomes so large that the CO_2 concentration at the surface becomes zero, and therefore fully diffusion controlled. The modeled potentials of -1.31V and -1.57V, for which the operational regime changes, are close to the actual values found in the experiment. The modeled limiting partial current densities for $HCOO^-$ and CO at 5 atm are found to be respectively 63 $mAcm^{-2}$ and 1.4 $mAcm^{-2}$. This is in good agreement with the experimental data in which i_{lim} was found to be between approximately 40-80 $mAcm^{-2}$ for $HCOO^-$ and 1.0-1.9 $mAcm^{-2}$ for CO. H_2O is reduced independent of the CO_2 surface concentration, and follows Tafel type kinetics within the entire potential range from 0.0V to -2.0V.

With increasing pressure the CO_2 concentration increases, and this will have a direct effect on the Tafel plots for $HCOO^-$ and CO formation. This modeled effect of an elevated CO_2 pressure on the Tafel plot can be seen in Figure 8.2b, which shows the modeled Tafel plots of $HCOO^-$, CO and H_2 together with experimental data points for operation at 40 atm. It is clearly seen that within the charge transfer region the modeled results deviate from the experimental results. The difference in slope between operation at 5 atm (~125$mVdec^-$) and 40 atm (~60$mVdec^-$) to $HCOO^-$ and CO, is interesting. As described in Chapter 6, this Tafel slope is primarily determined by α_c, which is assumed to be independent of pressure in this research. However, this assumption may be inaccurate for larger pressures, which can ex-

plain the deviation in slope. The current densities increase exponentially with overpotential, thus the deviation in slope results in a relatively large absolute error of up to 100 $mAcm^{-2}$ for $HCOO^-$, within the charge transfer region. Despite the different slope, the model qualitatively follows experimental data, though this is helped by the log scale. When looking at the limiting partial current densities towards $HCOO^-$ and CO, the modeled results are very similar to the results found experimentally. At 40 atm the limiting partial current density towards $HCOO^-$ is predicted to be 490 $mAcm^{-2}$ compared to 440-450 $mAcm^{-2}$ found experimentally.

The modeled partial current densities (PCD) allow us to calculate the Faradaic (i.e. current) efficiency towards each product species. The FE to product species i (with i being either $HCOO^-$, CO or H_2) is calculated as:

$$CE_i = \frac{PCD_i}{PCD_{HCOO^-} + PCD_{CO} + PCD_{H_2}} \cdot 100\% \tag{8.1}$$

In Figure 8.3 the modeled effect of current density on the Faradaic efficiencies towards $HCOO^-$, CO and H_2 is shown for a CO_2 pressure of 20 atm. In addition, experimental data by Todoroki et al. [1] at 20 atm on Indium electrodes is plotted. The model predicts that at a current density of 1 $mAcm^{-2}$ all three product are formed with significant selectivities (respectively ~35% to $HCOO^-$, ~15% to H_2 and ~50% to CO). This distribution is roughly in line with the experimental data and all the modeled efficiencies lie within a $10\%_{pp}$- range. For an increasing current density from 1 $mAcm^{-2}$ to approximately 300 $mAcm^{-2}$, the model shows a clear increase in selectivity towards $HCOO^-$ with the FE to CO and H_2 dropping to levels below 10%; a trend which is also observed experimentally. At even higher current densities (300+ $mAcm^{-2}$), the selectivity towards $HCOO^-$ rapidly drops and H_2 becomes the dominant product species. This rapid change occurs due to a CO_2 shortage at the electrode surface, which initiates the mass transfer controlled regime. Simplified, the formation of the CO_2 reduction products: formate and carbon monoxide is limited, and remains constant for higher current densities. As HER is not limited within the range observed, H_2 formation becomes dominant rapidly.

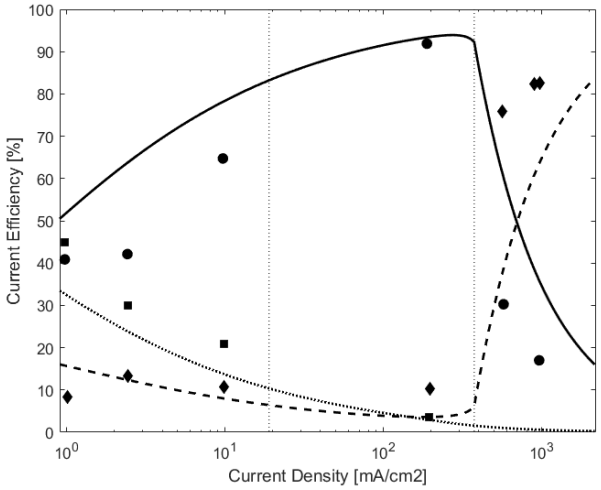

Figure 8.3: The modeled effect of current density on the Faradaic efficiency of $HCOO^-$ (—), CO (····) and H_2 (- -) at 20 atm on In electrodes (T=298.15K & 0.5M $KHCO_3$). Data points from Todoroki et al. [1] for $HCOO^-$ (●), CO (■) and H_2 (♦) at 20 atm on In electrodes (T=298.15K & 0.5M $KHCO_3$)

In Figures 8.4a and 8.4b, the predicted effects of current density on the FE at 5 atm and 40 atm are plotted. Generally speaking the same trends as at 20 atm are seen, with a rapid increase in selectivity towards $HCOO^-$ up to a certain current density, after which H_2 becomes the dominant species. Interestingly, is the fact that both the maximum FE (up

to 90-95%) to $HCOO^-$ and the current density at this maximum efficiency increase with an increasing CO_2 pressure. At 5 atm a maximum CE of 85% is predicted at a current density of 60 $mAcm^{-2}$. For 40 atm a maximum CE of 95% at 530 $mAcm^{-2}$ is modeled. As (partial) current density is directly related to the formation of a product, an increase of CO_2 pressure from 5 atm to 40 atm is predicted to result in a yield increase of $HCOO^-$ of 8 times.

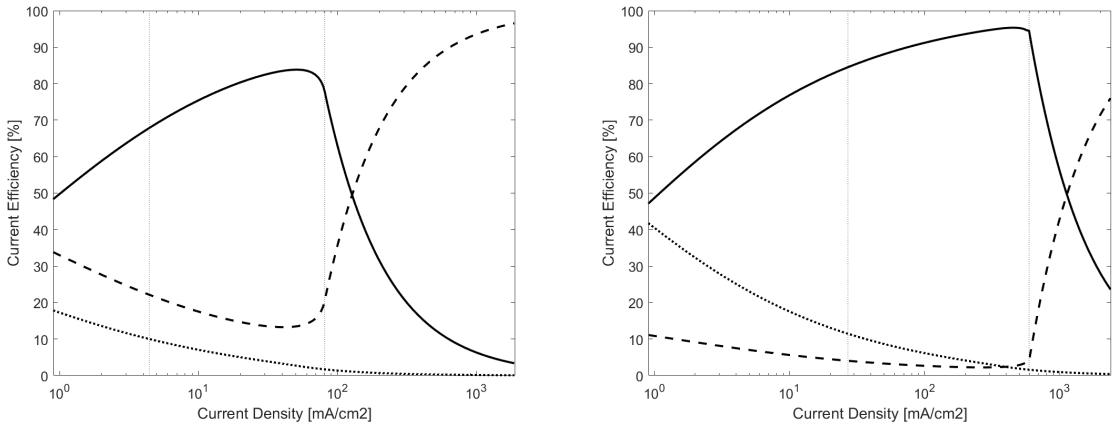

(a) 5 atm (T=298.15K & 0.5M $KHCO_3$) (b) 40 atm (T=298.15K & 2.0M $KHCO_3$)

Figure 8.4: The modeled effect of current density on the Faradaic efficiency of $HCOO^-$ (—), CO (····) and H_2 (- -) on In electrodes

During mass transfer control, the kinetics are fully determined by the diffusional flux of CO_2 from the bulk to the surface and are therefore completely independent of charge transfer. Thus, for an increasing potential, the partial current densities to ERC products have a maximum, and any additional current will go to the reduction of H_2O to hydrogen. In Figure 8.5, the modeled (●) and experimentally found (**x**) limiting partial current densities to $HCOO^-$ are plotted for CO_2 pressures between 1-60 atm. The modeled results are in agreement with the experimental data, increasing from <30 $mAcm^{-2}$ at 1 atm to ~ 600 $mAcm^{-2}$ at 60 atm in a near linear trend. At pressures above 40 atm the difference between the modeled results and the experimental data seems to get larger. This error may lie within the experimental error, but may also be caused by other limitations occurring at high pressure which are assumed negligible for the model (e.g. migrational effects).

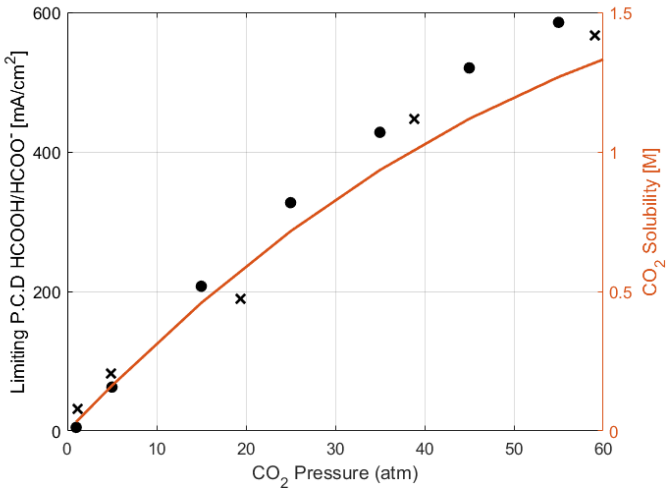

Figure 8.5: Modeled effect of CO_2 pressure on the limiting partial current density of $HCOO^-$ (●) (left axis) and the effect of pressure on the CO_2 solubility (—) (right axis). Data points from Todoroki et al. [1] for $HCOO^-$ (**x**) on In electrodes

Current efficiency is not the only metric that matters, other interesting aspects are the actual rate of $HCOO^-$ production per unit area and the production of formate per unit power. From the partial current density to formate, the rate of formation, $\dot{R}_{HCOO^-}$, can be calculated via Equation (8.2) and is plotted as the blue solid line in Figures 8.6a and 8.6b for varying current density at respectively 5 atm and 40 atm CO_2 pressure.

$$\dot{R}_{\mathrm{HCOO^-}}[\mathrm{gcm^{-2}s^{-1}}]=10^{-3}\,\mathrm{M_{HCOO^-}}\left(\frac{\mathrm{i_{HCOO^-}}}{\mathrm{nF}}\right) \tag{8.2}$$

Here M_{HCOO^-} is the molar mass of formate in $gmol^{-1}$, i_{HCOO^-} the partial current density to formate in $mAcm^{-2}$, n the number of electrons transfered in the reduction reaction to formate and F Faraday's constant.

As the rate of formation is directly proportional to the partial current density to $HCOO^-$, it increases exponentially up to the limiting partial current density, at which the kinetics become mass transfer controlled and from where it remains constant with increasing current density. The benefit of operation at an elevated CO_2 pressure with respect to the production rate becomes clear, as a near factor 8 increase in maximum production rate to formate is observed with ~$1.5e^{-5}$ $gcm^{-2}s^{-1}$ at 5 atm and ~$1.2e^{-4}$ $gcm^{-2}s^{-1}$ at 40 atm. For a cell with a superficial cathodic area of $600cm^{-2}$ (i.e. ~ 25cm x 25cm) [110], this relates to a daily production of ~0.8kg at 5 atm and ~6.2kg at 40 atm.

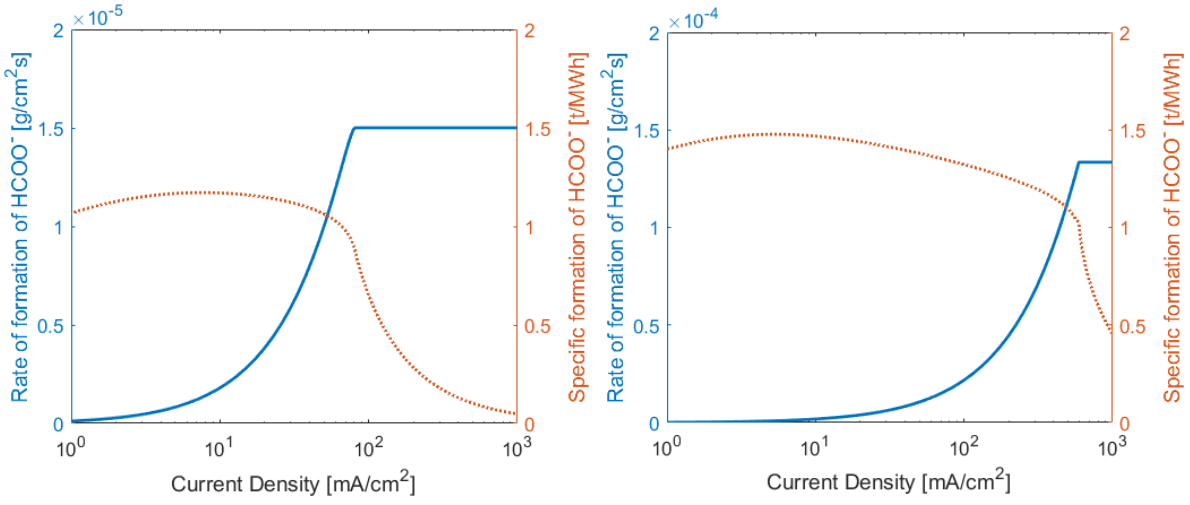

(a) 5 atm (T=298.15K & 0.5M $KHCO_3$) (b) 40 atm (T=298.15K & 0.5M $KHCO_3$)

Figure 8.6: Modeled effect of current density on rate of formation of $HCOO^-$ and specific energy consumption

The total specific energy input, $\dot{P}_{in}$ $[Jcm^{-2}s^{-1}]$, to the system is calculated via the product of the cell potential, E_{cell}, and the current density, i_{tot}. The cell potential is the sum of the cathodic reduction potential and the anodic oxidation potential. As explained in Chapter 3, the anodic oxidation potential is assumed to be equal to the theoretical oxidation potential of H_2O at pH 7: E_{ox} = -0.81V.

$$\dot{P}_{\mathrm{in}}\,[\mathrm{Jcm^{-2}s^{-1}}] = 10^{-3}(\mathrm{i_{tot}E_{cell}}) \tag{8.3}$$

The quotient of the rate of formation of $HCOO^-$ and the total specific energy input, gives the specific formation of formate per unit power. With $3.6e^9$ J per MWh and 10^6 gt^{-1}, the specific formation of formate per MWh, $\dot{F}_{HCOO^-}[tMWh^{-1}]$, is calculated via:

$$\dot{F}_{\mathrm{HCOO^-}}\,[\mathrm{tMWh^{-1}}] = 3.6\,\mathrm{e}^3\frac{\dot{R}_{\mathrm{HCOO^-}}}{\dot{P}_{\mathrm{in}}}=3.6\,\mathrm{e}^3\frac{\mathrm{M_{HCOO^-}}\left(\frac{\mathrm{i_{HCOO^-}}}{\mathrm{nF}}\right)}{(\mathrm{i_{tot}E_{cell}})} \tag{8.4}$$

The production of formate in tonnes per MWh is plotted for 5 atm and 40 atm in respectively Figures 8.6a and 8.6b. It is clear that the peak (i.e. highest production per unit energy)

is not at the limiting current density but for both 5 atm and 40 atm around 10 $mAcm^{-2}$. For both pressures, the production of formate is ~1 $tMWh^{-1}$ at the limiting current density. For higher current densities, the formation drops rapidly as extra H_2 is produced instead of formate. With an assumed energy price of €850 per MWh, this is in rough accordance with the energy cost calculated in Chapter 3, where ~0.95 $tMWh^{-1}$ was calculated based on typical experimental results. From the modeled results it appears that increasing the electrode surface area (i.e. increasing the size of the reactor itself) will always be beneficial as more formate can be formed with increasing surface area. In reality however, the trade-off between financial gain due to a production rate increase and increased capital costs should be researched carefully. For a certain desired production rate, a choice should be made to either build a larger reactor, resulting in increased capital costs, or to run a smaller reactor slightly more inefficiently, with associated increased production costs.

8.2. Bulk Specific Results

In this section, the predicted bulk conditions will be discussed. In Tables 8.1, 8.2 and 8.3, the modeled bulk concentrations for varying electrolyte concentrations are shown for 1 atm, 5 atm and 40 atm CO_2 pressure, respectively. With increasing pressure the concentration of CO_2(aq) is found to become higher, because the solubility of CO_2 increases. It is also found that an increase in electrolyte concentration will have have a minor effect on the CO_2 concentration. For sufficiently large electrolyte concentrations the electrolyte will shift to form extra CO_2(aq) as is predicted at 2.0M at 1 atm CO_2 pressure. Furthermore, the HCO_3^- concentration is practically equal to the electrolyte concentration and only a small fraction is deprotonated to form CO_3^{2-}. The amount of CO_3^{2-} increases with an increasing pH, as is expected from the equilibrium conditions described in Chapter 2.

Table 8.1: Bulk species concentrations for different electrolyte concentrations at 25°C and 1 atm

Electrolyte [M]	CO_2(aq) [M]	HCO_3^-[M]	CO_3^{2-}[M]	OH^-[M]	pH
0.05	0.0334	0.050	7.8e-6	3.3e-8	6.5
0.1	0.0335	0.100	3.1e-5	6.7e-8	6.8
0.2	0.0335	0.200	1.2e-4	1.3e-7	7.1
0.5	0.0342	0.498	7.6e-4	3.3e-7	7.5
1.0	0.0363	0.994	2.9e-3	6.1e-7	7.8
2.0	0.0430	1.981	9.6e-3	1.0e-6	8.0

Table 8.2: Bulk species concentrations for different electrolyte concentrations at 25°C and 5 atm

Electrolyte [M]	CO_2(aq) [M]	HCO_3^-[M]	CO_3^{2-}[M]	OH^-[M]	pH
0.05	0.1668	0.050	1.6e-6	6.7e-9	5.8
0.1	0.1669	0.100	6.3e-6	1.3e-8	6.1
0.2	0.1669	0.200	2.5e-5	2.7e-8	6.4
0.5	0.1670	0.499	1.6e-4	6.7e-8	6.8
1.0	0.1675	0.999	6.2e-4	1.3e-7	7.1
2.0	0.1693	1.995	2.5e-3	2.6e-7	7.4

Table 8.3: Bulk species concentrations for different electrolyte concentrations at 25°C and 40 atm

Electrolyte [M]	CO_2(aq) [M]	HCO_3^-[M]	CO_3^{2-}[M]	OH^-[M]	pH
0.05	1.0504	0.050	2.49e-7	1.07e-9	5.0
0.1	1.0504	0.100	9.97e-7	2.13e-9	5.3
0.2	1.0504	0.200	3.99e-6	4.26e-9	5.6
0.5	1.0505	0.500	2.49e-5	1.07e-8	6.0
1.0	1.0505	1.000	9.96e-5	2.13e-8	6.3
2.0	1.0508	1.999	3.98e-4	4.26e-8	6.6

In Figure 8.7a, the modeled effect of CO_2 pressure and electrolyte concentration on the bulk pH is shown. As expected, it is clearly seen that the pH will become lower with increasing pressure. For an electrolyte concentration of 0.5M the pH drops quickly from 7.5 to 6.3 between 1 and 20 atm, after with the drop in pH becomes more graduate and reaches ~6 at 60 atm. The same trend is seen for all electrolyte concentrations, but with increasing electrolyte the overall pH will become higher, as expected from the equilibrium reactions. At 2.0M the pH drops from 8 at 1 atm to 6.5 at 60 atm and this overall drop in pH of about 1.5 pH is observed for all electrolyte concentrations.

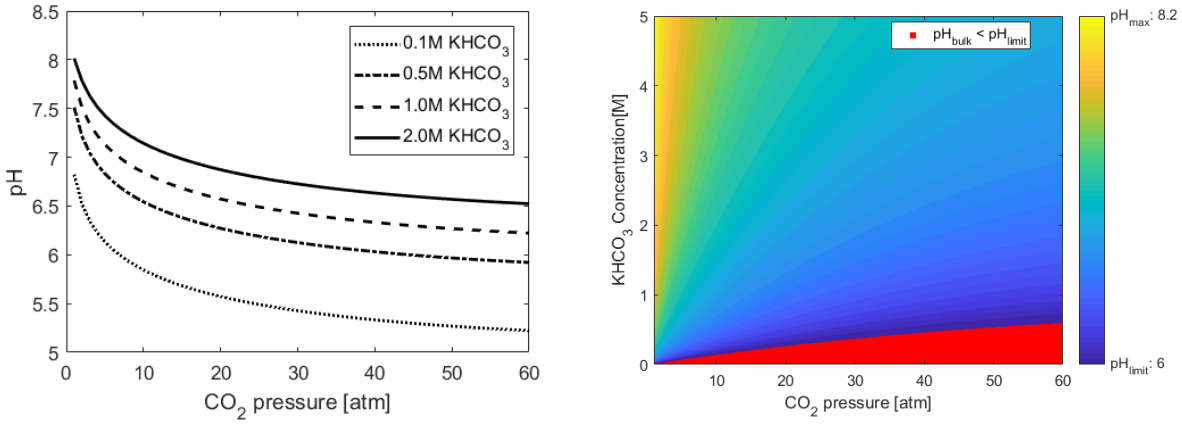

(a) Effect of CO_2 pressure on the bulk pH for varying electrolyte concentrations (T=298.15K)

(b) Surface plot for the effect of CO_2 pressure and electrolyte concentration on the bulk pH

Figure 8.7: Modeled effect of CO_2 pressure on the bulk pH for varying electrode concentrations (T=298.15K)

With an increasing pressure and an increasing CO_2 concentration, the solution will become more acidic and this is in accordance with the modeled results. This acidifying effect can be (partly) countered by increasing the electrolyte concentration. Due to the assumption that H_2O is the proton donor and that reaction b1 and b2 in Table 2.1 are dominant, the modeled results are only valid for sufficiently alkaline conditions. Therefore, while operating at high CO_2 pressures, care must be taken to add sufficient $KHCO_3$ to ensure neutral to basic conditions. The minimum bulk pH for which the model will be valid, pH_{limit}, is arbitrarily assumed to be 6.0 as explained in Chapter 7. In Figure 8.7b, the modeled effect of CO_2 pressure on the bulk pH for varying electrode concentrations is plotted on a surface plot. The red area indicates the region of operation for which the combination of pressure and electrolyte concentration will result in a modeled bulk pH below this minimum. At a CO_2 pressure of 60 atm, the highest pressure studied, the pH is found to be sufficiently high at an electrolyte concentration of approximately 0.5M.

8.3. CSR Specific Results

In this section, the predicted CSR conditions will be discussed. In Figure 8.8, the modeled concentration profile of CO_2 within the cathode surface region is plotted for ERC at 5 atm at the maximum FE (i_{HCOO^-}=~50 $mAcm^{-2}$). The step size Δt = 0.1s, with 51 spacial intervals. From 0-3 seconds the concentration profile appears transient, after which the system reaches steady state. It is seen that for operation at the maximum Faradaic efficiency, the concentration of CO_2 at the electrode surface is approximately zero. This indicates the start of the mass transfer controlled regime. In the Appendix, concentration profiles for the other species are plotted, as well as the 2D steady state concentration profiles for a CO_2 pressure of 1 atm (0.5M $KCHO_3$), 5 atm (0.5M $KCHO_3$) and 40 atm (2.0M $KCHO_3$). Gupta et al. [27] investigated the cathode surface concentrations for ERC in $KHCO_3$ solutions (based on experimental work at 1 atm by Hori et al. [71]) and the modeled results are in good agreement with their findings. As example, in accordance with the results found for this research, they

found an comparable increase of pH from ~7.5 to ~9.4 at the electrode surface.

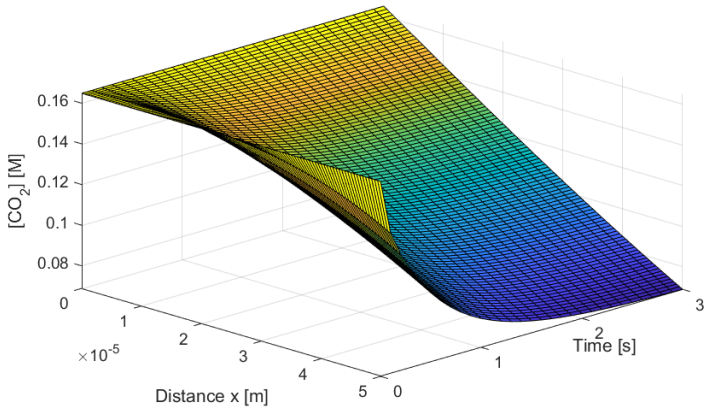

Figure 8.8: Modeled CO_2 profile at CO_2 pressure of 5 atm at maximum CE (i=~50 $mAcm^{-2}$) (T=298.15K & 0.5M $KHCO_3$)

In Figure 8.9, the modeled cathode bulk pH and surface pH for varying electrolyte concentration between 0M and 3M is plotted for a CO_2 pressure of 5 atm, 20 atm and 40 atm. It is observed that the difference between the bulk pH and surface pH increases with increasing CO_2 pressure for all electrolyte concentrations. First of all, the bulk pH decreases with increasing pressure due to the acidifying effect of a higher CO_2 solubility (see Chapter 2). Secondly, the surface pH will actually increase with increasing pressure, due to an increase in OH^- formation at the surface with increasing current density. With an increasing electrolyte concentration, the bulk pH and surface pH will approach each other. This effect is partly explained by the fact that the buffer capacity of the electrolyte increases with concentration and therefore the pH is less effected by the OH^- production at the surface. Furthermore, the bulk pH will become higher for increasing electrolyte concentration due to the increase in HCO_3^- within the solution as elaborated in Section 8.2.

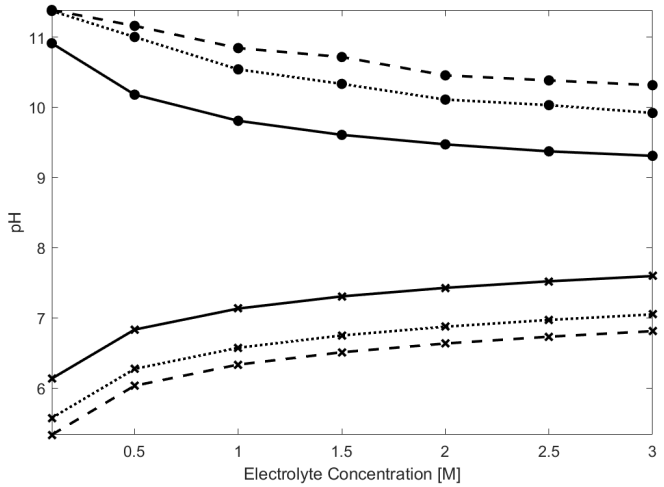

Figure 8.9: Modeled bulk pH (**x**) and surface pH (●) at CO_2 pressure of 5 atm (—), 20 atm (⋯) and 40 atm (- -) at $E_{mixed,MT}$ for varying $KHCO_3$ concentration between 0.1M and 3.0M on In electrodes (T=298.15K)

8.4. Sensitivity Analysis

The results presented in this chapter are based on certain assumptions about the value of input parameters such as the diffusion coefficients, diffusion layer thickness and the rate constants. The values of these parameters are based on reported values in literature or simple calculations, but reality may differ. In order to get a sense of the sensitivity of the model to variations of these variables, a sensitivity analysis has been conducted. This analysis will show how the uncertainty in the output of a numerical model may be apportioned to different sources of uncertainty in its inputs. Also, it will give an insight on the effect of wildly varying parameters, on the model outputs.

The analysis will be done using an one-factor-at-a-time approach (OFAT), where each input variable is changed separately while keeping all others at their nominal values. After analysis of one variable all variables are changed back to their nominal values, after which the next variable is changed. The input variables which are identified as most critical, and of which the effect of variation is analyzed are:

- Diffusion layer thickness (δ)
- Diffusion coefficients (D_i's)
- Diffusion coefficient of CO_2 (D_{CO_2})
- CO_2 solubility due to temperature
- Reaction rate constants (k_i's)
- Electrolyte concentration

The effect of variation of the inputs on several output variables is monitored. The critical output variables have been identified to be:

- Limiting current density to $HCOO^-$ ($i_{lim}^{HCOO^-}$)
- Limiting current density to CO (i_{lim}^{CO})
- Maximum Faradaic efficiency to $HCOO^-$ (FE_{max})
- Cathodic potential at CE_{max} (E_{opt})

The base case conditions which will act as base value are listed in Table 8.4:

Table 8.4: Base case conditions as used for the sensitivity analysis

Parameter:	**Value:**	**Unit:**
Temperature	298.15	K
Pressure	5	atm
Electrolyte concentration	0.5	M
Diffusion layer thickness	0.05e-3	m
Diffusion coefficients	see Table 5.1	m^2s^{-1}
Reaction rate constants	see Table 2.1	dependent

The most interesting findings will be discussed here and all results of the sensitivity analysis are shown in tabular form in the Appendix.

Diffusion layer thickness

The effect of the diffusion layer thickness on the output variables was found to be most striking. In Figures 8.10a and 8.10b, the modeled effects of δ on respectively the limiting partial current density to $HCOO^-$ and the maximum FE's to $HCOO^-$ are shown. It is clearly seen that a decrease in thickness both significantly increases the limiting partial current density to $HCOO^-$ and the maximum FE to $HCOO^-$. This effect is explained by the fact that mass transfer of CO_2 from the bulk to the electrode surface is significantly increased when the thickness decreases. At the nominal thickness of 0.05mm a limiting PCD of ~60 $mAcm^{-2}$ is predicted, together with a maximum FE of 83.8%. On the other hand, by halving the diffusion layer thickness to 0.025mm the limiting PCD to formate increases with 150% to ~150 $mAcm^{-2}$ and the maximum FE increases to 88.2%. Ways to decrease the thickness, and thus increasing both production rate and selectivety, may include stirring or increased flow of electrolyte solution within the cell.

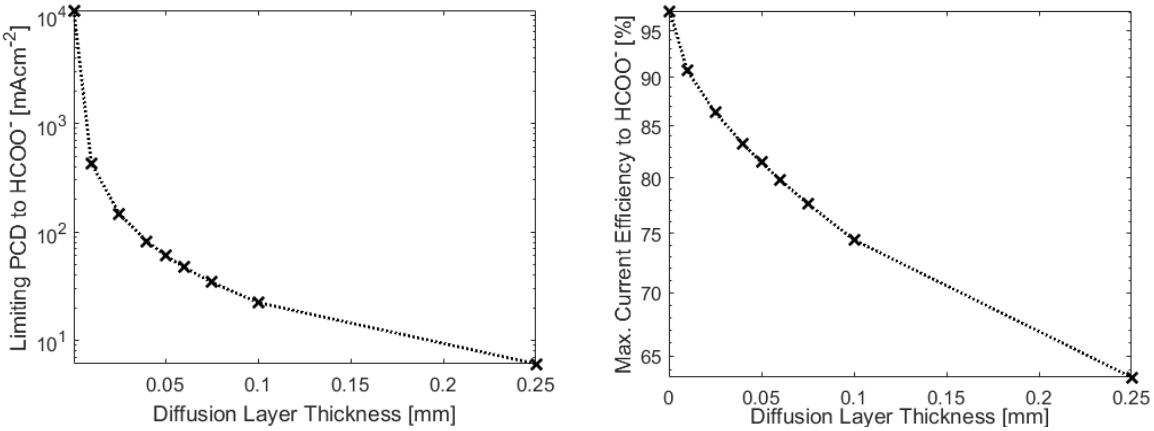

(a) Limiting partial current density to $HCOO^-$ (b) Maximum Faradiac efficiency to $HCOO^-$

Figure 8.10: Modeled sensitivity of varying diffusion layer thickness on the limiting partial current density to $HCOO^-$ and maximum Faradiac efficiency to $HCOO^-$ (dotted line shows the trend)

Diffusion Coefficients

The sensitivity of the model with respect to the diffusion coefficient is also evaluated. It has been found that the diffusion coefficient of CO_2 has a substantial influence of the outputs of the model, whereas the diffusion coefficients of the other species have very little influence. If D_{CO_2} becomes larger, both the limiting partial current densities of the CO_2 reduction products (i.e. $HCOO^-$ and CO) and the FE increase. A 30% increase from the nominal value, results in an increase of $i_{lim}^{HCOO^-}$ with 20 $mAcm^{-2}$ and the FE increases $1.8\%_{pp}$. This effect is also explained by the fact that the transfer of CO_2 from the bulk to the electrode surface is increased for a larger diffusion coefficient of CO_2. The diffusion coefficient will increase with an increased temperature.

CO_2 solubility due to temperature

As explained in Chapter 2, both an increasing pressure and a decreasing temperature have a positive influence on the solubility of CO_2 in water and aqueous systems. The sensitivity of the model for variations in the CO_2 solubility caused by temperature is tested. In reality a changing temperature may cause other factors to change as well (i.e. reaction rates, diffusion coefficients, etc...), but for this analysis they are kept constant at their nominal values. As expected, the model shown that a decreasing temperature will increase the CO_2 concentration in the electrolyte solution, directly influencing the model outputs. For a decreasing temperature, $i_{lim}^{HCOO^-}$ is observed to increase exponentially as seen in Figure 8.11a. FE_{max} is observed to increase linearly with a decreasing temperature, as seen in Figure 8.11b.

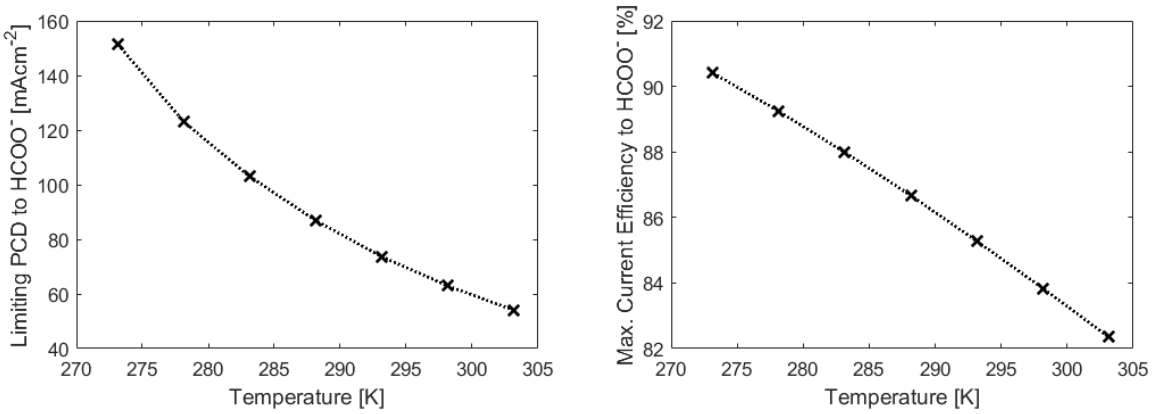

(a) Limiting partial current density to $HCOO^-$ (b) Maximum Faradiac efficiency to $HCOO^-$

Figure 8.11: Modeled sensitivity of varying CO_2 concentration due to temperature on the limiting partial current density to $HCOO^-$ and maximum Faradiac efficiency to $HCOO^-$

Reaction rate constants

As a rule of thumb, a temperature increase of 10 degrees will cause the rate constants to double [111]. The sensitivity of the model for changing reaction rates due to changing temperatures is investigated. It is found that the effect of the reactions rates on the model outputs is fairly small. Doubling the reaction rates will cause a decrease of $i_{lim}^{HCOO^-}$ with $7\%_{pp}$ and a decrease of the Faradiac efficiency of $<1\%_{pp}$. Interesting is the fact however, that a decrease of $i_{lim}^{HCOO^-}$ and CE_{max} is observed for increasing reaction rates.

Electrolyte Concentration

The pH of the bulk is found to be highly dependent of the electrolyte concentration. As explained, the pH of the electrolyte solution must be sufficiently high for the model to be valid. Beside the pH, the electrolyte concentration is found be have little effect on other outputs as $i_{lim}^{HCOO^-}$ and maximum Faradaic efficiency to formate.

9

Conclusions & Recommendations

9.1. Conclusions

In this research ERC has been investigated from two perspectives. First, the feasibility of commercial production for a selection of possible products of ERC has been evaluated and compared to formic acid. Secondly, ERC and the effect of an elevated CO_2 pressure has been researched and a numerical model has been developed.

Both thermodynamic theory and experimental research shows that a variety of products can be made by electrochemically reducing CO_2. It has been found that overall, formic acid is a promising product with some large advantages compared to the other ERC products. Interestingly it was found that, for best-known FE and when assessing for energy- and carbon costs, the production to $HCOO^-$ is found to cost ~€310 per tonne. Compared to a current market price for formate of €600 per tonne, formic acid formation was found to gave the highest profitability margin. Also, formic acid and methanol are liquid at atmospheric conditions. Therefore, they can store relatively large amounts of energy and hydrogen volumetrically, compared to the other products. Both species can be effectively used to store energy or act as hydrogen carrier without the need of additional compression or cooling.

The second objective of this research has been to further investigate this proposed beneficial effect of an elevated CO_2 pressure on selectivity and production rate, and to start the development of a numerical model. In this model, key thermodynamic principles (Chapter 4), diffusion (Chapter 5) and Tafel-type kinetics (Chapter 6) are combined. The model has shown to be capable of modeling the performance of a cell for various operating conditions with reasonable accuracy and the trends observed in experimental work are successfully reproduced. Interestingly, the effect of CO_2 pressure on the FE towards $HCOO^-$, CO and H_2 was predicted within a maximum deviation of approximately $20\%_{pp}$ for a current density of 200 $mAcm^{-2}$, compared to experimental results [1]. Also the trend of increasing FE towards $HCOO^-$ up to 20 atm, after which it remains constant with increasing pressure, was predicted accurately.

For increasing potential, the consumptive flux of CO_2 is found to increase exponentially and for sufficiently high overpotentials the diffusion of CO_2 from the bulk to the surface becomes limiting as the CO_2 surface concentration drops to (approximately) zero. At that point, all CO_2 that reaches the electrode surface is immediately reduced and no additional CO_2 is available to be reduced with increasing potential. As experimentally observed and reproduced with the model, both the production rate of $HCOO^-$ and the FE to $HCOO^-$ reach a maximum at approximately the point where CO_2 surface concentration becomes zero. The amount of CO_2 in the bulk and the transport of CO_2 from the bulk to the electrode surface are therefore identified as the main limitation for achieving high production rates. The effect of high CO_2 pressures on the selectivity and production rate has been modeled and is found to be significant. The maximum production rate per cm^2 to formate at a CO_2 pressure of 40 atm is calculated to be almost 8 times higher compared to 5 atm, with a production of $1.2e^{-4}$ $gcm^{-2}s^{-1}$ and $1.5e^{-5}$ $gcm^{-2}s^{-1}$ respectively. Also, for the same pressure increase, a rise of $10\%_{pp}$ in FE to $HCOO^-$ is found.

The development of specie concentration over time and for varying operating conditions within the vicinity of the electrode surface are numerically solved as a initial- and boundary problem. Besides the constant and equilibrated concentrations at the bulk-CSR interface, the flux of species due to electrochemical reactions are introduced as boundary conditions at the surface-CSR interface. Due to the formation of OH^- ions at the electrode surface, the pH is found to increase significantly near the electrode. The results numerically found for the local surface concentrations are in good accordance with modeling work on the cathode surface concentrations in ERC in $KCHO_3$ solutions by Gupta et al. [27].

9.2. Recommendations

The mathematical modeling involved several simplifications of the actual processes in the cell, which are expressed in a set of assumptions. In order to make the model more reliable and relevant for a wider range of applications, many improvements can be made. A selection of the most important recommendations for future work is mentioned below:

1. **Include the anodic half-cell to the model** - Anodic limitations on the process, and losses due to overpotential will be then accounted for. This may be done in a similar manner as for the cathodic half-cell, separating the half-cell in a bulk, surface region and electrode surface.
2. **Research on effects of convection and migration and include in model** - The developed numerical model assumes that diffusion is the only mass transfer phenomena. Although experiments can be specifically designed for this assumption to be valid, it also narrows the usability of the model. In reality, additional mass transfer phenomena will be present.
3. **Research the effect of temperature on cell performance and include in model** - The solubility of CO_2 is also temperature dependent and therefore an effect of temperature on both selectivity and production rate may be expected. In addition to CO_2 solubility, temperature will also have an effect on many other factors such as reaction rates, diffusion coefficients and conductivity of the electrolyte solution.
4. **Research on the direct usability of formate and conversion to formic acid** - This work has focused on the effect of an elevated CO_2 pressure on the selective production of formate, as the pH was assumed sufficiently high for the direct production of formic acid to be negligible. Little attention is given to the distinction between formic acid and formate however. Therefore, research on the post-process treatment, possible by acidification of formate or formate salts, and the associated costs is recommended. Also, a study on the separation and purification process to commercial purities is advised.

Other recommended additions include:

- Making the standard reduction potentials of $HCOO^-$, CO and H_2 pH dependent
- Improve the model to be valid at all pH levels, by adding additional chemical and electrochemical relations to the model
- Correcting D_i for a varying viscosity of the electrolyte solution

Finally, as mentioned, reliable experimental data on ERC at elevated pressures is scarcely available. For this research, experimental data by Todoroki et al. [1] is used to fit the kinetic parameters and to validate the modeled results. In order to successfully continue research on the usability of the model, more independent experimental data, especially on ERC at elevated CO_2 pressures and at different electrocatalysts, is necessary. With more experimental data for varying cell conditions and with a better understanding of the actual kinetic mechanisms, the selective production of other products such as CO or methanol may be also researched using the model. Also more clarity on the effect of pressure on both charge transfer coefficient and on the exchange current density will be beneficial to the accuracy of the model.

Bibliography

[1] Makoto Todoroki, Kohjiro Hara, Akihiko Kudo, and Tadayoshi Sakata. Electrochemical reduction of high pressure co2 at pb, hg and in electrodes in an aqueous khco3 solution. *Journal of Electroanalytical Chemistry*, 394(1-2):199–203, 1995.

[2] Sichao Ma, Paul JA Kenis, et al. Electrochemical conversion of co2 to useful chemicals: current status, remaining challenges, and future opportunities. *Current Opinion in Chemical Engineering*, 2(2):191–199, 2013.

[3] NIST. Carbon dioxide - phase change data, . URL `http://webbook.nist.gov/cgi/cbook.cgi?ID=C124389&Mask=1`. Accessed: 2018-01-18.

[4] B Patrick Sullivan, K Krist, and HE Guard. *Electrochemical and Electrocatalytic Reactions of Carbon Dioxide*. Elsevier, 2012.

[5] Masashi Azuma, Kazuhito Hashimoto, Masahiro Hiramoto, Masahiro Watanabe, and Tadayoshi Sakata. Electrochemical reduction of carbon dioxide on various metal electrodes in low-temperature aqueous khco3 media. *Journal of the Electrochemical Society*, 137(6):1772–1778, 1990.

[6] Mary Rakowski Dubois. Development of molecular electrocatalysts for co2 reduction and h2 production/oxidation. *Accounts of Chemical Research*, 42(12):1974–1982, 2009.

[7] Jeremy T Feaster, Chuan Shi, Etosha R Cave, Toru Hatsukade, David N Abram, Kendra P Kuhl, Christopher Hahn, Jens K Nørskov, and Thomas F Jaramillo. Understanding selectivity for the electrochemical reduction of carbon dioxide to formic acid and carbon monoxide on metal electrodes. *ACS Catalysis*, 7(7):4822–4827, 2017.

[8] National Oceanic and Atmospheric Administration Cameo Chemicals. Database of hazardous materials, 2018. URL `https://cameochemicals.noaa.gov`. Accessed: 2018-2-9.

[9] IPCC (Press Release). Concluding installment of the fifth assessment report: Climate change threatens irreversible and dangerous impacts, but options exist to limit its effects. 2014.

[10] HM Government. Carbon plan. URL `https://www.gov.uk/government/uploads/system/uploads/attachment_data/file/47621/1358-the-carbon-plan.pdf`. Accessed: 2018-2-4.

[11] Government of the Netherlands. Climate change - dutch goals within the eu. URL `https://www.government.nl/topics/climate-change/eu-policy`. Accessed: 2018-2-4.

[12] World Resources Institute. The u.s. greenhouse gas reduction targets, . URL `https://www.wri.org/sites/default/files/WRI14_Fact_Sheet_US_GHG_singles.pdf`. Accessed: 2018-2-4.

[13] Arun S Agarwal, Yumei Zhai, Davion Hill, and Narasi Sridhar. The electrochemical reduction of carbon dioxide to formate/formic acid: engineering and economic feasibility. *ChemSusChem*, 4(9):1301–1310, 2011.

[14] Daniel Yergin. *The quest: Energy, security, and the remaking of the modern world*. Penguin, 2011.

[15] Mar Pérez-Fortes, Jan C Schöneberger, Aikaterini Boulamanti, Gillian Harrison, and Evangelos Tzimas. Formic acid synthesis using co2 as raw material: Techno-economic and environmental evaluation and market potential. *international journal of hydrogen energy*, 41(37):16444–16462, 2016.

[16] Kohjiro Hara, Akihiko Kudo, and Tadayoshi Sakata. Electrochemical reduction of carbon dioxide under high pressure on various electrodes in an aqueous electrolyte. *Journal of Electroanalytical Chemistry*, 391(1-2):141–147, 1995.

[17] Derek Pletcher and Frank C Walsh. *Industrial electrochemistry*. Springer Science & Business Media, 1982.

[18] Macrotrends. Oil prices between 1965-1995. URL `http://www.macrotrends.net/1369/crude-oil-price-history-chart`. Accessed: 2017-05-05.

[19] Arun S Agarwal, Edward Rode, Narasi Sridhar, and Davion Hill. Conversion of co2 to value-added chemicals: Opportunities and challenges. *Handbook of Climate Change Mitigation and Adaptation*, pages 1–40, 2014.

[20] Jiujun Zhang Jinli Qiao, Yuyu Liu. *Electrochemical Reduction of Carbon Dioxide: Fundamentals and Technologies*. CRC Press, 2016.

[21] Matthew Jouny, Wesley W Luc, and Feng Jiao. A general techno-economic analysis of co2 electrolysis systems. *Industrial & Engineering Chemistry Research*, 2018.

[22] Xu Lu, Dennis YC Leung, Huizhi Wang, Michael KH Leung, and Jin Xuan. Electrochemical reduction of carbon dioxide to formic acid. *ChemElectroChem*, 1(5):836–849, 2014.

[23] Qi Lu, Jonathan Rosen, Yang Zhou, Gregory S Hutchings, Yannick C Kimmel, Jingguang G Chen, and Feng Jiao. A selective and efficient electrocatalyst for carbon dioxide reduction. *Nature communications*, 5:3242, 2014.

[24] Jingjie Wu, Frank G Risalvato, Fu-Sheng Ke, PJ Pellechia, and Xiao-Dong Zhou. Electrochemical reduction of carbon dioxide i. effects of the electrolyte on the selectivity and activity with sn electrode. *Journal of the Electrochemical Society*, 159(7):F353–F359, 2012.

[25] Hui Li and Colin Oloman. Development of a continuous reactor for the electro-reduction of carbon dioxide to formate–part 1: Process variables. *Journal of Applied Electrochemistry*, 36(10):1105, 2006.

[26] Colin Oloman and Hui Li. Electrochemical processing of carbon dioxide. *ChemSusChem*, 1(5):385–391, 2008.

[27] N Gupta, M Gattrell, and B MacDougall. Calculation for the cathode surface concentrations in the electrochemical reduction of co2 in khco3 solutions. *Journal of applied electrochemistry*, 36(2):161–172, 2006.

[28] Chariklia Georgopoulou, Swati Jain, Arun Agarwal, Edward Rode, George Dimopoulos, Narasi Sridhar, and Nikolaos Kakalis. On the modelling of multidisciplinary electrochemical systems with application on the electrochemical conversion of co2 to formate/formic acid. *Computers & Chemical Engineering*, 93:160–170, 2016.

[29] Charles Delacourt, Paul L Ridgway, and John Newman. Mathematical modeling of co2 reduction to co in aqueous electrolytes i. kinetic study on planar silver and gold electrodes. *Journal of The Electrochemical Society*, 157(12):B1902–B1910, 2010.

[30] Shinji Nakagawa, Akihiko Kudo, Masashi Azuma, and Tadayoshi Sakata. Effect of pressure on the electrochemical reduction of co2 on group viii metal electrodes. *Journal of electroanalytical chemistry and interfacial electrochemistry*, 308(1-2):339–343, 1991.

[31] Shoichiro Ikeda, Takehiko Takagi, and Kaname Ito. Selective formation of formic acid, oxalic acid, and carbon monoxide by electrochemical reduction of carbon dioxide. *Bulletin of the Chemical Society of Japan*, 60(7):2517–2522, 1987.

[32] GS Frankel, Arun Agarwal, Narasi Sridhar, et al. Degradation and deactivation of sn catalyst used for co2 reduction as function of overpotential. *Electrochimica Acta*, 133: 188–196, 2014.

[33] Fatih Köleli and Didem Balun. Reduction of co2 under high pressure and high temperature on pb-granule electrodes in a fixed-bed reactor in aqueous medium. *Applied Catalysis A: General*, 274(1-2):237–242, 2004.

[34] Hui Li and Colin Oloman. The electro-reduction of carbon dioxide in a continuous reactor. *Journal of Applied Electrochemistry*, 35(10):955–965, 2005.

[35] Kohjiro Hara, Akihiko Kudo, and Tadayoshi Sakata. Electrochemical reduction of high pressure carbon dioxide on fe electrodes at large current density. *Journal of Electroanalytical Chemistry*, 386(1-2):257–260, 1995.

[36] Kazuya Nakata, Takuya Ozaki, Chiaki Terashima, Akira Fujishima, and Yasuaki Einaga. High-yield electrochemical production of formaldehyde from co2 and seawater. *Angewandte Chemie International Edition*, 53(3):871–874, 2014.

[37] Karl W Frese. Electrochemical reduction of co2 at intentionally oxidized copper electrodes. *Journal of the Electrochemical Society*, 138(11):3338–3344, 1991.

[38] Minh Le, Maoming Ren, Ziyu Zhang, Phillip T Sprunger, Richard L Kurtz, and John C Flake. Electrochemical reduction of co2 to ch3oh at copper oxide surfaces. *Journal of the Electrochemical Society*, 158(5):E45–E49, 2011.

[39] Ko W Frese and S Leach. Electrochemical reduction of carbon dioxide to methane, methanol, and co on ru electrodes. *Journal of the Electrochemical Society*, 132(1):259–260, 1985.

[40] David P Summers, Steven Leach, and Karl W Frese Jr. The electrochemical reduction of aqueous carbon dioxide to methanol at molybdenum electrodes with low overpotentials. *Journal of electroanalytical chemistry and interfacial electrochemistry*, 205(1-2):219–232, 1986.

[41] Jianping Qu, Xiaogang Zhang, Yonggang Wang, and Chengxi Xie. Electrochemical reduction of co2 on ruo2/tio2 nanotubes composite modified pt electrode. *Electrochimica Acta*, 50(16-17):3576–3580, 2005.

[42] Md Meser Ali, Sato Hiroyasu, Mizukawa Tetsunori, Tsuge Kiyoshi, Haga Masa-aki, and Tanaka Koji. Selective formation of hco2 - and c2o4 2- in electrochemical reduction of co2 catalyzed by mono-and di-nuclear ruthenium complexes. *Chemical Communications*, (2):249–250, 1998.

[43] Y Hori, H Wakebe, T Tsukamoto, and O Koga. Adsorption of co accompanied with simultaneous charge transfer on copper single crystal electrodes related with electrochemical reduction of co2 to hydrocarbons. *Surface science*, 335:258–263, 1995.

[44] R. Sander. Compilation of henry's law constants (version 4.0) for water as solvent. *Atmos. Chem. Phys.*, 15:4399–4981, 2015.

[45] EW Aldrich and OC Bridgeman. Vapor pressure tables for water. *J. Heat Transfer*, 86: 279–286, 1964.

[46] NIST. Water - antoine equation parameters, . URL `http://webbook.nist.gov/cgi/cbook.cgi?ID=C7732185&Mask=4&Type=ANTOINE&Plot=on#ANTOINE`. Accessed: 2017-10-05.

[47] Shell Internationale Petroleum Maatschappij BV. Physical and engineering data, The Hague, 1978.

[48] R Wiebe and VL Gaddy. The solubility of carbon dioxide in water at various temperatures from 12 to 40 and at pressures to 500 atmospheres. critical phenomena. *Journal of the American Chemical Society*, 62(4):815–817, 1940.

[49] Stephen K Lower. Carbonate equilibria in natural waters. *Simon Fraser University*, 544, 1999.

[50] Zhenhao Duan, Nancy Møller, and John H Weare. An equation of state for the ch4-co2-h2o system: I. pure systems from 0 to 1000 c and 0 to 8000 bar. *Geochimica et Cosmochimica Acta*, 56(7):2605–2617, 1992.

[51] Kenneth S Pitzer. Thermodynamics of electrolytes. i. theoretical basis and general equations. *The Journal of Physical Chemistry*, 77(2):268–277, 1973.

[52] Zhenhao Duan and Rui Sun. An improved model calculating co2 solubility in pure water and aqueous nacl solutions from 273 to 533 k and from 0 to 2000 bar. *Chemical geology*, 193(3):257–271, 2003.

[53] Zhenhao Duan, Rui Sun, Chen Zhu, and I-Ming Chou. An improved model for the calculation of co2 solubility in aqueous solutions containing na+, k+, ca 2+, mg 2+, cl-, and so4 2-. *Marine Chemistry*, 98(2):131–139, 2006.

[54] National Institude of Standards and Technology (NIST). Carbon dioxide. URL `http://webbook.nist.gov/cgi/cbook.cgi?ID=C124389&Mask=10`. Accessed: 2017-05-05.

[55] MCAT. Rate processes in chemical reactions - kinetics and equilibrium. URL `http://mcat-review.org/rate-kinetics-equilibrium.php`. Accessed: 2018-2-5.

[56] Chemistry LibreTexts Jim Clark. The effect of pressure on rate of reaction, 2017. URL `https://chem.libretexts.org/Core/Physical_and_Theoretical_Chemistry/Kinetics/Rate_Laws/Reaction_Mechanisms/Reaction_Mechanisms/The_Effect_of_Pressure_on_Rate_of_Reaction`. Accessed: 2017-11-15.

[57] Alibaba.com. Oxalic acid wholesale per tonne, . URL `https://www.alibaba.com/product-detail/Oxalic-Acid-Wholesale-Price_60558184674.html?spm=a2700.7724857.main07.40.23e791c3730nxm&s=p`. Accessed: 2018-1-11.

[58] Research and Markets. Research and markets: China's oxalic acid industry, 2010-2012. URL `https://www.businesswire.com/news/home/20110111006011/en/Research-Markets-Chinas-Oxalic-Acid-Industry-2010-2012`. Accessed: 2017-06-1.

[59] Werner Reutemann and Heinz Kieczka. Formic acid. *Ullmann's encyclopedia of industrial chemistry*, 1996.

[60] Molbase.com. Formic acid price inquiry per tonne, . URL `http://www.molbase.com/en/cas-64-18-6-cate-p1n4-p7n10-p4n1.html`. Accessed: 2018-1-11.

[61] S. Moret, P. J. Dyson, and G. Laurenczy. Direct synthesis of formic acid from carbon dioxide by hydrogenation in acidic media. *Nature Communications*, 5(4017), 2014.

[62] Arun Agarwal Narasi Sridhar and Edward Rode. Electrochemical production of chemicals - applicability to co2 conversion. URL `https://www.arpa-e.energy.gov/sites/default/files/documents/files/3_Narasi_Sridhar_DNV.pdf`. Accessed: 2018-1-11.

[63] Agency for Toxic Substances and Disease Registry. Medical management guidelines for formaldehyde. URL `https://www.atsdr.cdc.gov/mmg/mmg.asp?id=216&tid=39`. Accessed: 2017-05-02.

[64] Alibaba.com. Formaldehyde wholesale per tonne, . URL https://www.alibaba.com/trade/search?fsb=y&IndexArea=product_en&CatId=&SearchText=formaldehyde. Accessed: 2018-1-11.

[65] Ltd. Merchant Research & Consulting. World formaldehyde production to exceed 52 mln tonnes in 2017. URL https://mcgroup.co.uk/news/20140627/formaldehyde-production-exceed-52-mln-tonnes.html. Accessed: 2017-06-01.

[66] Peng Tian, Yingxu Wei, Mao Ye, and Zhongmin Liu. Methanol to olefins (mto): from fundamentals to commercialization. *Acs Catalysis*, 5(3):1922–1938, 2015.

[67] Terry Helton, Mitch Hindman (ExxonMobil Research, and Engineering Company). Methanol to gasoline technology - an alternative for liquid fuel production, 2014. URL http://sycomoreen.free.fr/docs_multimedia/MTGexoonmobil.pdf. Accessed: 2018-2-9.

[68] Prachi Patel. Mit technology review - hydrogen fuel from formic acid, 2008. URL https://www.technologyreview.com/s/410135/hydrogen-fuel-from-formic-acid. Accessed: 2018-01-25.

[69] Methanol Institute. The methanol industry, . URL http://www.methanol.org/the-methanol-industry/. Accessed: 2017-06-01.

[70] Molbase.com. Methanol price inquiry per tonne, . URL http://www.molbase.com/en/cas-67-56-1-cate-p1n4-p7n10-p4n1.html. Accessed: 2018-1-11.

[71] Yoshio Hori, Katsuhei Kikuchi, Akira Murata, and Shin Suzuki. Production of methane and ethylene in electrochemical reduction of carbon dioxide at copper electrode in aqueous hydrogencarbonate solution. *Chemistry Letters*, 15(6):897–898, 1986.

[72] US Energy Information Administration. Natural gas weekly update. URL https://www.eia.gov/naturalgas/weekly/#tabs-prices-2. Accessed: 2018-1-11.

[73] Eurostat. Electricity price statistics. URL http://ec.europa.eu/eurostat/statistics-explained/index.php/Electricity_price_statistics. Accessed: 2017-06-05.

[74] Tom Mikunda, Filip Neele, Frank Wilschut, and Maurice (TNO) Hanegraaf. A secure and affordable co2 supply for the dutch greenhouse sector. 2015.

[75] Kamaruzzaman Sopian, Mohd Zamri Ibrahim, Wan Ramli Wan Daud, Mohd Yusof Othman, Baharuddin Yatim, and Nowshad Amin. Performance of a pv–wind hybrid system for hydrogen production. *Renewable Energy*, 34(8):1973–1978, 2009.

[76] Stephan Enthaler, Jan von Langermann, and Thomas Schmidt. Carbon dioxide and formic acid—the couple for environmental-friendly hydrogen storage? *Energy & Environmental Science*, 3(9):1207–1217, 2010.

[77] Brian Vad Mathiesen, Henrik Lund, David Connolly, Henrik Wenzel, Poul Alberg Østergaard, Bernd Möller, Steffen Nielsen, Iva Ridjan, Peter Karnøe, Karl Sperling, et al. Smart energy systems for coherent 100% renewable energy and transport solutions. *Applied Energy*, 145:139–154, 2015.

[78] Cheméo High Quality Chemical Properties. Chemical properties of oxalic acid. URL https://www.chemeo.com/cid/37-223-3/Oxalic%20acid. Accessed: 2018-1-11.

[79] The Engineering Toolbox. Heat of combustion, . URL https://www.engineeringtoolbox.com/standard-heat-of-combustion-energy-content-d_1987.html. Accessed: 2018-1-11.

[80] Naoya Onishi, Gábor Laurenczy, Matthias Beller, and Yuichiro Himeda. Recent progress for reversible homogeneous catalytic hydrogen storage in formic acid and in methanol. *Coordination Chemistry Reviews*, 2017.

[81] Gabriele Centi, Elsje Alessandra Quadrelli, and Siglinda Perathoner. Catalysis for co2 conversion: a key technology for rapid introduction of renewable energy in the value chain of chemical industries. *Energy & Environmental Science*, 6(6):1711–1731, 2013.

[82] Jörg Eppinger and Kuo-Wei Huang. Formic acid as a hydrogen energy carrier. *ACS Energy Letters*, 2(1):188–195, 2016.

[83] Karaked Tedsree, Tong Li, Simon Jones, Chun Wong Aaron Chan, Kai Man Kerry Yu, Paul AJ Bagot, Emmanuelle A Marquis, George DW Smith, and Shik Chi Edman Tsang. Hydrogen production from formic acid decomposition at room temperature using a ag–pd core–shell nanocatalyst. *Nature nanotechnology*, 6(5):302, 2011.

[84] National Fire Protection Agency. Frequently asked questions on nfpa 704, 2012. URL `https://www.nfpa.org/Assets/files/AboutTheCodes/704/704_FAQs.pdf`. Accessed: 2018-2-9.

[85] Keith Oldham, Jan Myland, and Alan Bond. *Electrochemical science and technology: fundamentals and applications*. John Wiley & Sons, 2011.

[86] Khan Academy. The reaction quotient q. URL `https://www.khanacademy.org/science/chemistry/chemical-equilibrium/factors-that-affect-chemical-equilibrium/a/the-reaction-quotient`. Accessed: 2018-2-9.

[87] Yoshio Hori. Electrochemical co2 reduction on metal electrodes. In *Modern aspects of electrochemistry*, pages 89–189. Springer, 2008.

[88] Ming Ma and Bernard Dam. Selective electrocatalytic co2 conversion on metal surfaces. *Doctoral Thesis, Delft University of Technology*, 2017.

[89] David Harvey. *Modern analytical chemistry*, volume 381. McGraw-Hill New York, 2000.

[90] William M Haynes. *CRC Handbook of Chemistry and Physics*. CRC press, 2014.

[91] John Newman and Karen E Thomas-Alyea. *Electrochemical Systems*. John Wiley & Sons, 2012.

[92] Javor K Novev and Richard G Compton. Natural convection effects in electrochemical systems. *Current Opinion in Electrochemistry*, 2017.

[93] Comsol Multiphysics Cyclopedia. What is ionic migration? URL `https://www.comsol.com/multiphysics/what-is-ionic-migration`. Accessed: 2017-11-6.

[94] PA Christensen and A Hamnet. *Techniques and mechanisms in electrochemistry*. Springer Science & Business Media, 2007.

[95] Yuliy D Gamburg and Giovanni Zangari. *Theory and practice of metal electrodeposition*. Springer Science & Business Media, 2011.

[96] Joseph Wang. *Analytical electrochemistry*. John Wiley & Sons, 2006.

[97] Edmund JF Dickinson, Juan G Limon-Petersen, Neil V Rees, and Richard G Compton. How much supporting electrolyte is required to make a cyclic voltammetry experiment quantitatively “diffusional”? a theoretical and experimental investigation. *The Journal of Physical Chemistry C*, 113(25):11157–11171, 2009.

[98] Clement H Bamford, CFH Tipper, and RG Compton. *Electrode kinetics: Principles and methodology*, volume 26. Elsevier, 1986.

[99] Yoshio Hori, Hidetoshi Wakebe, Toshio Tsukamoto, and Osamu Koga. Electrocatalytic process of co selectivity in electrochemical reduction of co2 at metal electrodes in aqueous media. *Electrochimica Acta*, 39(11-12):1833–1839, 1994.

[100] Tatsuya Shinagawa, Angel T Garcia-Esparza, and Kazuhiro Takanabe. Insight on tafel slopes from a microkinetic analysis of aqueous electrocatalysis for energy conversion. *Scientific reports*, 5, 2015.

[101] Nix R. M. An introduction to surface chemistry. URL http://www.chem.qmul.ac.uk/surfaces/scc/. Accessed: 2017-10-6.

[102] Corrosionpedia. Exchange current density. URL https://www.corrosionpedia.com/definition/477/exchange-current-density. Accessed: 2017-12-10.

[103] Rolando Guidelli, Richard G Compton, Juan M Feliu, Eliezer Gileadi, Jacek Lipkowski, Wolfgang Schmickler, and Sergio Trasatti. Definition of the transfer coefficient in electrochemistry (iupac recommendations 2014). *Pure and Applied Chemistry*, 86(2):259–262, 2014.

[104] Laurence A Belfiore. *Transport phenomena for chemical reactor design*. John Wiley & Sons, 2003.

[105] The Engineering Toolbox. Solubility of gases in water, . URL https://www.engineeringtoolbox.com/gases-solubility-water-d_1148.html. Accessed: 2017-11-27.

[106] P. Howard. *Partial Differential Equations in MATLAB 7.0*. Texas A&M University, Department of Mathematics, 2010.

[107] Mathworks. Mathworks pdepe documentation. URL https://nl.mathworks.com/help/matlab/ref/pdepe.html#f93-998627. Accessed: 2017-11-8.

[108] Robert D Skeel and Martin Berzins. A method for the spatial discretization of parabolic equations in one space variable. *SIAM journal on scientific and statistical computing*, 11(1):1–32, 1990.

[109] Lawrence F Shampine and Mark W Reichelt. The matlab ode suite. *SIAM journal on scientific computing*, 18(1):1–22, 1997.

[110] DNV GL. Carbon dioxide utilization: Electrochemical conversion of co2 – opportunities and challenges. URL https://issuu.com/dnv.com/docs/dnv-position_paper_co2_utilization/2. Accessed: 208-12-2.

[111] General Chemistry Virtual Textbook. Collision and activation. URL http://www.chem1.com/acad/webtext/dynamics/dynamics-3.html. Accessed: 2018-01-18.

Appendix

Diffusion Layer Thickness (δ):

	δ:	**$i_{lim,HCOOH}$:**	**$i_{lim,CO}$:**	**$FE_{max,HCOO}$:**	**E_{opt}:**
	mm	*mA/cm2*	*mA/cm2*	*%*	*V*
1%	**0.001**	5217.3	13.7	97.0	-1.72
20%	**0.010**	436.7	3.8	92.0	-1.59
50%	**0.025**	151.7	2.2	88.2	-1.53
80%	**0.040**	84.5	1.6	85.4	-1.50
100%	**0.050**	**62.9**	**1.4**	**83.8**	**-1.49**
120%	**0.060**	49.0	1.2	82.4	-1.48
150%	**0.075**	35.8	1.0	80.4	-1.46
200%	**0.100**	23.5	0.8	77.4	-1.44
500%	**0.250**	7.7	0.4	65.5	-1.38

Diffusion Coefficient (all):

D:	**$i_{lim,HCOOH}$:**	**$i_{lim,CO}$:**	**$FE_{max,HCOO}$:**	**E_{opt}:**
m2/s	*mA/cm2*	*mA/cm2*	*%*	*V*
70%	39.9	1.1	81.1	-1.47
80%	47.4	1.2	82.2	-1.47
90%	55.1	1.3	83.1	-1.48
100%	**62.9**	**1.4**	**83.8**	**-1.49**
110%	70.9	1.5	84.5	-1.49
120%	78.9	1.5	85.1	-1.50
130%	87.3	1.6	85.6	-1.50

Diffusion Coefficient (CO2 only):

D_{CO2}:	**$i_{lim,HCOOH}$:**	**$i_{lim,CO}$:**	**$FE_{max,HCOO}$:**	**E_{opt}:**
m2/s	*mA/cm2*	*mA/cm2*	*%*	*V*
70%	41.7	1.1	81.4	-1.5
80%	48.7	1.2	82.4	-1.5
90%	55.8	1.3	83.2	-1.5
100%	**62.9**	**1.4**	**83.8**	**-1.5**
110%	70.1	1.4	84.4	-1.5
120%	77.3	1.5	85.0	-1.5
130%	84.5	1.6	85.4	-1.5

CO_2 Solubility (due to temperature):

T:	$C_{CO2,BULK}$	$i_{lim,HCOOH}$:	$i_{lim,CO}$:	$FE_{max,HCOO}$:	E_{opt}:
K	*M*	*mA/cm2*	*mA/cm2*	*%*	*V*
273.15	0.339	151.3	2.6	90.4	-1.41
278.15	0.288	123.0	2.3	89.2	-1.43
283.15	0.247	102.9	2.0	88.0	-1.44
288.15	0.214	86.8	1.7	86.7	-1.46
293.15	0.187	73.7	1.5	85.3	-1.47
298.15	**0.165**	**62.9**	**1.4**	**83.8**	**-1.49**
303.15	0.147	54.1	1.2	82.3	-1.5

Electrolyte Concentration:

$C_{ELEC.}$:	$pH_{BULK:}$	$i_{lim,HCOOH}$:	$i_{lim,CO}$:	$FE_{max,HCOO}$:	E_{opt}:	$C_{CO2,BULK:}$
M	-	*mA/cm2*	*mA/cm2*	*%*	*V*	*M*
0	3.567	43.7	1.1	81.6	-1.47	0.1644
0.01	5.134	44.5	1.1	81.7	-1.47	0.1647
0.1	6.133	50.1	1.2	82.5	-1.48	0.1647
0.2	6.434	55.0	1.3	83.1	-1.48	0.1647
0.5	**6.832**	**62.9**	**1.4**	**83.8**	**-1.49**	**0.1649**
1	7.131	67.3	1.4	84.3	-1.49	0.1654
2	7.427	70.7	1.5	84.7	-1.49	0.1672
5	7.793	79.2	1.6	85.6	-1.50	0.1792

Reaction Kinetics (rate constants):

	± T :	$i_{lim,HCOOH}$:	$i_{lim,CO}$:	$FE_{max,HCOO}$:	E_{opt}:
	K	*mA/cm2*	*mA/cm2*	*%*	*V*
1/8x	**268.15**	69.8	1.5	84.6	-1.49
1/4x	**278.15**	68.4	1.4	84.5	-1.49
1/2x	**288.15**	66.2	1.4	84.2	-1.49
1x	**298.15**	**62.9**	**1.4**	**83.8**	**-1.49**
2x	**308.15**	58.7	1.3	83.3	-1.49
4x	**318.15**	53.9	1.2	82.7	-1.48
8x	**328.15**	49.1	1.2	82.1	-1.48

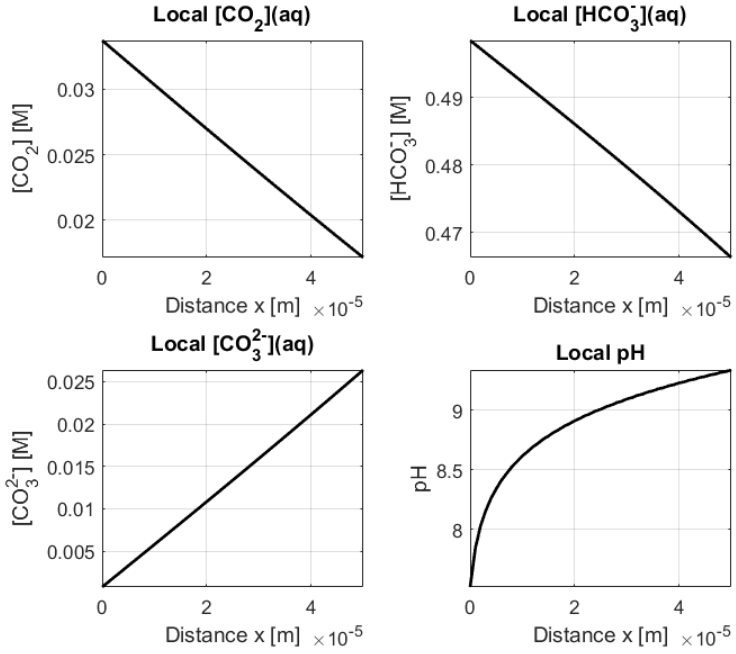

Figure 9.1: Steady state concentration profiles within the CSR at 1 atm and 0.5M $KHCO_3$

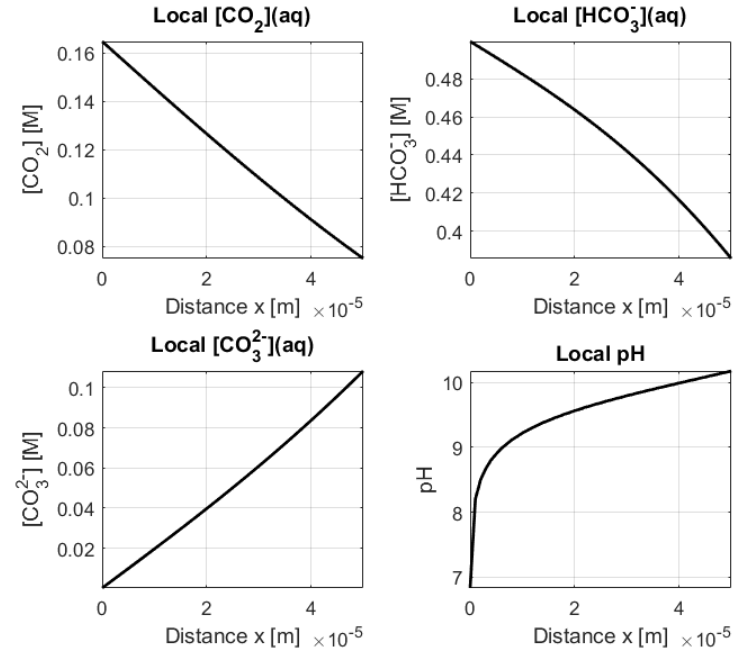

Figure 9.2: Steady state concentration profiles within the CSR at 5 atm and 0.5M $KCHO_3$

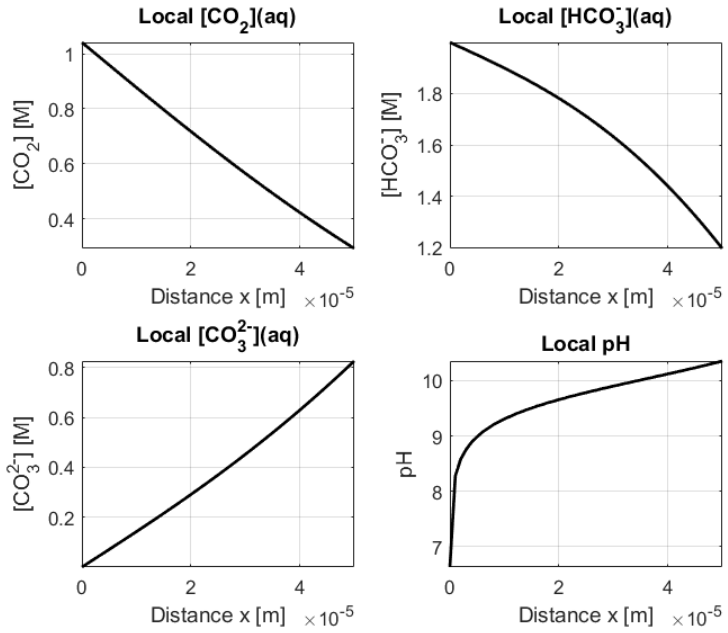

Figure 9.3: Steady state concentration profiles within the CSR at 40 atm and 2.0M $KHCO_3$

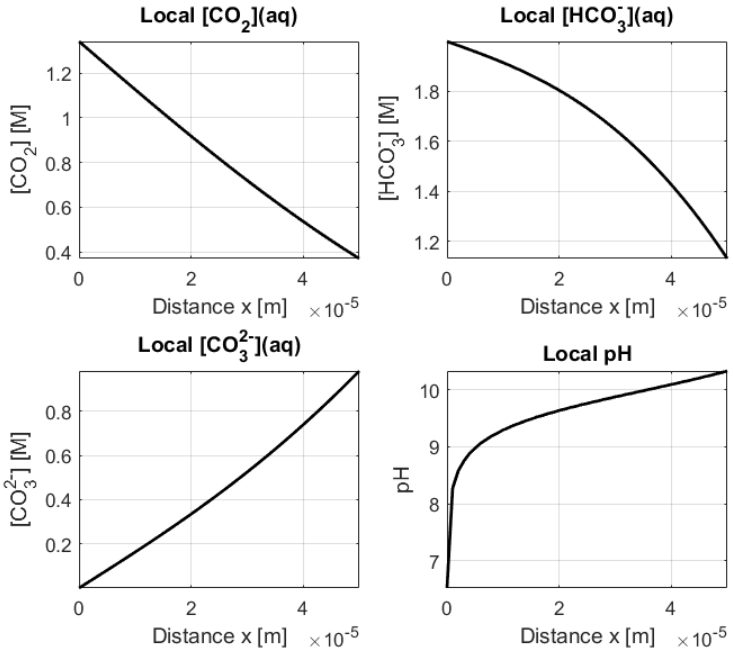

Figure 9.4: Steady state concentration profiles within the CSR at 60 atm and 2.0M $KCHO_3$

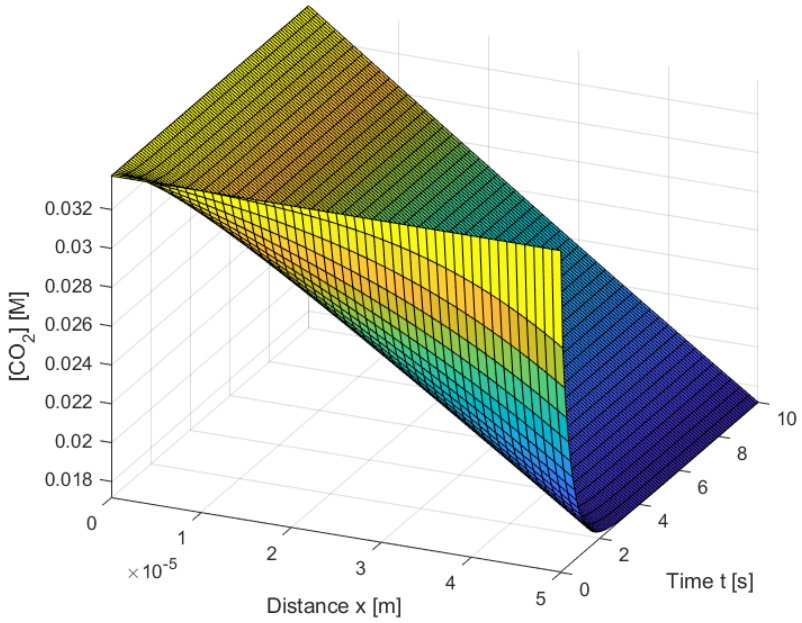

Figure 9.5: Transient 3D concentration profile for CO_2 within the CSR at 5 atm and 0.5M $KHCO_3$

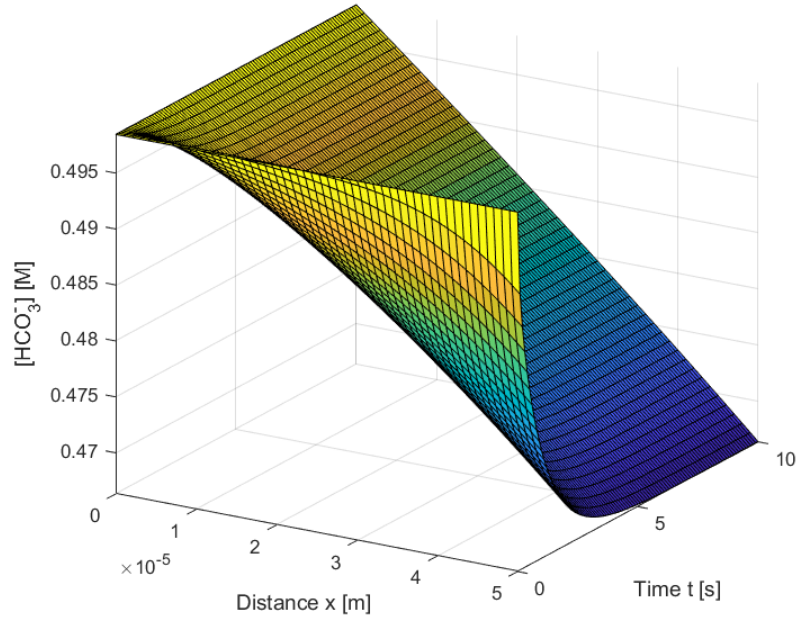

Figure 9.6: Transient 3D concentration profile for HCO_3^- within the CSR at 5 atm and 0.5M $KHCO_3$

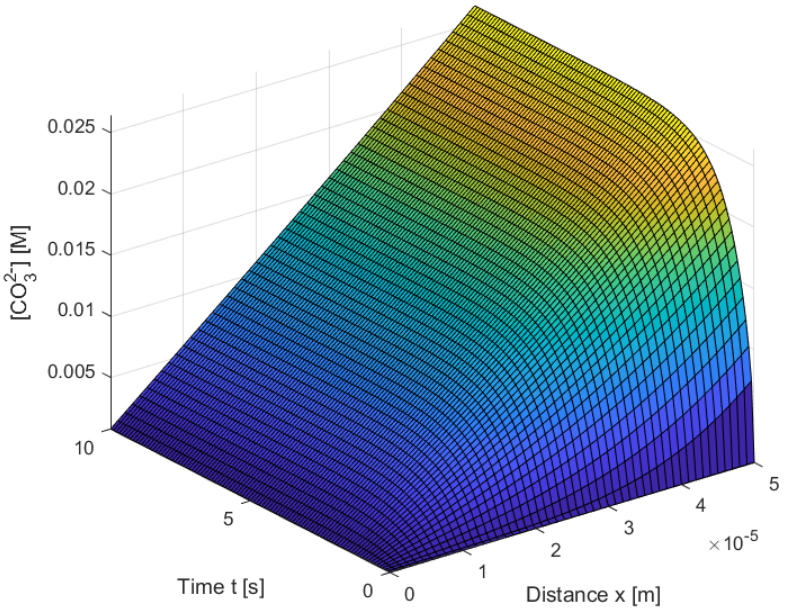

Figure 9.7: Transient 3D concentration profile for CO_3^{2-} within the CSR at 5 atm and 0.5M $KHCO_3$

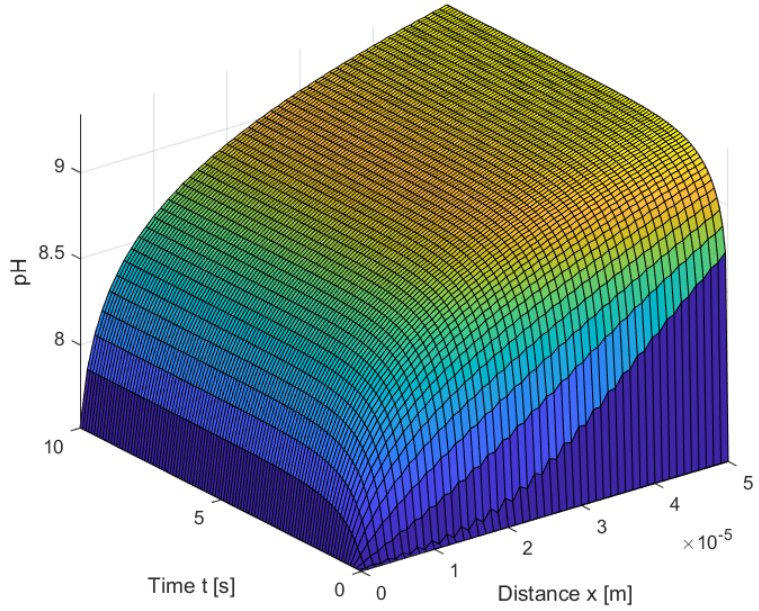

Figure 9.8: Transient 3D pH profile within the CSR at 5 atm and 0.5M $KCHO_3$